UNIVERSITÉ DE REIMS CHAMPAGNE-ARDENNE

ÉCOLE DOCTORALE SCIENCES DU NUMERIQUE ET DE L'INGENIEUR n°620

THÈSE

Pour obtenir le grade de

DOCTEUR DE L'UNIVERSITÉ DE REIMS CHAMPAGNE-ARDENNE

Discipline* : *GENIE CIVIL

Spécialité :Thermique du bâtiment

Présentée et soutenue publiquement par

ALI EL SAIED

Optimisation de la réduction des échanges géothermiques tridimensionnels des bâtiments

---

Thèse dirigée par **CHADI MAALOUF ET ETIENNE WURTZ**

Encadrement : **TIMEA BEJAT**

JURY

M. Jean-Jacques ROUX,	Professeur,	INSA Lyon,	**Rapporteur**
M. Patrick SALAGNAC,	Professeur	Université de La Rochelle,	**Rapporteur**
Mme Monika WOLOSZYN,	Professeur	Université Savoie Mont Blanc,	**Examinateur**
M. Pierre TITTELEIN,	Maître de Conférences	Université d'Artois,	**Examinateur**
M. Etienne WURTZ,	Directeur de Recherche,	CEA LITEN,	**Directeur de thèse**
M. Chadi MAALOUF,	Maître de Conférences HDR,	Université de Reims,	**Directeur de thèse**
Mme Timea BEJAT,	Ingénieur de recherches,	CEA LITEN,	**Encadrante de thèse**

ACKNOWLEDGMENTS

This thesis represents the outcome of three years of work within the MATIM laboratory, at the University of Reims-ChampagneArdenne and LELA laboratory at the French National Institute for Solar Energy (INES-CEA).

First of all, I would like to thank the Grand Reims and the French Alternative and Atomic Energies Commission (CEA) for funding this thesis.

I would like to express my sincere gratitude to my supervisors, Mr. Chadi MAALOUF, Mr. Etienne WURTZ, and Mrs. Timea BEJAT, whose encouragement, guidance and support enabled me to complete this thesis and prepared me for my following research career.

I would like to thank the members of my dissertation committee, Mrs. Monika WOLOSZYN, Mr. Jean-Jacques ROUX, Mr. Patrick SALAGNAC and Mr. Pierre TITTELEIN, for their discussion, ideas and feedback that have been absolutely invaluable.

I would like to express my gratitude to all my friends, without whom these three years would not have been the same. A big thank you for the moments of conviviality that we shared together. Thank you Samah, Sleiman, Farah, Hasan, Wassim, Sara, Rim, Karin, Hussein, Abbass, Bachar, Mohamad and Ali.

Finally, my deepest gratitude and special thanks go to my lovely parents, my sisters Amani and Majd. It is their unconditional love, patience and support that led me through this long, yet fulfilling journey.

ABSTRACT

The building sector is the highest energy-consuming sector in France. Hence, renovation should be considered to overcome high energy consumption. Naturally, heat rises and escapes through roofs, windows, and walls rather than the ground, acting as a natural insulator and thermal reservoir. Ground heat loss has been considered negligible compared to heat losses from other building surfaces for a long time. Therefore, heat transfer at this level should be included in the whole energy simulation for slab-on-grade buildings.

In this context, the thesis describes significant ground physical phenomena to understand ground behavior, boundary conditions and soil thermal parameters. This is followed by the presentation of different studies evaluating heat transfer phenomena through the soil and the thermal bridges.

In addition to that, a detailed three-dimensional analysis of ground heat transfer using WUFI Plus software is presented. Considering ground thermal bridges in whole building calculations is strongly highlighted in this analysis. Several boundary conditions, climates, insulations, slabs materials, and soil thermal properties are widely compared and discussed.

Finally, the thesis concludes with an optimization study. The last chapter compares and validates a 2D heat transfer model (KIVA) in EnergyPlus to the 3D model in WUFI Plus. Several insulations or renovation solutions are proposed, and other thermal and economic parameters are described in an optimization work using GenOpt and EnergyPlus (KIVA) software.

Key words: ground heat transfer, 3D calculation, slab on grade building, thermal bridges, renovation, optimization.

RÉSUMÉ

Le bâtiment est le plus grand secteur consommateur d'énergie en France. Ainsi, la rénovation doit être appliquée pour réduire les fortes consommations énergétiques. Dans un bâtiment sur terre-plein, la chaleur a tendance à s'échapper via les toits, les fenêtres et les murs plutôt que via le sol, qui agit comme un isolant naturel et un réservoir thermique. La perte de chaleur dans le sol a été considérée comme négligeable ou mal prédit par rapport aux pertes de chaleur des autres surfaces d'un bâtiment. Par conséquent, les fuites de chaleur à ce niveau doivent être incluses et bien étudiées dans les calculs des énergétiques des bâtiments.

C'est dans ce contexte que s'inscrit le travail de thèse. Dans un premier temps, ce rapport décrira les principaux phénomènes physiques du sol afin de mieux comprendre son comportement vis-à-vis des différentes conditions aux limites et matériaux. Les études bibliographiques des transferts de chaleur dans le sol et les ponts thermiques seront discutés.

La prochaine étape présentera une analyse tridimensionnelle détaillée sur le transfert de chaleur dans le sol à l'aide du logiciel WUFI Plus. Les résultats montrent l'importance de la prise en compte des ponts thermiques au niveau de la dalle et le sol dans les calculs énergétiques du bâtiment. Plusieurs conditions aux limites, climats, isolations, matériaux de la dalle et propriétés thermiques du sol sont largement comparés et discutés.

Enfin, la thèse se conclura par une étude d'optimisation. Le dernier chapitre commencera par une comparaison et validation d’un modèle de transfert de chaleur 2D (KIVA) dans EnergyPlus avec le modèle 3D dans WUFI Plus. Des solutions d'isolation et rénovation sont proposées dans ce travail. Des nombreux paramètres thermiques et économiques sont présentés dans un travail d'optimisation à l'aide des logiciels GenOpt et EnergyPlus (KIVA).

Mots clés : transfert de chaleur dans le sol, calcul 3D, dalle sur terre-plein, ponts thermiques, rénovation, optimisation.

TABLE OF CONTENTS

LIST OF FIGURES

LIST OF TABLES

LIST OF SYMBOLS AND ABBREVIATIONS

Symbol	Definition	Unit
A	Area	m^2
A^*	Water absorption coefficient	$kg/m^2s^{1/2}$
b	Width	m
C_p	Heat capacity	J/kg.K
Ct	Cost	€
d	Ground depth	m
D	Diffusion coefficient	m^2/s
E	Energy	kWh
e	Thickness	m
F	Payback period	year
g	Water vapor flux density	$kg/m^2.s$
H	Enthalpy	J/kg
h	Heat transfer coefficient	$W/m^2. K$
h_{matric}	Matric potential	m
J_v	Vapor diffusion flux density	$kg/m^2.s$

k_B	Boltzmann constant	-
knd	Knudsen diffusion coefficient	-
L_v	Latent heat of vaporization	J/kg
L_{2D}	2D thermal coupling coefficient	W/m.K
L_{3D}	3D thermal coupling coefficient	W/m.K
l	length	m
m	mass	kg
mfp	Mean free path	m
M	Molar mass	kg/m^3
Q	flux	W
q	flux density	W/m^2
p	pressure	Pa
r	radius	m
R	Gas constant	J/mol.K
R_m	Thermal resistance	m^2.K/W
S_e	Effective saturation	-
T	Temperature	°C

U	Thermal conductance	$W/m^2. K$
V	Volume	m^3
w	Water content	Kg/m^3
x	Coordinate	m
y	Coordinate	m
z	Coordinate	m

Greek alphabet

Symbol	**Definition**	**Unit**
α	Albedo	-
ε	emissivity	-
ϵ	scalar	
σ	Stefan-Boltzmann constant	$W/m^2.K^4$
λ	Thermal conductivity	W/m.K
λ_l	Hydraulic conductivity	kg/Pa.m.s
ρ	Density	Kg/m^3
ϕ	Relative humidity	%

μ	dynamic viscosity	kg m^{-1} s^{-1}
ξ	Structure factor	-
δ_v	Vapor permeability	kg.m^{-1}. s^{-1}. Pa^{-1}
ψ	Linear thermal transmittance coefficient	W/m.K
χ	Point thermal transmittance coefficient	W/m.K

Index

Symbol	**Definition**
a	Air
c	convective
cr	Convective-radiative
cs	Sensible convection
ex	exterior
g	ground
is	insulation
in	interior
l	liquid

n	nodal
ni	No insulation
sat	saturated
s	Soil
T	Total
v	vapor

Abbreviations

Symbol	**Definition**
ACH	Air change per hour
BC	Boundary condition
GPS	Generalized Pattern Search
HAMT	Heat and moisture transfer
HJ	Hooke-Jeeves
NM	Nelder-Mead
PSO	Particle Swarm Optimization
REV	Representative elementary volume

SD	Standard deviation
TB	Thermal bridges

CHAPTER 1. INTRODUCTION

1.1. RÉSUMÉ EN FRANÇAIS:

Le domaine du bâtiment est un secteur important pour les économies d'énergie et la réduction des gaz à effet de serre. En France, il représente 44% de la consommation d'énergie finale et 24% de ces émissions [1]. Cependant, l'un des défis environnementaux majeurs est la réduction des consommations énergétiques. Les déperditions thermiques des bâtiments affectent ces consommations, la chaleur étant dissipée à travers les différentes surfaces (murs, fenêtres, sols...). L'une des sources critiques de la dissipation de chaleur est le sol et les fondations. Dans les années 90, les pertes de chaleur à ce niveau étaient d'environ 15% contre 35% pour les murs, 25% pour la toiture, 15% pour les diverses fuites d'air et 10% pour les fenêtres. Les pertes de chaleur via le sol dans les bâtiments sur terre-plein jouent un rôle essentiel dans le comportement thermique [3]. Actuellement, elles sont devenues plus importantes en raison de la haute performance thermique de l'enveloppe et de l'ajout des systèmes de ventilation efficaces. Il est donc intéressant d'étudier les fuites de chaleur dans le sol et de proposer des solutions lors de l'évaluation de la performance énergétique d'un bâtiment lors de la rénovation [4].

Dans cette thèse, nous nous intéressons aux défis suivants : Comment prédire les pertes de chaleur tridimensionnelles via le sol et la dalle ? Quelle est l'importance de ces déperditions par rapport aux consommations énergétiques de l'ensemble du bâtiment ? Quels sont les paramètres qui affectent ces déperditions et comment les réduire ? Et enfin, quelles sont les solutions optimales pour rénover les bâtiments ? Toutes ces questions seront abordées dans les chapitres suivantes.

1.2. CONTEXT AND MOTIVATIONS:

The residential and tertiary building domain is an important sector for energy saving and reducing greenhouse gases. In France, it represents 44% of final energy consumption and 24% of greenhouse gas emissions[1]. However, one of the environmental challenges in this sector is energy reduction. Building thermal losses highly affect energy consumption, where heat is dissipated through different building levels (walls, windows, floors…). Many solutions are proposed to overcome this problem, like improving insulation properties, reducing air leakage and using efficient heating methods. Therefore, a renovation will present an effective solution to overcome thermal losses. The National Housing Agency [2] recorded 155,000 renovated house units in 2019 (almost double 2017).

One of the critical heat dissipation sources is the ground and its foundations. In the 90's, heat losses at this level were around 15% compared to 35% for walls, 25% for a roof, 15% for various air leaks and 10% for windows. Heat losses through ground floors in slab-on-grade buildings play an essential role in a building's thermal behavior [3]. Nowadays, it has become more important due to the high thermal performance of walls, roofs, windows and the addition of efficient ventilation systems. Therefore, it is interesting to study ground heat losses and propose solutions (retrofitting) when assessing a building's energy performance [4].

In addition to that, ground and foundation heat transfers earn their importance due to its multidimensional heat transfer aspect. Hence, it is necessary to predict the ground thermal behavior using detailed models and correlations. In the literature, several articles are found on multi-dimensional ground heat transfer. A great number of research paper study ground heat losses under variable temperatures using 2D and 3D models.

However, ground thermal bridges' dynamic effect during seasonal variation (winter and summer) are among conditions that are not widely studied. Moreover, a small number of research work discuss this calculation at the building scale. So, it is necessary to use a dynamic multi-dimensional model to include all TB effects at the slab and the global building level.

Once this detailed calculation is done, renovating the building against ground heat losses and thermal bridges should be a constant concern. Exterior thermal insulation at the foundation wall and the junction is considered a good renovation technology to keep heat inside homes and reduce energy consumption.

In this thesis, we are interested in the following challenges: How to predict three-dimensional heat losses via soil and slab? What is the effect of ground heat losses on whole building energy calculations? What are the parameters that affect ground calculations? What is the importance of soil thermal properties and coupled heat and moisture transfer? How to reduce energy consumption due to ground heat losses? And finally, what are the optimal solutions to renovate buildings under different conditions? All these questions will be discussed in the next chapters.

The thesis is divided into six chapters, the first being the present introduction.

Chapter 2 reviews the state of the art of various physical parameters of the soil and the coupled transfer of moisture and heat. It presents different ground physical phenomena used in following application chapters. Equations are presented at a micro and macro scale.

Chapter 3 describes ground thermal bridges associated numerical model and the modelling process. It presents a literature review about thermal bridges, especially at ground level. Different calculation methods, norms, and insulation solutions are presented to study thermal bridges for slab on grade.

In chapter 4, the results of different simulations will be displayed and explained. The analysis of ground heat loss using a 3D heat transfer model in WUFI Plus software is presented. This chapter describes the numerical studies of ground thermal bridges influence on whole building energy calculation. First, and through several simulation studies, the effect of ground boundary variation on building results is studied. Then, soil and slab thermal behavior under seasonal variations are described. The building energy performance is presented in winter and summer conditions for different soil thermal properties. The comparison of exterior insulation (polystyrene) technique with respect to uninsulated case and under different climate conditions is also carried out. Moreover, two slab types (hempcrete and concrete) are compared using a heat moisture transfer model.

Chapter 5 discusses different exterior insulation solutions under various conditions. Insulations are made of polystyrene and polyurethane: They are applied at the exterior foundation wall and the slab on grade junction. Then, a coupling numerical study is carried out between EnergyPlus with the foundation KIVA model and an optimization software called GenOpt. Many solutions are studied under different soil, interior and economic conditions. Finally, optimal results are found based on the building thermal performance and the insulation price.

The thesis concludes in Chapter 6.

CHAPTER 2. SCIENTIFIC BACKGROUND OF GROUND PHYSICS

2.1. RÉSUMÉ EN FRANÇAIS:

Ce chapitre présente une description des phénomènes de transfert de chaleur et d'humidité dans le sol et la dalle, ainsi que les conditions aux limites à ce niveau. D'abord on présente les transferts de chaleur ensuite les transferts couplés d'humidité et de chaleur.

Le transfert de chaleur est représenté par l'équation de la chaleur (2D et 3D). Le bilan thermique est appliqué à la surface supérieure de la dalle et du sol en contact avec le bâtiment et avec l'extérieure. L'interaction directe entre le bâtiment et le sol se fait via les conditions aux limites : transfert de chaleur avec l'environnement intérieur, transfert de chaleur vers l'environnement extérieur avec les conditions du champ lointain et la condition du sol profond.

Le sol est considéré comme un milieu poreux siège de différents phénomènes physiques: Le transfert de chaleur par conduction, transfert de chaleur latente couplé à un changement de phase, transfert de liquide par montée capillaire, transfert de vapeur par diffusion ou effusion. Ces phénomènes seront représentés par le modèle de Kunzel : Les potentiels des transferts dans ces deux équations sont la teneur en eau w et la température T.

To understand ground heat transfer, we define physical behavior via soil and ground layers. This chapter presents a description of ground heat and moisture transfer phenomena in soil in contact with building. These phenomena are considered in this work in next chapters.

2.2. SOIL IN BUILDING ENERGY ANALYSIS

All buildings are in contact with soil (Figure 2-1) which is considered as boundary conditions same as weather or exterior climate. Therefore, soil influences thermal losses and should be considered during building energy efficiency analysis.

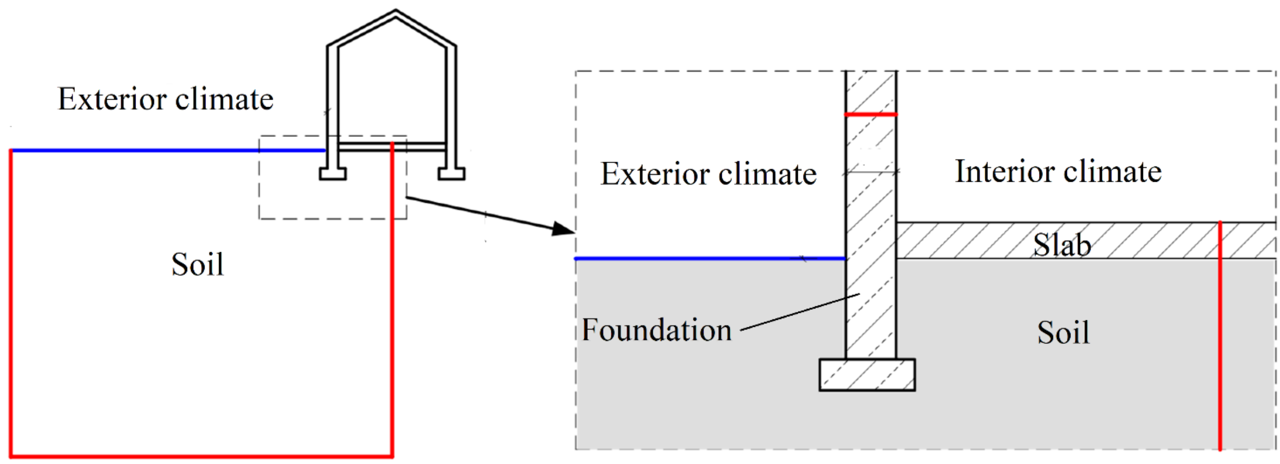

Figure 2-1: Foundation and building with soil [5].

Over the past twenty years, soil thermal research became more important with respect to building energy balance and ground thermal losses calculation. Ground heat losses can represent up to 30% of the total heat losses in buildings [6]. Therefore, soil has an important effect on whole building energy balance and should not be neglected.

The knowledge of thermal and hydric properties of soils is necessary to study their heat or coupled heat and moisture transfers. We distinguish several soil types (Figure 2-2) according to their physical characteristics: density, water content, mineralogy, size and grains arrangement, which influence their thermal behavior.

Figure 2-2: Considered soil types [7]

2.2.1. Soil types in building studies

Twelve classes of soil are described in Figure 2-3 with specific thermal and hydric properties. They are defined based on three components: sand, silt and clay. The most important properties for hygrothermal calculation are liquid water content, dry bulk density, porosity, thermal conductivity and specific heat capacity [8].

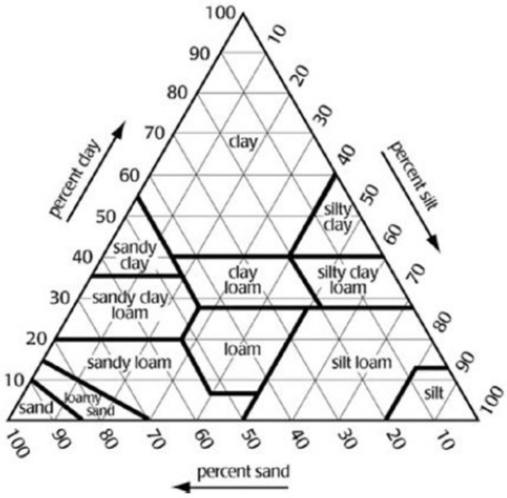

Figure 2-3: Twelve classes of soil texture [9].

Several studies have shown that thermal conductivity increases with dry density and water content of the material [10], [11] as does the thermal capacity[12]. Meanwhile the impact of water content and moisture transfer in soil is not widely discussed in the literature. [13], [14] showed a proportional relationship between soil's moisture content and soil's thermal conductivity.

2.2.2. Soil hydraulic properties

Table 2-1 represents average hydraulic properties of the above-mentioned soil types (except silty clay loam). We consider this table as a good reference for calculating moisture transfer in soil in building simulations.

Table 2-1: Average hydraulic properties for different types of soil [15].

Texture	Residual water content	Saturated water content	f	n	Saturated hydraulic conductivity
	l^3/l^3	l^3/l^3	cm^{-1}		$m\ d^{-1}$
Sand	0.045	0.43	0.145	2.68	7.128
Loamy sand	0.057	0.41	0.124	2.28	3.502
Sandy loam	0.065	0.41	0.075	1.89	1.061
Loam	0.078	0.43	0.036	1.56	0.249
Silt	0.034	0.46	0.016	1.37	0.06
Silt loam	0.067	0.45	0.02	1.41	0.108
Sandy clay loam	0.1	0.39	0.059	1.48	0.314
Clay loam	0.095	0.41	0.019	1.31	0.062
Sandy clay	0.1	0.38	0.027	1.23	0.028
Silty clay	0.07	0.36	0.005	1.09	0.005
Clay	0.068	0.38	0.008	1.09	0.048

Saturated water content is the maximum amount of water a soil can store. It is closely related to the t otal soil porosity. The residual water content presents the maximum moisture amount in soil that won't contribute to water flow.

The data in this table are based on Heathman experimental measures [16], for Micronet sites (Oklahoma USA) and pedotransfer functions from Carsel and Parrish work on soil water retention characteristics [17] where f and n are the traditional parameters of the soil retention formulation [18]:

$$S_e = \frac{1}{[1 + (f.h_{matric})^n]^{(1-1/n)}} \quad \text{2-1}$$

S_e is the effective saturation expressed as function of residual and saturated water contents; h_{matric} is the matric potential. This hydraulic input data is applicable to a depth of 30 cm or as an average for an entire soil profile if soil texture is uniform with depth. The saturated soil hydraulic conductivity represents the fluid potential to pass through soil pores.

Soil type is defined depending on particle diameter: clay (<2 µm), silt (2 to 50 µm) and sand (50 µm to 2 mm) [19]. Spatial arrangement and the connections between grains define structure of the porous medium [20]. It was clearly showed that soil particle size has a direct effect on moisture transport and storage [9]. For example (Table 2-1): Sand, Loamy sand and sandy loam have the largest hydraulic conductivity compared to other types (larger pores diameter).

2.2.3. Soil thermal properties

The properties associated with the thermal behavior of ground are thermal conductivity "λ" which represents the amount of heat transmitted per unit area and time under a temperature gradient, and thermal capacity "C_p" which corresponds to the energy needed to increase the temperature of a body by one kelvin.

2.2.3.1. Thermal conductivity:

Based on literature, it is concluded that soil's thermal conductivity (λ_S) is highly dependent on its temperature (T) and water content (w) [21]. Its variation with temperature is due to water phase transition during drying. Therefore, λ_S will be proportional to T and w [14] (Figure 2-4).

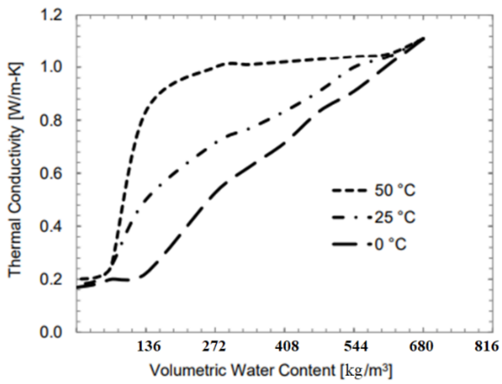

Figure 2-4: Ground thermal conductivity variation with soil (loam) temperature and volumetric water content [22].

It is shown from Figure 2-4 that ground thermal conductivity will rise when water content increases. Each line from this graph represents a soil temperature: for awater content between 68 and 680 kg/m^3, thermal conductivity has a significant variation.

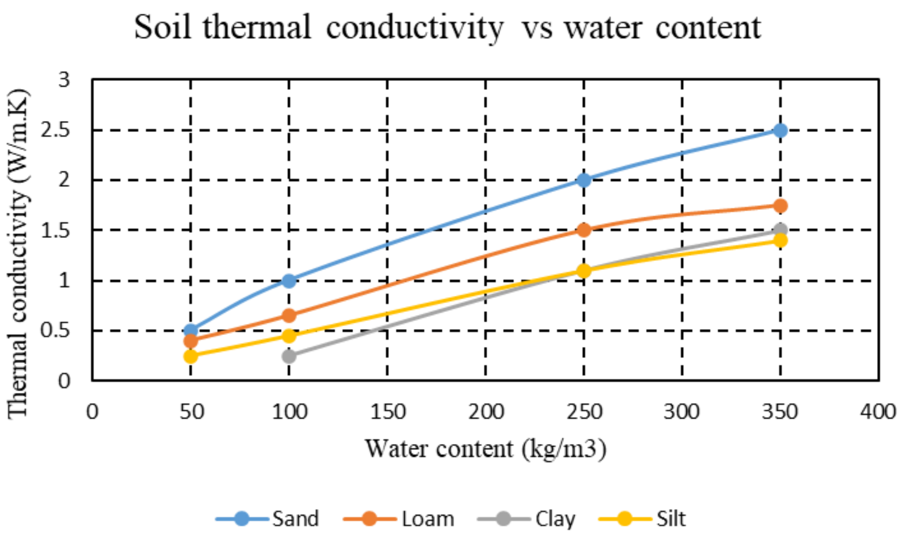

Figure 2-5: Soil conductivity as a function of water content for several soil types (at T=20°C).

Figure 2-5 represents thermal conductivity in function of water content for four soil types [9]. It is clearly shown that the λ of each type will increase when water content increase. Therefore, more the soil contains water, more its thermal conductivity is higher, thus its thermal resistance is less.

2.2.3.2. Thermal capacity

Thermal capacity is dependent on temperature and water content (w): more the porous material is filled by water, more its specific heat increased [17] upon a linear relation [9], [12]. It will vary from 0.83 to 1.67 KJ/kg.°C (sand) and from 1.17 to 2.25 kJ/kg.°C (clay) for water contents from 30 to 375 kg/m^3 [12].

2.2.4. Moisture in soils:

Soil has the ability to adsorb and store water from the surrounding environment; therefore, it is considered as a "hygroscopic" material. The amount of water accumulated in soil, at equilibrium, depends on the level of relative humidity of soil’s surroundings. Figure 2-6 presents the sorption curve of a hygroscopic material in general. Sorption isotherm is a curve reflecting water content increase in a material as a function of relative humidity at a given temperature. If the variation of water content starts from a saturated state, the curve is called "desorption" and if it starts from a dry state, the curve is called "adsorption isotherm".

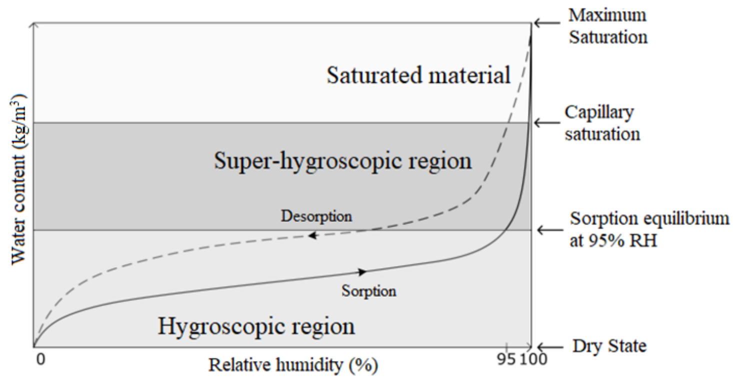

Figure 2-6: General form of the sorption curve of a hygroscopic material [23].

In function of water content of the material, we separate three regions:

- Hygroscopic region where water is transported mainly in vapor form as surrounding relative humidity remains low (under 40%). As Piot expressed [18], at low RH a first layer of water molecules is adsorbed on pore's surface, which receive second and more molecule layers with RH increase. In case of a pore totally filled by water, capillary condensation occurs.
- Super-hygroscopic region where no dominant moisture is identified as vapor and liquid transports are present. In case of maximum water content in a pore, capillary saturation is observed.
- Saturated region where soil is filled with water therefore no vapor transmission is possible. Instead, we observe maximum saturation, and no air transfer is possible through this soil.

Finally, the ability of soil to store moisture, are strongly depends on the dimension of the pores, as well as their diameter.

2.3. PHYSICS OF ENERGY AND MASS TRANSFER IN POROUS MATERIALS

Physical phenomena that we take into account during the study of porous materials in building physics are:

- Heat transfer by conduction,
- Latent heat transfer coupled by phase change,
- Liquid transfer by capillary suction
- Vapor mass transfer by diffusion or effusion.

2.3.1. Energy and mass balance at micro-scale

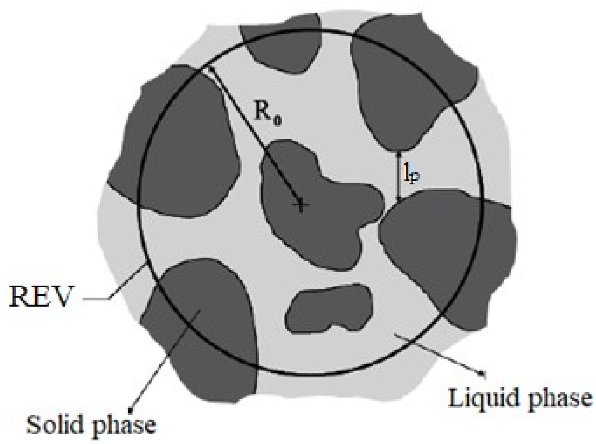

Figure 2-7:representative elementary volume REV [24].

Micro-scale correspond to the representative elementary volume (REV) [25] which is the minimum volume to be taken into consideration so that, once the homogenization theory is applied, the results obtained are representative of the macroscopic behavior of the heterogeneous medium. Therefore, the following sections concern the REV (Figure 2-7) of the studied domain.

One must choose the size of a REV in a way to capture the global movement of the fluid, the solid, the heat transfer and to smooth out the morphological complexities. The REV must meet the following condition so that it capture the global movement and phenomena's of the fluid or the solid:

l_p<< R_0 (radius of the REV) <<l_c where l_c is the characteristic dimension of the whole material and l_p is the characteristic size of the porosity). Therefore, R_0 should be very small compared to particle material size.

2.3.1.1. Heat transfer and storage

Heat transfer by conduction is governed by Fourier's law:

$$d\vec{q} = -\lambda . \vec{\nabla} T . dS \qquad 2\text{-}2$$

which describes the heat flux crossing a unit volume by conduction induced by temperature gradient within this solid. As we consider here only buildings with direct contact with the soil, convective and radiation heat transfer are neglected. Heat transfer due to phase change (condensation or evaporation) within the control volume could be written by the next equation:

$$d\,\overrightarrow{q_v} = L_v \overrightarrow{J_v} \qquad 2\text{-}3$$

where L_v is the latent heat of phase change [J/kg] and $\overrightarrow{J_v}$ is the vapor diffusion flux density [kg/m².s]. We apply the energy conservation law to the representative elementary volume REV (Figure 2-7):

$$\frac{\partial(\rho . C_p . T)}{\partial t} = -\nabla . \left(\lambda . \vec{\nabla} T\right) + r \qquad 2\text{-}4$$

where r is the source term corresponding to heat generation within the control volume (for example vapor condensation in our case).

2.3.1.2. Mass transfer

Under the influence of gradients of different potentials (total pressure, vapor pressure, temperature, etc.). Moisture in porous materials can be transported in liquid or gaseous phase. Two types of approaches are developed to describe this transfer:

1. The microscopic approach where the transfer is studied at REV.
2. The macroscopic approach where the moisture flux is linked to the gradient of driving potential.

Vapor moisture transfer by molecule-wall and intermolecular collisions

Vapor molecular transport takes place under the effect of a vapor concentration gradient according to the Fick's law [26]:

$$\overrightarrow{q_v} = -D_v.\vec{\nabla}(\rho_v) \quad \text{2-5}$$

q_v is the vapor flux density, D_v is the vapor diffusion coefficient in a porous medium and ρ_v is water vapor density. Water vapor is assumed to be an ideal gas, therefore:

$$p_v.V = N_v.R.T_v \quad \text{2-6}$$

$$\rho_v = \frac{M_v}{R.T} p_v$$

M_v is the vapor molar mass, R is the ideal gas constant and T_v the absolute vapor temperature. Replacing equation (2-6) in (2-5). The vapor flux in a pore will be:

$$\overrightarrow{q_v} = -D_v.\frac{M_v}{R.T_v}.\vec{\nabla}(p_v) \quad \text{2-7}$$

Now to determine D_v it is important to consider the mean free path (mfp) which represents the static distance traveled by the molecule between two molecular shocks. Thus, it depends on the pore size and molecular density. The vapor diffusion coefficient in the porous medium is proportional to the vapor diffusion coefficient in the free air D_{air} and to the Knudsen number [27]:

$$D_v = \frac{D_{air}}{1 + knd} \quad \text{2-8}$$

and

$$D_{air} = 2.10^{-7} \frac{T^{0.81}}{p_a} \quad \text{2-9}$$

T is the ambient temperature and p_a is the air ambient pressure. knd is the Knudsen number which is related to pore geometry:

$$knd = \frac{mfp}{d_p} \quad \text{2-10}$$

d_p is the pore diameter. The mean free path of water molecule in (in the air of a pore) is expressed as:

$$mfp = \frac{k_B . T_v}{r_p^2 . P_T . \pi \sqrt[2]{2}} \qquad 2\text{-}11$$

k_B is the Boltzmann constant, r_p is the radius of the molecule's protective sphere and P_T is the moist air total pressure.

Therefore, depending on the pore size and the molecular density, we can distinguish two vapor transfer mechanisms in a porous medium:

In the pores with a radius greater than the mean free path r_p>> mfp, collisions between pores walls are negligible compared to collisions between molecules, the vapor transfer will mainly be molecular diffusion.

In pores with a radius less than the mean free path r_p<< mfp, the vapor transfer will be effusion or so-called Knudsen diffusion.

In pores with a radius equal to the mean free path r_p= mfp, the molecules transport is determined both by molecule-wall collisions and by intermolecular collisions. D_v in function of pore diameter and Knudsen coefficient is shown in Figure 2-8:

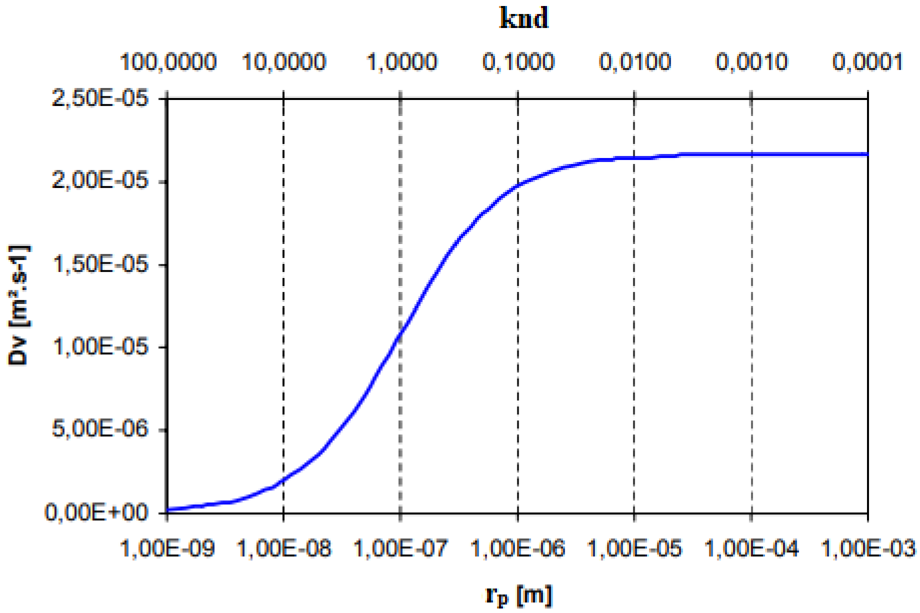

Figure 2-8: Vapor diffusion coefficient as a function of pore diameter and Knudsen coefficient [25].

For a pore with radius < 5.10^{-9}m, Knudsen diffusion is dominant. But if the radius is > 10^{-6}m than Fick's diffusion is applied. For a value between 10^{-6} and 5.10^{-9}, one observes a mixed transport.

Liquid moisture transfer

The presence of water in the porous medium is due either to the adsorption of water molecules or to capillary condensation. The adsorbed water has a very low mobility which is difficult to quantify. The mass transfer due to the adsorbed layer is not taken into account in this thesis [28].

The water due to capillary condensation in the pores moves under the effect of a capillary liquid pressure gradient. The mass flow rate within a tube of radius r, in the absence of external forces is described by Poiseuille's law [29]:

$$\vec{q_l} = \rho_l \frac{\pi . r^4}{8. \mu} . \vec{\nabla}(p_l) \tag{2-12}$$

q_l is liquid flux density, ρ_l is the liquid's density, p_l is the liquid's pressure and μ is the dynamic viscosity. Liquid and vapor phase equilibrium in a pore makes it possible to calculate liquid pressure as a function of relative humidity ϕ using Kelvin's law [30]:

$$p_l = \frac{R.T.\rho_l}{M_l}.ln(\phi) \quad \text{2-13}$$

M_l is the liquid molar mass and ϕ is the relative humidity. It is equal to the ratio of vapor pressure to saturated vapor pressure p_{sv} (T):

$$\phi = \frac{p_v}{p_{sat,v}(T)} \quad \text{2-14}$$

2.3.2. Energy and mass balance at macro-scale

At the macroscopic scale, the humidity accumulated in a material, depends on the ambient relative humidity. For a sorption isotherm curve, water content "w" is added for every relative humidity [31]:

$$w = w_{sat}.\frac{(B-1)*\phi}{B-\phi} \quad \text{2-15}$$

Where w_s is the moisture content at free saturation, and B is an approximation factor.

2.3.2.1. Vapor transfer in porous materials

Vapor transfer by diffusion or effusion

Vapor diffusion takes place if a difference in the concentration of water vapor or a vapor partial pressure gradient is present while the total pressure remains constant. Fick's law can describe water vapor diffusion in a gaz. Through porous materials, effusion exist when the pores are very small so that the collision between solid matrix walls (pores) and water molecules are more frequent than collision between water molecules. Within a porous material, water vapor can also migrate by diffusion or effusion under the effect of a partial vapor pressure gradient which can be described as follows:

$$\overrightarrow{q_v}(w,T) = -\delta_v(w).\vec{\nabla}(p_v(w,T)) \quad \text{2-16}$$

and δ_v is the vapor permeability of the material calculated based on a diffusion or effusion case.

2.3.2.2. Liquid transfer in porous material

Liquid transfer mechanisms exist based on capillary migration (Suction pressure).

Liquid transfer by capillary migration

The liquid water flow is due to a liquid pressure gradient within the water. It is directed in the direction of smaller pressure. The liquid flux density, $g_{l,c}$, is described by Darcy's law [32] as follows, with λ_l the hydraulic conductivity:

$$\overrightarrow{q_l}(w,T) = -\lambda_l(w).\vec{\nabla}(p_l) \qquad 2\text{-}17$$

p_l is the suction pressure. Hydraulic conductivity is the ability of the fluid to pass through pores expressed in kg/Pa.m.s. Based on equations (2-13),(2-14) and 2-15), equation (2-17) is re written as [31]:

$$\overrightarrow{q_l}(w,T) = -D_w(w).\vec{\nabla}(w) \qquad 2\text{-}18$$

the liquid transport coefficient D_w can be calculated by [31]:

$$D_w(w) = 3.8 * \left(A^*/w_f\right)^2 1000^{(w/w_{sat})-1} \qquad 2\text{-}19$$

where A^* is the water absorption coefficient.

The total liquid flux is:

$$\overrightarrow{q_{liquid}}(w,T) = -D_w(w).\vec{\nabla}(w) \qquad 2\text{-}20$$

2.3.2.3. Coupled heat and moisture transfer

In the case of soil materials, moisture present in pores in the form of vapor and liquid influences the storage and transfer of heat. Different parameter and variables interact to couple heat and moisture in a porous material. Through this interaction, coupling phenomena is established:

1. Water phase transition, where the material enthalpy is related to water transition from phase to phase (in the material).
2. Dependence of material thermal properties on moisture transfer and content (thermal conductivity).
3. The direct effect of material temperature on its absolute relative humidity.

Mass equation:

By applying conservation law, we can write mass conservation equation for the two phases as:

$$\frac{\partial w}{\partial t} = \nabla.(\overrightarrow{q_{liquid}} + \overrightarrow{q_{vapor}}) \qquad \text{2-21}$$

Therefore, the left-hand side can be re written as [33]:

$$\frac{\partial w}{\partial \phi}.\frac{\partial \phi}{\partial t} = \nabla.(\overrightarrow{q_{liquid}} + \overrightarrow{q_{vapor}}) \qquad \text{2-22}$$

ϕ is the relative humidity and $\frac{\partial w}{\partial \phi}.\frac{\partial \phi}{\partial t}$ will represent material moisture storage.

Heat equation:

By applying conservation law, heat equation is represented by:

$$\frac{1}{V}\frac{\partial H}{\partial t} = -\nabla.\left(\lambda\,(w,T).\vec{\nabla}T\right) + r \qquad \text{2-23}$$

The total energy E is defined as the sum of the internal energy U, the kinetic energy and the potential one. The variations of potential and kinetic energy are neglected in buildings. In an ideal gas, the internal energy and the enthalpy are related by:

$$u = H - p.V \qquad \text{2-24}$$

P is the pressure and V is the constant volume. p.V is negligible with respect to “u”. The enthalpy H are based on water, and material equations:

$$H = H_{water} + H_{material} \qquad \text{2-25}$$

H_{water} can be expressed as a function of liquid and vapor masses of the material:

$$H_{water} = m_{vapor}.C_{p,v}.T + m_{liquid}.C_{p,l}.T + m_{vapor}.L_v \qquad \text{2-26}$$

m_{vapor} $C_{p,v}$, m_{liquid} and $C_{p,l}$ are vapor and liquid masses and heat capacities. The density and specific heat of the material assumed to be constant.

Finally, the heat equation can be expressed as [33]:

$$\frac{1}{V}\frac{\partial H}{\partial \phi}\frac{\partial \phi}{\partial t} = -\nabla.\left(\lambda\,(w,T).\vec{\nabla}T\right) - \nabla.(\overrightarrow{q_{liquid}}.C_{p,l}.T - \overrightarrow{q_{vapor}}.(C_{p,v}.T + L_v)) \qquad \text{2-27}$$

Equation’s system:

Therefore, our equations for coupled heat and moisture transfer are:

$$\begin{cases} \frac{1}{V}\frac{\partial H}{\partial \phi}\frac{\partial \phi}{\partial t} = -\nabla.\left(\lambda\,(w,T).\vec{\nabla}T\right) - \nabla.(\overrightarrow{q_{liquid}}.C_{p,l}.T - \overrightarrow{q_{vapor}}.(C_{p,v}.T + L_v)) & \text{2-28} \\ \frac{\partial w}{\partial \phi}.\frac{\partial \phi}{\partial t} = \nabla.\left(\overrightarrow{q_{liquid}} + \overrightarrow{q_{vapor}}\right) & \text{2-29} \end{cases}$$

The three terms of equation 2-28 represent the storage, transport and generation of heat. The terms of equation 2-29 represent the storage of moisture, the transport of liquid moisture and the transport of vapor. The driving potentials in these two equations are water content w and temperature. To obtain the system of 2-28 and 2-29, we recall the assumptions made:

1. The porous medium consists of three phases: solid, liquid and gaseous. It is considered non-deformable, homogeneous and isotropic.
2. The fluids are considered incompressible.
3. Hysteresis is not taken into account.
4. The influence of gravity is negligible compared to the forces exerted by the suction pressure.
5. All interactions between plants and ground medium are not considered.
6. The part of the internal energy is dominant in front of the other energies (kinetic, potential...). The internal energy is assimilated to the enthalpy given the low-pressure differences involved.
7. No vapor transfer by advection.

2.3.2.4. Heat balance at soil surface

The heat balance now is applied at slab and soil upper surface of ground volume in contact with building (Figure 2-9). The direct interaction between building and soil is via slab interior surface boundary conditions.

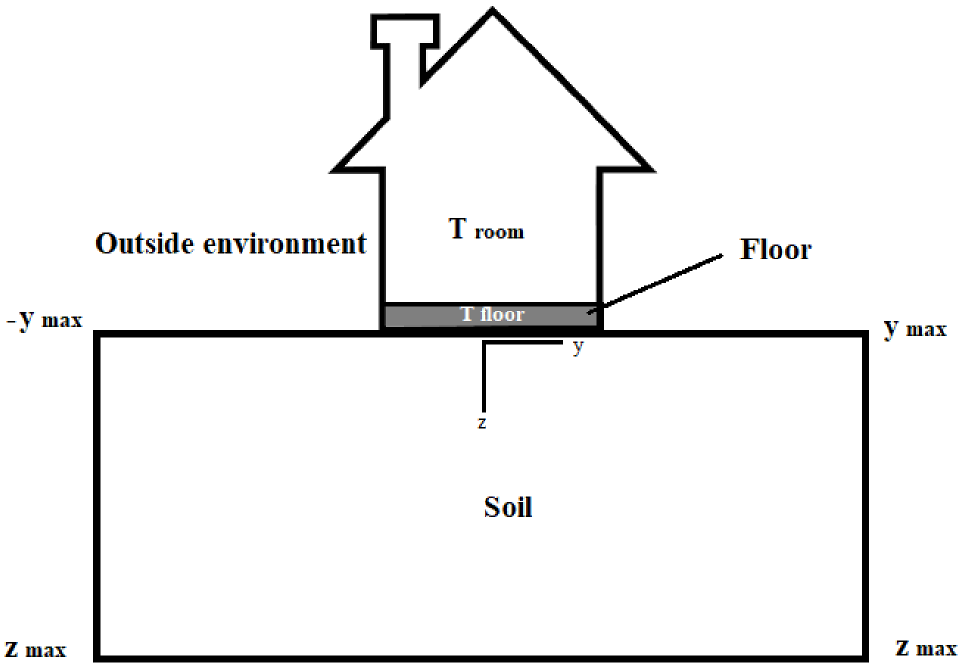

Figure 2-9: Ground domain with building.

Heat transfer with the indoor environment: It can be represented by convection and radiation phenomenon:

$$Q = h_{cr}.A.(T_{room} - T_{floor}) \tag{2-30}$$

where Q is the thermal flux [W], h_i is the combined convective-radiative surface conductance [W/m^2.K], A is the slab surface in contact with interior [m^2], T_{room} and T_{floor} are the room and floor temperatures [°C].

Heat transfer towards outside environment: It can be represented by equation 2-31 at soil surface where we consider heat transfer is in the z direction:

$$q = \lambda.\frac{\partial T}{\partial z} = q_{soil} + q_{sky} - q_g - q_{cs} \tag{2-31}$$

where q is the conduction heat flux density into ground [W/m^2], q_{soil}, q_g , q_{sky} and q_{cs} represent the net radiation absorbed and reflected at the ground surface , incoming infrared sky radiation, and sensible convection [W/m^2].

$$q_{soil} = q_{soil,i}(1 - \alpha_{soil}) \quad 2\text{-}32$$

$q_{soil,\,i}$ is the incident solar radiation heat flux on a horizontal surface [W/m^2], α_{soil} is the albedo of the ground. The albedo of the Earth-atmosphere system is the fraction of solar energy that is reflected back into space [6].

q_{sky} will be determined from climate file for every location. q_g can be represented by:

$$q_g = \varepsilon_g.\sigma.T_g^4 \quad 2\text{-}33$$

T_g is the ground temperature [°C].

$$q_{cs} = \rho_{air}.C_{p,air}.D_h(T_g - T_{db}) \quad 2\text{-}34$$

ρ_{air} is the air density [kg/m^3], $C_{p,air}$ is the air heat capacity [J/kg.K], T_{db} is the exterior air dry bulb temperature [°C] and D_h is the turbulent transport coefficient for heat [m/s] [34].

Boundary conditions at soil's volume surfaces:

The domain of study illustrated below is for ground and floor (Figure 2-10).

At $x = \pm x_{max}$ and $y = \pm y_{max}$, far-field conditions exist with a zero flux.

At $z = z_{max}$, a deep ground condition is imposed with a constant temperature or zero flux.

At $z = 0$, there are heat transfer with **the indoor environment** and **the outside environment**.

Far field condition:

Far field boundary condition is a zero-lateral heat flux in the horizontal directions. It exists at distance far enough from the building where no longer ground heat transfer will exist. Most of studies [3], [34]–[36] determine this distance to be between 5 m and 15 m.

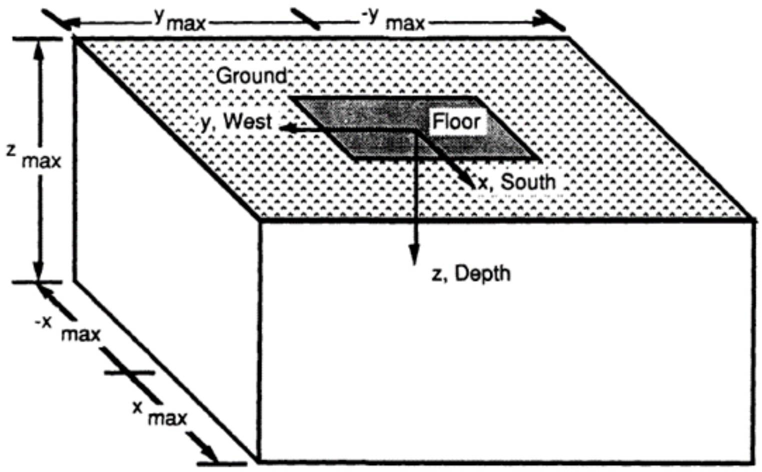

Figure 2-10: Rectangular domain [37].

Deep Ground Conditions:

A specified temperature condition is particularly appropriate when water conditions exist (such as a high-water table) that tend to maintain a fixed temperature at a finite depth. Based on the European norm [38], an adiabatic boundary condition is applied at a distance represented by floor width multiplied by 2.5. From literature, this depth is considered between 5 m and 20 m based on location and water table level. This temperature will be equal to the average outdoor air temperature.

2.4. CONCLUSION

Chapter 2 presents a theoretical description on ground heat and moisture transfer. All equations and phenomena described in this chapter will be considered in next chapters using several softwares (WUFI, EnergyPlus). Soil thermal properties (conductivity, heat capacity) can differ from one soil to another (Clay, Silt, Sand, and Loam) based on its moisture content or temperature. Therefore, it seems important to study coupled ground heat and moisture transfer (liquid and vapor transfer).

The driving potentials that are considered for moisture transfer in this study are: capillarity and phase change for liquid transfer. For vapor transfer, diffusion and effusion are considered as driving phenomenon. Concerning boundary conditions, convection, radiation, far field and deep ground conditions are used in this work. They have a direct effect on ground heat transfer [34].

This theoretical chapter will be followed by a literature review about different theoretical aspects and prediction to calculate ground thermal bridges.

CHAPTER 3. SLAB-ON-GRADE THERMAL BRIDGES LITERATURE REVIEW

3.1. RÉSUMÉ EN FRANÇAIS:

Ce chapitre traite la question générale liée à l'augmentation progressive des consommations énergétiques et des émissions de gaz à effet de serre, dues à l'effet des ponts thermiques au niveau du sol. Il traite des études et des travaux réalisés afin de modéliser et de prédire le comportement des ponts thermiques tout en proposant des solutions pour réduire leur effet en particulier pour les liaisons au niveau du sol pour les bâtiments sur terre-plein en rénovation. Il est publié dans Energy and Buildings Volume 257, 2022, https://doi.org/10.1016/j.enbuild.2021.111770.

Un pont thermique est la zone de l'enveloppe d'un bâtiment où la résistance thermique change considérablement en raison d'un changement de forme, d'épaisseur ou de matériau. Dans les zones perturbées par les PT, le flux thermique devient bidimensionnel (2D) ou tridimensionnel (3D), alors qu'il est unidimensionnel (1D) dans les zones non perturbées [39].

Trois méthodes principales sont utilisées dans la littérature pour identifier les PT. Elles sont basées sur les équations de la conservation de la chaleur, l'état du système (état transitoire/état stationnaire) et les propriétés thermiques : Méthode dynamique 3D, U équivalente, et mur équivalent.

La littérature concernant ce type de PT est peu abondante, il est donc important de les décrire. Dans ce chapitre, les ponts thermiques (2D) sont calculés en régime statique (méthode U équivalente) au niveau du sol et de la liaison dalle-mur à l'aide du logiciel THERM (Norme 10211). Pour réduire les PT et les déperditions de chaleur, diverses solutions d'isolation sont disponibles pour rénover les bâtiments existants : intérieure (verticale ou horizontale) et extérieure (verticale, en L, incliné, conique, trapézoïdal, trapézoïdal avec deux types d'isolant).

Les simulations montrent que l'isolation extérieure est plus pratique que l'isolation intérieure et permet de réduire l'effet des PT (de 54% à 61%) par rapport à un cas sans isolation. L'augmentation de l'épaisseur et de la profondeur de l'isolation ne réduit pas nécessairement l'effet du PT, celui-ci dépend aussi de la hauteur d'isolation H (que la jonction soit isolée ou non).

This literature chapter deals with the general issue related to the gradual increase in energy consumption and greenhouse gas emissions, due to the effect of ground thermal bridges in building sector, that are not widely discussed with respect to building total energy calculation. It deals with the studies and works carried out in order to model and predict thermal bridges behavior and propose different solution to reduce their effect and renovate buildings at grounds level. It is published in Energy and Buildings Volume 257, 2022, https://doi.org/10.1016/j.enbuild.2021.111770.

3.2. INTRODUCTION

In general, heat loss in buildings occurs via walls, roofs, windows, doors, slabs, thermal bridges (TB), [39] and the air exchange between indoor and outdoor areas. A TB is the area of a building's envelope where the thermal resistance changes considerably due to a change in shape, thickness, or material. In areas disturbed by TBs, the heat flow becomes two dimensional (2D) or three dimensional (3D), whereas the heat flow is one dimensional (1D) in undisturbed areas [40]. Ground heat loss has been considered negligible compared to heat loss from other surfaces of a building. After the improvement of building insulation, the relative importance of heat losses through foundation increases and becomes an important factor in the energy efficiency of a dwelling. Nowadays, the heat losses by the foundation are rather between 10 and 30% [41]. Neglecting this heat loss can lead to inaccuracies in the results (up to 50% error for surface temperature [42]), which are no longer negligible because new buildings aim to achieve low energy consumption. Accordingly, TBs are gaining more attention from researchers [43]. Actual new constructions tend to decrease heating and cooling energy and become zero energy consumption [44]. Therefore, national building standards, such as RT2012 [45], impose rules to achieve this goal.

Hence, renovation should be applied to overcome high energy consumption. Insulation types are described in the literature and can be used to renovate existing buildings at ground level such as vertical insulation or exterior horizontal insulation [46]. These types are recommended in most of articles, they will ensure good thermal insulation without harming building (foundation, slab).

During the heating season, heat loss between the building interior and exterior is affected by TBs or weak points through the construction envelope [47]. In particular, TBs are responsible in increasing energy use due to heating requirements [48], [49]. TBs also affect the cooling of interior surfaces, leading to condensation and mold risk, which affects indoor-air quality [50], [51]. Levin and Mao [52] simulated the effect of TBs on the total energy consumption of three buildings in Stockholm; the results suggest that, due to TBs, the total energy consumption increases by 2%–21%, and the heat flux through the building envelope increases by 5%–39%, especially through foundation and external walls. They recommend that TBs should be considered when simulating building thermal losses.

Several studies have proposed models to describe TBs. Hassid [53], [54] built a simplified model to consider TB-induced heat transfer (for homogeneous walls and multilayer walls) based on a 2D conduction heat transfer equation incorporating a steady-state TB effect. Zalewski, Lassue, and Rousse [55] conducted a numerical and experimental study to determine the TBs of prefabricated steel walls, in which 3D modeled walls were examined using heat flow meters, infrared cameras, and thermocouples data. Mao [56] compared experimental measurements to validate numerical correlation that uses electrical analogy (resistance) of the studied wall. Martin, Erkoreka, and Flores [57] studied the dynamic effect of TBs (thermal inertia) for two wall models: one with a strong-inertia concrete pillar and other with a low-inertia hollow metallic pillar. Seven simulations were realized, the results of which suggest that simplified models can be used to calculate transient heat transfer, but models with inertia are optimal to capture all effects.

The first part of this chapter presents a state of the art on TBs: definition, types and influence on energy consumption and indoor comfort. The second part discusses existing standards used in building industry introducing theoretical calculation methods (U-value, equivalent wall, 3D dynamic methods). We carried out a numerical study which covers the comparison of these standardized methods with available software. Our literature review highlights that slab on grade thermal bridges are not widely studied, therefore the following section is dedicated to ground TB insulation types available in the literature (interior and exterior insulation: vertical or horizontal). This section enabled understanding of the major impact of the soil thermal conductivity on TB linear thermal transmittance coefficient. Above mentioned technical solutions were finally implemented into THERM software [58] to reduce slab on grade thermal bridges. Analysis of the simulated cases permit to recommend some of the studied solutions in order to reach optimized energy savings. These recommendations for decision making on building retrofitting and for reducing literature gaps close the chapter as conclusions.

3.3. THERMAL BRIDGES: OVERVIEW

3.3.1. Types

There are three types of TBs: geometrical, material, and structure TBs. Geometrical TBs [59] (Figure 3-1 (a)), also called 2D or 3D TBs, define the energy loss between two walls, such as the connection between a slab on grade and an exterior wall. In this case, the structure has no material change; rather, it only has geometrical variation.

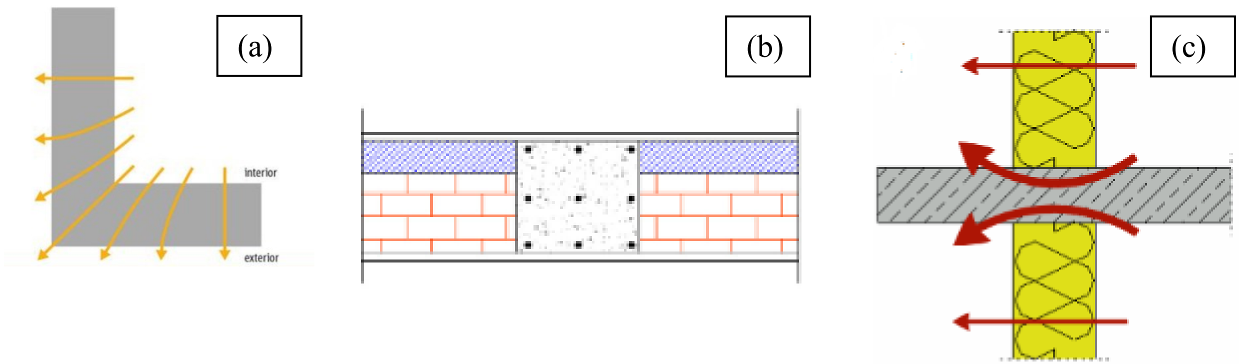

Figure 3-1: TB types: Geometrical TB [60] (a) Material TB [61] (b)Structure TB [40] (c).

Material TBs [40] (Figure 3-1 (b)) refer to the energy loss generated by changes in the wall structure constitution. For example, thermal insulation can cause TBs if the insulation technique used is inadequate. In this case, the geometry does not change but the material does. Structure TBs [40] (Figure 3-1 (c)) are a combination of the two previous types, where building materials and geometry change for the studied surface, e.g., a slab of a cantilevered balcony.

3.3.2. Energy consumption and condensation impact

If a weak point exists at the floor–wall junction, heat flows from the hot zone to the cool one, which cools the room. To maintain a constant temperature, it is necessary to heat the room, which results in energy overconsumption.

In addition, TBs have an effect on surface condensation, which can result in mold growth, thereby reducing indoor-air quality [62]. Condensation can be attributed to two parameters: water-vapor absolute humidity (grams of water per kilogram of dry air) and temperature. Basically, the higher the temperature, the more water vapor retained in the air. Warm air that passes by cold surfaces (weak points, i.e., TBs) is cooled [63], and, therefore, the vapor in the warm air condenses on the cold surface. Table 3-1 sum up several studies and approaches to consider thermal bridges effect on building energy consumption and condensation risk.

Table 3-1: Effect of TBs on energy consumption and condensation risk.

	Approach	**Effect of TB on energy consumption and condensation risk**
Evola et al. [48]	Numerical	Energy heating demands can be reduced between 17% and 25% by reducing the TB effect (depending on the type of houses) under Mediterranean climate.
Building envelope thermal bridging guide [64]	Numerical (U-value method)	Building energy consumption can be decreased by 14% due to reducing the TB effect

Theodosiou et al. [65]	Numerical (TRNSYS 16)	The heating energy demand increases by 30% for the studied building compared with the case where no-TB effects are considered
Krus et al. [66]	(WUFI Bio)	The surface temperature of the interior decreases below the dew point, causing condensation risk; this will affect indoor conditions and comfort
Ilomets et al. [67]	Experimental	Measurements were conducted using a thermal camera (infrared); it was found that the moisture condensation risk is 51% for concrete buildings and 50% for wooden and brick ones (Estonia climate) for external wall and window junctions
Fantucci et al. [68]	Numerical (Delphin 5.8.3)	To reduce mold growth and condensation, an insulating coat should be placed on the interior side of vertical walls;

		this can decrease the risk of mold growth, which improves indoor-air quality; however, verification is required before installation to avoid interstitial condensation risks

From Table 3-1, it is evident that energy consumption increases due to TBs, and it can be affected by climate conditions, building envelope, and TB type.

Also, condensation is responsible for 40% of aesthetic problems and wall damages [69]. It can also affect occupants' comfort due to the associated low air quality (Table 3-1). Condensation risk can be reduced by introducing interior-wall insulation (Fantucci et al. [68]), which decreases mold-growth risk and thus improves indoor-air quality. This technique requires occupant acceptance to reduce interior space because considerable area will be removed from living area and people will have to pay expensive bills to insulate from the inside. Hence, exterior insulation is more appropriate when possible [70].

Heat flux is dependent on material thermal properties, and the surface area varies with geometry. It is important to accurately predict TBs [71]. Therefore, many norms and standard were created to determine and organize methods of their calculation.

3.4. TB STANDARDS

The treatment of TBs is dependent on climate in the area. Accordingly, many countries have adopted standardization. Table 3-2 represents different standards in the European Union and North America.

Table 3-2: Different TB standards.

	EN ISO 10211 [38]	**EN ISO 13370** [72]	**EN ISO 13789** [73]	**EN ISO 6946** [74]	**EN ISO 14683** [75]	**NECB** [76]	**ANSI/ASHRAE/IES Standard 90.1** [77]
Calculates linear and point TBs (steady state)	x						
Describes calculation method of heat transmission			x	x			
Describes calculation method of thermal resistance				x			
Surface resistance (wind dependent)				x			
Catalog of TBs (2D steady state)					x		
Heat transfer of building in contact with ground	x	x		x	x		
Heat transfer of building component (walls/roofs)	x			x	x		

Heat transfer of building component (windows/doors)	x				x		
Provides solutions without any heat flow or temperature distribution calculations						x	x
Provides U-values for different building envelope components with metal studs and wooden frames							x

It should be mentioned that EN ISO 10211 refers to EN ISO 13370, 13789, and 6946 to calculate thermal coefficients (e.g., calculation methods for ground conductance). This standard is a TB reference for most national building standards in the European Union [78].

ISO standards are mainly used in Europe, NECB standards are used in Canada, and ANSI/ASHRAE/IES standards are used in the US. According to ISO standards, adjacent TBs do not affect each other, and, therefore, no thermal effect will be considered (TB has no influence on other TB). However, for the US and Canada, buildings are constructed with dense conductive framing and high elevations (adjacent TBs can affect each other); therefore, new theoretical descriptions should be considered [79].

3.5. CALCULATION METHODS

Three main methods are used in literature studies and papers to identify TBs. These are based on heat conservation equations and differ in system state (transient/steady state) and thermal properties.

3.5.1. Equivalent U-value method

The U-value approach is based on EN ISO 10211 to calculate TB effects in building components under steady-state conditions. Moreover, two coefficient categories are widely used to describe TBs [80]: linear/2D TBs and point/3D TBs. On the one hand, linear or 2D TBs [81] are characterized by a linear thermal transmittance coefficient (Ψ). Heat loss through a linear TB is calculated by multiplying its coefficient by the TB length. On the other hand, point or 3D TBs [82] are characterized by a point coefficient (χ).

Accordingly, in the U-value approach, for the case of a 2D TB, the linear thermal transmittance coefficient can be calculated as follows [83]:

$$\boldsymbol{\psi}_j = L_{2D} - \sum_{j=1}^{N} U_j\, l_j \tag{3-1}$$

For a 3D TB, the point coefficient can be expressed as follows:

$$\boldsymbol{\chi} = L_{3D} - \sum_{j=1}^{N} U_j\, A_j - \sum_{j=1}^{N} \boldsymbol{\psi}_j\, l_j \tag{3-2}$$

Where L_{2D} and L_{3D} are the thermal coupling coefficients obtained from the 2D and 3D analysis of the modeled element by multiplying the averaged thermal transmittance (U) and the joint length (l_j), U_j is the thermal transmittance coefficient of the envelope element, and A_j is the area where U_j applies. The values of U_j and L_{2D} are calculated using 2D heat transfer software.

Then, the equivalent U value is computed using the following equation:

$$U_{w,new}A_w = \boldsymbol{\psi}.\, l_T + U_wA_w \tag{3-3}$$

Where A_w is the area of the wall, U_w is the thermal conductance of the wall without considering TBs, $U_{w, new}$ is the new wall thermal conductance (with thermal bridges), and l_T is the joint total length between the wall and floor. Thereafter, $U_{w, new}$ is applied for the wall to calculate the energy consumption using simulation software such as EnergyPlus.

3.5.2. Equivalent wall method

In the equivalent wall method, a multilayered wall is designed with the same thermal properties and dynamic behavior as the original wall (with TB). It will simplify the numerical treatment of thermal bridge [84]. This method considers the envelope thermal inertia, and, therefore, additional thermal properties are calculated for each layer. The first step is the determination of adiabatic planes based on EN ISO 10211. Then, three important dimensionless parameters are introduced that represent the energy-storage fraction of the envelope, i.e., the structure factors $\xi_{in.ex}$, $\xi_{in,in}$, and $\xi_{ex,ex}$ [85] [86]:

$$\xi_{in,ex} = \int \rho C_p (1 - T_n) dV \quad \text{3-4}$$

$$\xi_{in.in} = \int \rho C_p (1 - T_n)^2 dV \quad \text{3-5}$$

$$\xi_{ex,ex} = \int \rho C_p T_n^2 dV \quad \text{3-6}$$

where *in* and *ex* represent interior material and exterior material respectively. These three factors satisfy the following relation:

$$\xi_{in,in} + \xi_{ex,ex} + 2\xi_{in,ex} = 1 \quad \text{3-7}$$

where ρ is the density of each element, C_p is the specific heat capacity, T_n is the nodal temperature, and dV is the differential volume. Finally, to determine the thermal properties of each layer, the following equations are used:

$$\xi_{in,in} + \xi_{in,ex} = \frac{1}{RC} \sum_{i=1}^{N} C_{p,i} \left(-\frac{R_{m,i}^2}{3} + \frac{R_{m,i} R}{2} + R_{m,i-ex} \right) \quad \text{3-8}$$

$$\xi_{in,ex} = \frac{1}{R^2 C} \sum_{i=1}^{N} C_{p,i} \left(\frac{R_i}{2} + R_{m,i-in} + R_{m,i-ex} \right) \quad \text{3-9}$$

$$C_{p,total} = \sum_{i=1}^{N} C_{p,i} \quad \text{3-10}$$

$$R_{m,total} = \sum_{i=1}^{N} R_{m,i} \qquad 3\text{-}11$$

where C is the total thermal capacity of the element, R is the total thermal resistance per unit area for the elements with TBs, C_m is the thermal capacity of the m-th layer, R_m is the thermal resistance of the m-th layer, and $R_{i\text{-}m}$ and $R_{m\text{-}o}$ are the inside and outside thermal resistances of the m-th layer, respectively.

3.5.3. Three-dimensional dynamic method

The 3D dynamic method is a transient method (implemented in WUFI Plus and HEAT3 software). It uses 3D objects to define TBs and can be expressed as follows:

$$\rho C_p \frac{\partial T}{\partial t} = \nabla.(\lambda \nabla T) \qquad 3\text{-}12$$

where ρ is the material density, C_p is the material heating capacity, and λ is the material thermal conductivity. The model is coupled with WUFI energy calculations via TB boundary conditions. The importance of this method compared to the U-value and equivalent wall method (paragraph 4.1 and 4.2) is that it combines transient thermal calculation with a complete 3D geometry model of the studied structure.

3.5.4. Method comparison

Martin and Viot [57], [87] studied transient and steady-state methods. They found that the dynamic model (when considering thermal behavior variation in time) is more reliable compared to the permanent one (phase lag and different amplitude variations for internal heat flux). Concerning thermal inertia, [88] compared five 1D methods: structure factor, harmonic, matrix transfer function, identification, and mixed (harmonic + structure factor) methods. The advantage of the mixed method is the combination between dynamic and thermal structure calculations. It is accurate in estimating 2D TBs. Furthermore, [84] compare three cases: without considering TBs, considering TBs without thermal inertia, and considering TBs with thermal inertia (using the equivalent wall method). The results highlight the difference (25%) between the first and second methods (for total energy consumption) and the time delay in heat flux between the second and the third methods.

Baba [89] compares the 3D dynamic, the U-value method, and no-TB methods for a balcony made of lightweight and heavyweight concrete for a typical multi-unit residential building. For the heavy concrete, TBs have a higher impact on heating load (7.6%) compared with the lightweight case (3.2%); a similar aspect is observed for cooling loads (11.4% and 15.6%, respectively). This suggests that increasing the thermal mass (heavy concrete case) increases the dynamic impact of TBs, which means that transient models are suitable in these situations.

Baba [90] [91] uses three methods: U-value method, equivalent wall method, and direct 3D dynamic modeling method. Compared with the 3D method (reference case), the heating and cooling loads (for cold and hot climate) are underestimated by the U-value (8% to 17%) and equivalent wall techniques (3% to 14%), for a low-rise residential building. The equivalent wall method performs better than the U-value method in cold climates for a material with high density and heat capacity. Furthermore, the difference between the 3D dynamic and equivalent wall methods decreases when thermal inertia increases.

Table 3-3: Comparison between the three methods (based on [89]).

Method	**Thermal Inertia**	**Transient calculation**	**Complex geometry**	**Prediction of high insulation level**	**Simulation time**
3D dynamic	Yes	Yes	Yes	Yes	Moderate
Equivalent wall	Yes	Yes	No*	No*	Slow*
Equivalent U-value	No	No	No	No	Fast

* New improvements exist

From Table 3-3, it is evident that the 3D dynamic model should be used in most cases. The equivalent U-value model is appropriate for a material with a low thermal mass. The equivalent wall method is widely recommended to replace the 3D dynamic method due to its simplified correlation and the fact that it considers thermal property variation; however, it is slow for complex cases (complex geometry with a high level of insulation). As such, many researchers have attempted to improve this method: a new modified equivalent wall method was described by [92], [84], and [88] to represent 2D complex geometry as a 1D equivalent wall. This new approach is also based on EN ISO 10211 (similar to the equivalent method used by [90]) and is validated against analytical solutions.

3.6. THERMAL BRIDGES AT GROUND LEVEL AND SOIL PROPERTIES

It is clearly shown that this aspect of TB is tightly discussed in literature with respect to other one that focuses on different types of thermal bridges. Therefore, it is important to describe slab-on-grade TBs. Compared with other TB types, TBs for slab-on-grade buildings are in direct contact with soil, which means that heat losses occur via soil through to the exterior. Therefore, ground thermal properties (e.g., heat capacity, thermal conductivity, etc.) play a role in reducing heat losses. These properties are dependent on soil properties: density, water content, mineralogy, size, and grain arrangement. Several studies have shown that thermal conductivity increases with dry density and water content [10], [11], as does thermal capacity [12] [93]. References [13], [14] showed a proportional relationship between soil moisture content and soil thermal conductivity. Therefore, these properties must be considered when examining ground TBs as they have a direct effect on TB calculations [34], [38], [72].

Soil thermal conductivity (λ_S) is highly dependent on temperature and moisture content [21]. It varies significantly with temperature due to the phase transition during dehydration [94]. Concerning water content, it has a large effect on thermal conductivity, λ_S will increase from a dry soil to saturated one [14].

Therefore, to examine building energy performance, the hygrothermal behavior should be examined with respect to variations in soil temperature and relative humidity (Table 3-4).

Table 3-4: Soil properties affecting ground and building heat loss.

	Approach	**HT or HAMT**	**Soil type**	**Effect on ground and building heat loss**
Deru et al. [14], [35]	Numerical (Fortran 90)	HAMT	Sandy loam and clay	Soil thermal conductivity increases by a factor of 10 with water content
Mendes et al. [95]	Numerical (C++)	HAMT	Sand and sandy silt	Difference of 15% (when considering soil study) in the zone-humidity ratio. Energy consumption is increased due to soil's latent heat
Janssen et al. [21], [96]	Numerical	HAMT	Sand, silt, and clay	Greater amplitude of soil surface temperature

Doughty et al. [97]	Experimental and numerical (Fortran 90)	HAMT	Sand and silty clay	Soil conductivity is proportional to water content and ground thermal heat loss
Sinka et al. [98]	Numerical (WUFI, DELPHIN, and GAHMT)	Review article	-	It is important to include moisture transport via soil (moisture safety design to prevent mold growth)
Bahnfleth [34]	Numerical (Fortran 90)	HT	Different soil thermal properties (thermal parameter variation)	It is incorrect to calculate ground heat loss without considering soil properties (12% change of annual ground heat loss when diffusivity changed by factor of two)

Note. HT denotes heat transfer and HAMT denotes heat, air, and moisture transfer.

Table 3-4 highlights the importance of taking into account the variation of soil thermal properties when calculating ground heat losses [98]. It leads to more important changes in ground heat loss than variation in climate conditions [34]. Main impact on these properties is due to moisture transfer in soils which increases water content and thermal conductivity resulting an increase in ground heat loss [14], [97]. Neglecting soil effect can cause a high error in ground heat transfer calculations (up to 50%) [34].

It is important to recall that to study heat and moisture transfer in soil, reliable experimental measurements are needed covering several types of soil. Literature review shows a lack of experimental data in this field.

To highlight the effect of soil properties on slab TBs, a simulation test shown in Figure 3-2 (a) was conducted in THERM software. Figure 3-2 (b) represents the linear thermal transmittance coefficient as a function of soil thermal conductivity. The equation governing this variation (based on this curve) can be expressed as follows:

$$\psi = -0.15\lambda_s + 1 \qquad \text{3-13}$$

where λ_s is the soil thermal conductivity and ψ is the linear thermal transmittance coefficient (of ground TBs). From Figure 3-2, it is evident that, if Λ_S is increased from 0.5 to 3 W/m.K, the linear thermal transmittance coefficient decreases from 0.97 to 0.61 W/m.K, equivalent to reduction of 37%. Based on Table 3-4, it is shown that soil thermal properties should be considered when calculating TBs. For example, soil thermal conductivity can change by factor of 10 with respect to water content. Moreover, it is directly related to thermal calculations as well as slab and ground heat loss (equation 3-13).

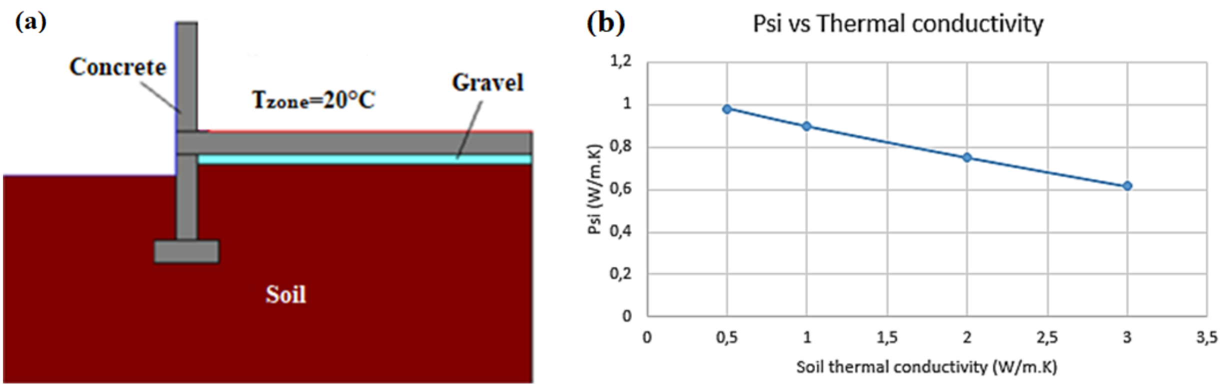

Figure 3-2: (a) No-insulation case and (b) linear thermal transmittance coefficient as a function of soil thermal conductivity.

Therefore, it is vital to consider soil types and properties when calculating ground TBs. Studies are lacking with respect to the occurrence of TBs for slab-on-grade buildings, as shown in Table 3-5.

Table 3-5: Different ground-TB studies.

	Approach	**Material**	**Insulation**	**Effect of TB**
Wróbel et al [99]	Experimental (thermographic measurements)	Ceramic brick	Vertical external but not extended to the foundation	Temperature difference and heat loss between vertical wall (19°C) and ground floor, especially at corners (14°C)
Ge et al. [100]	Numerical (COMSOL) and simplified approach	Reinforced concrete	Vertical external insulation (extruded polystyrene)	Improving insulation thickness or conductivities does not mean that TBs are reduced; a

				proper insulation strategy may reduce energy loss
Nyberg [101]	Numerical (HEAT2&3)	Simple timber joint on concrete floor with extruded-polystyrene floor insulation, sandwich wall on lightweight concrete, and low-conductivity concrete and extruded-polystyrene wall–floor junction	Internal extruded-polystyrene floor insulation and an external vertical one	Proper combination between slab material and insulation material can reduce the TB effect (Ψ = 0.05 W/m.K)
Tiziana et al.[102]	Numerical (THERM)	Concrete wall–slab construction	Vertical internal insulation	Inapplicability of existing catalogs to determine all wall–slab junction TB; a relationship exists between the linear

				thermal transmittance coefficient and the wall and slab thicknesses: Ψ is inversely proportional to wall thickness and proportional to slab thickness
Brzyski et al. [103]	Numerical (THERM)	Hemp-lime	No	Using hemp as a slab material will decrease the risk of condensation; Also, by increasing floors level with respect to ground, it is possible to reduce the TB effect and improve the thermal properties of the junction
Borelli et al. [104]	Numerical (THERM)	Concrete, wood, and aluminum	Floor-slab insulation (0.029 W/mK)	Validation of THERM software for wall–slab TB

				with respect to the analytical solution
Aguilar et al. [84]	Numerical (ANSYS-MATLAB)	Reinforced concrete (slab) and solid brick (wall)	Floor-slab insulation (extruded polystyrene)	The equivalent wall method can predict the ground-TB effect for simple transient calculations
Grudzińska et al. [105]	Experimental and numerical (THERM)	Hemp-lime	No	Using hemp-lime with s wooden frame will reduce the TB effect (Ψ = 0.035 W/m.K) and condensation risk.
Capozzoli et al. [106]	Numerical (TRISCO)	Concrete	External and internal (0.04 W/m.K; vertical and horizontal)	new correlation to predict the linear thermal transmittance coefficient for different TB cases
Brumă et al. [107]	Numerical (RENESTL)	Reinforced concrete	-	Significant difference concerning the TB effect in steady-state and transient

				calculations; (interior heat flow) simplified dynamic model to predict the TB effect
Hopfe et al. [108]	Numerical (THERM and Flixo)	Concrete	Cavity-wall insulation (polystyrene)	Importance of cavity insulation (U-value reduction to 0.15 W/m^2.K for slab and wall)
Staszczuk et al. [109], [110]	Numerical (WUFI 3D)	Concrete	Extruded polystyrene	Difference between transient and steady-state calculations can reach an error of 30% (uninsulated slab); the heating mode affects the difference between transient and steady-state methods (higher deviation for

				reduced heating mode)

In Table 5 authors demonstrated that considering slab on grade thermal bridges is necessary to achieve acceptable accuracy in building energy simulations. A comparison between a building with and without ground TB shows that the interior slab surface heat flow density has lower values for no TB case [107]. The difference between the dynamic and steady state approaches was studied in [109], [110] and [107] , results show an increase of 30% in heating demand for uninsulated slab on grade building. It is due to the fact that insulation will lower variations at boundaries (due to climate conditions) in comparison to other cases without thermal insulation (1 to 10%). Concerning solution strategies to reduce TB, most of these articles discuss insulation methods. They showed that, depending on building material and insulation position, thermal bridges can be reduced to psi value of 0.05 W/m.K [101]. As mentioned before, insulation of a slab on grade foundation reduces climate condition effects on heat exchange between ground and building and also decreases the difference between 2D and 3D calculation in simulations by lessening the 3D corner heat flow and reducing building geometry influence [110].

Table 3-6: Different software-based methods of calculating ground TBs.

Software	HT or HAMT	T or SS	2D or 3D	R or FF	Validated	F or C	Whole building energy software
WUFI Plus/3D [111]	HAMT	T	2D and 3D	FF	Yes	C	Yes
THERM [58]	HT	SS	2D	FF	Yes	F	No
DELPHIN [112]	HAMT	T	2D	R	Yes	C	No

HEAT2/3 [113], [114]	HT	T	2D and 3D	R	Yes	C	No
AnTherm [115]	HT	SS	3D	R	Yes	C	No
HAMLab [116]	HAMT	T	3D	FF	No	F	Yes
TerMus BRIDGE [117]	HT	SS	2D	FF	Yes	C	No
BISCO [118]	HT	SS	2D	FF	Yes	C	No
TRISCO [118]	HT	SS	2D and 3D	R	Yes	C	No
SOLIDO [118]	HT	SS	2D and 3D	FF	Yes	C	No
BISTRA [118]	HT	T	2D	FF	Yes	C	No
VOLTRA [118]	HT	T	2D and 3D	R	Yes	C	No
KIVA [119]	HT	T	2D	R	Yes	F	Yes
DOMUS [120]	HAMT	T	2D	R	No	C	Yes

These studies present also some limitations. Most of articles did not discuss soil's effect on thermal bridges. They focus on TB calculation with respect to material and climate boundary conditions [105], [109], [110], while the coupled heat and moisture effect is not considered. Most of articles calculates slab on grade TB effect on foundation level, however this effect is not widely discussed within whole building calculation. In addition, it was shown in Table 3-5 that the polystyrene was used in most of studies to reduce TB, however new insulation materials (ex: polyurethane) could have better performance. Nevertheless, the economic effect should be considered when choosing these materials to renovate slab on grade existing building.

3.6.1. Software-based calculation of ground thermal bridges

Many tools exist to determine TBs [121] with various capabilities: heat transfer only, or heat, air, and moisture transfer; transient or steady state; 2D or 3D; rectangular geometry or free form; validated according to EN ISO 10211 or not; and free or commercial. Table 3-6 summarizes the software that can be used to calculate the TBs (inspired from [122]).

Note. T denotes transient, SS denotes steady state, R denotes rectangular geometry, FF denotes free form, F denotes free software, and C denotes commercial software.

The most efficient software is WUFI Plus, wherein the TB effect is considered for the whole building. The only disadvantages here is that WUFI is not free. Therefore, it is difficult to couple other programs with WUFI and to access the model source codes.

Concerning other programs, KIVA is also an efficient model to predict ground heat losses (2D transient calculations [119]). KIVA uses some correlations to replace different 3D aspect (corner): It uses the rounded rectangle method [123] to predict heat transfer for 2D rectangular shapes. However, the influence of coupled heat and moisture transfer is not considered. Moreover, KIVA is limited to orthogonal geometries and adjacent multiple zones. However, it is linked to EnergyPlus, which is an important feature with respect to existing software (Table 6).

Heat2&3 [124] use heat equation to deal with TBs, ground heat loss (equation in 2D and 3D). This model includes transient and steady-state calculations, which means it is practical for all types of case studies. The originality of this work is the model applicability for different types of materials, and conditions (dynamic and static). In addition, calculation time is small, and suitable finite difference meshes and conditions are used (e.g., method of subdivision and the successive over-relaxation method for the steady-state case). Despite these advantages, Heat2&3 is not linked to any building energy software with a commercial license.

THERM is more practical than other software with respect to creating 2D geometries with different material properties, which is an important factor in calculating TBs. THERM is widely used in the literature for different geometry types and steady-state conditions. It is also free and uses the U-value method.

AnTherm [125] is a steady-state heat transfer model based on [126]. AnTherm TB equations are based and validated against EN ISO 10211. It can predict vapor diffusion via the TB surface, which means it can determine condensation risk.

HAMLab model [127] includes 2D and 3D geometries, heating, ventilation, and air conditioning systems' description, and TBs. TB models are based on Eq. (3-12). HAMLab is effective in predicting heat, air, and mass transfer in the building envelope. However, the main disadvantage is that TB models are not validated against actual standards.

3.6.2. Insulation solutions

3.6.2.1. Insulation solutions from literature

Interior insulation

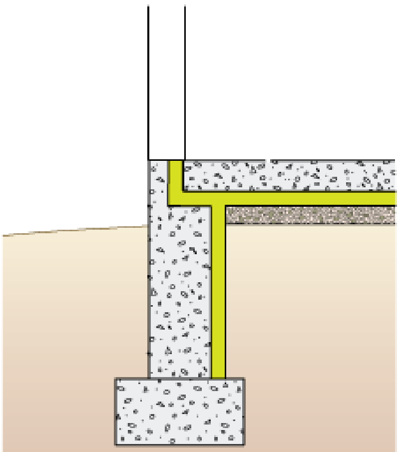

Figure 3-3: Interior insulation.

Internal installation techniques: below slab level or on the foundation wall (interior face) (Figure 3-3). These techniques are widely used in the construction industry [34], [128]–[130] and could reduce heat losses via slab and foundation. However, compared with interior vertical insulation (polystyrene, depth of 1 m, 0.025 m thick), 64% more material is required for the interior horizontal type [34] to have the same efficiency. In addition, during winter, heat losses from the inside to the outside exist mainly at the perimeter, so it is preferable to use interior vertical insulation.

Exterior insulation

Different positions for exterior heat insulation: vertically, horizontally, vertical sharped, trapezoidal insulations and inclined with the foundation wall. These positions are widely discussed in the literature [131], [132]. Exterior insulations can save energy up to 36% per year [46]. Compared with other exterior solutions, e.g., the sharped and trapezoidal ones, insulation volume and excavation cost are reduced.

The exterior solutions are much simpler to install for retrofitting compared with other solutions (interior solutions). For example: installing an insulation under the slab or into the foundation wall interior face is very difficult. Moreover, exterior insulations can increase the slab-surface temperature (near walls) and reduce condensation risk. Also, as the interior one, energy reduction is proportional with vertical insulation depth. Concerning costs, internal insulation is expensive and difficult to install under slabs, whereas external insulation is cheap and easy to install. However, drilling costs are a major obstacle [46].

3.6.3. Case Study

In this section, we study several external insulation types using THERM software: vertical (also called I), horizontal and vertical (also called L), and inclined, sharped, and trapezoidal.

The aim is to calculate the total ground heat transfer, the undisturbed fluxes, and thus the TB coefficient [38]. The heat flux crossing a wall (with homogeneous materials) without considering TBs is an undisturbed heat flow, which can be calculated analytically without numerical tools. These two undisturbed fluxes from the wall and the floor must be determined to deduce the disturbed flux corresponding to the TB. For this, we divide the model in Figure 3-4 (a) into two geometrical parts: wall part only and ground with soil only (Figure 3-4 (b)).

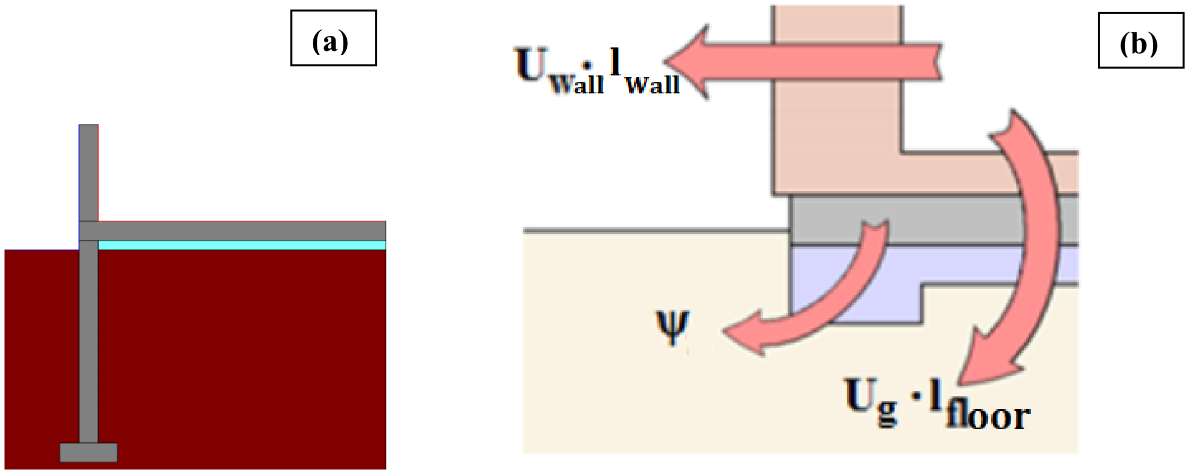

Figure 3-4: (a) Domain studied without insulation, (b) domain with different heat transfer coefficients.

The EN ISO 10211 standard

According to EN ISO 10211, the linear thermal transmittance coefficient can be calculated as follows:

$$\psi_j = L_{2D} - l_{wall}.U_{wall} - 0.5 * b * U_g \qquad 3\text{-}14$$

$$\psi_j = L_{2D} - (l_{wall} + l_{floor}).U_{wall} - (0.5b + e_{wall}).U_g \qquad 3\text{-}15$$

where l_{wall}, l_{floor}, b, and e_{wall} denote the distance from the junction to the horizontal adiabatic plane, the slab depth above the ground, the zone width, and wall thickness (above ground). The difference between the two equations is that Eq. 3-14 calculates the linear thermal transmittance coefficient with respect to interior dimensions (positive Ψ) and Eq. 3-15 with respect to exterior ones (negative Ψ).

Both equations are accurate, but, in the present example, Eq. 3-14 is used to calculate TBs, which is explained below.

Starting from point A (Figure 3-5), which represents the interior horizontal- and vertical-surface junction, the floor length must go to the plane of symmetry (half the floor=0.5b) or 4 m maximum; for example, if the floor width is 10 m, “0.5b” is 5 m but 4m will be considered (choose the smaller of the two values 0.5b and 4).

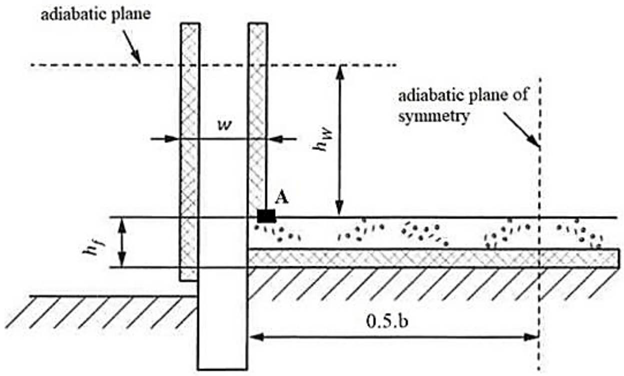

Figure 3-5: Wall–slab junction dimensions (slab on grade) based on EN ISO 10211 [38].

Again, starting from point A, the lower limit of the model (in the ground) must be 2.5 × (b) from the interior horizontal surface or 20 m (choose the smaller of the two values). The left limit of the model must be 2.5 × (b) from the interior vertical surface. As the wall thickness is 300 mm, the wall height must be 1 m (h_w) from point A (h_w is equal to 3.w or 1 m if 3.w < 1). The ground is 400 mm below the level of the slab.

3.6.4. Results

TBs were calculated for different cases: no insulation and exterior insulation with different depths, thicknesses, and heights (Figure 3-6and Figure 3-7). In the following paragraphs, *d*, *e*, x, H, and *z* represent insulation depth, thickness, width, height, and length, respectively. The height from ground to junction (wall-slab junction) is 0.3 m.

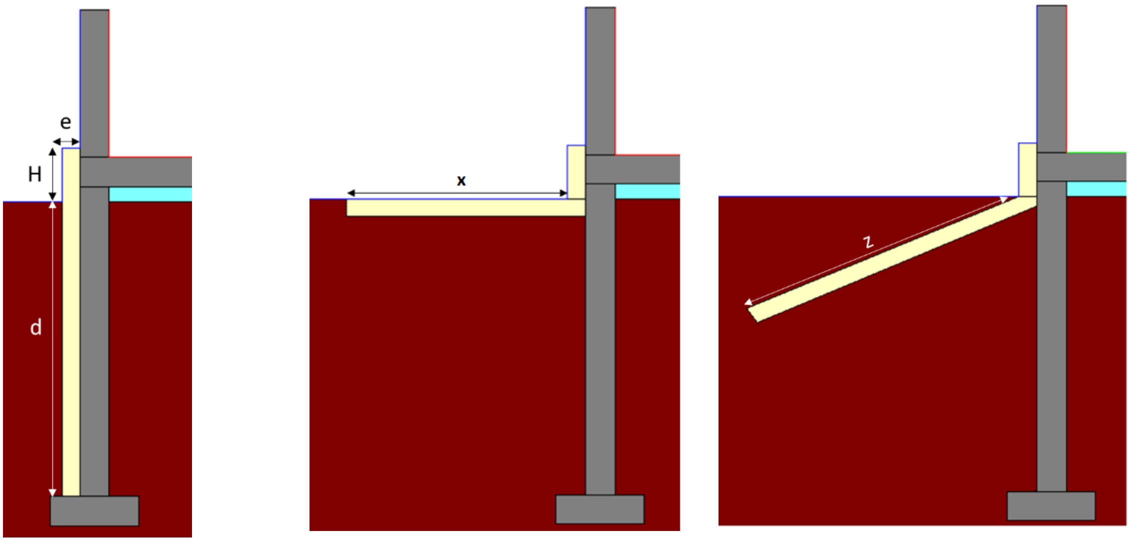

Figure 3-6: Exterior insulation (via foundation): I, L, and inclined.

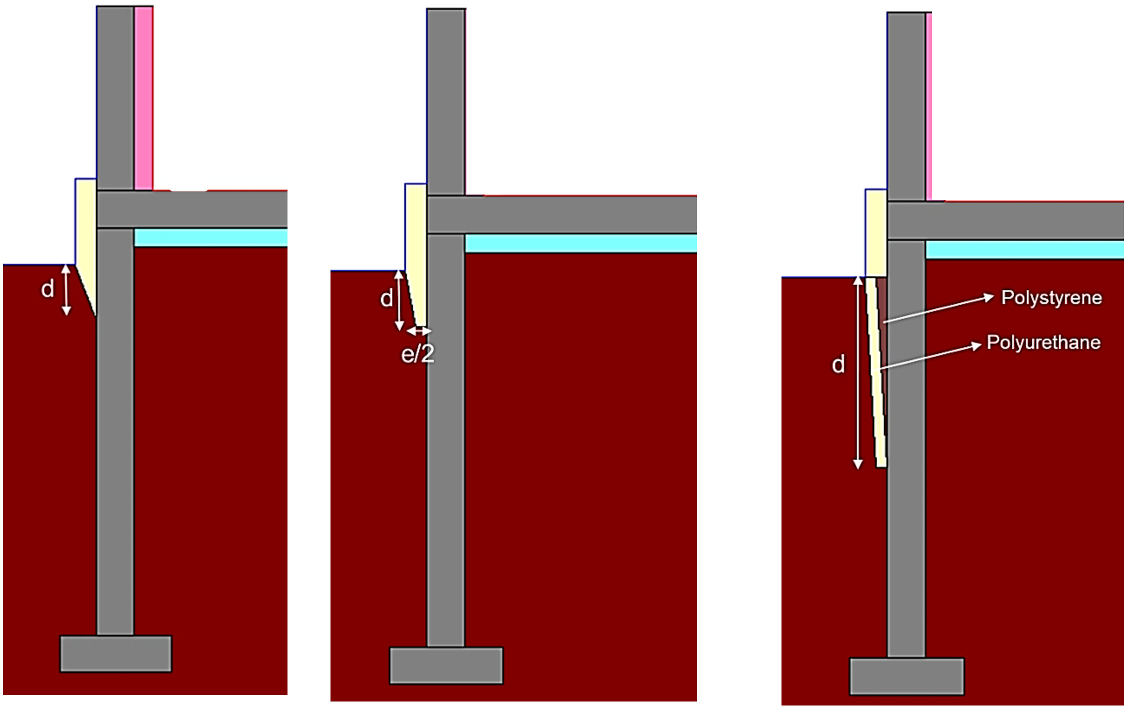

Figure 3-7: Exterior insulation (via foundation): conic, trapezoidal, and two insulations (trapezoidal).

The wall consists of 20-cm thick concrete (2.3 W/m.K). The slab consists of 20 cm of concrete (2.3 W/m.K) and 10 cm of gravel (2 W/m.K) and soil (2 W/m.K). The exterior wall insulation consists of polyurethane (0.04 W/m.K) and polystyrene (0.03 W/m.K).

3.6.4.1. No-insulation case

For the no-insulation case, based on Eq. (3-14), the linear thermal transmittance coefficient is 0.618 W/m.K.

3.6.4.2. Vertical exterior insulation

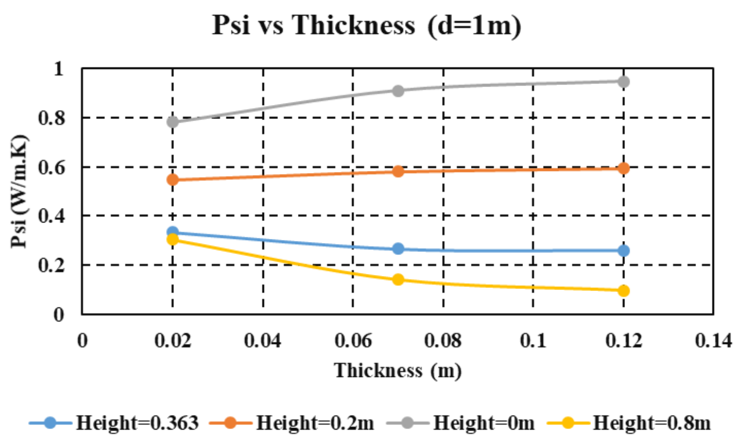

Figure 3-8: Linear thermal transmittance coefficient as a function of thickness for different H values (d = 1 m).

Exterior insulation was studied for two depths: 1 (Figure 3-8) and 0.6 m (Figure 3-9).

For H >0.3m (above junction), by increasing the depth and thickness of the insulation, the linear thermal transmittance coefficient decreases. This is due to the fact that the insulation blocked the heat flux from the interior to the exterior.

For H < 0.3 m, the linear thermal transmittance coefficient is proportional to depth and thickness. This is due to fact that the wall–slab junction (at 0.3 m) is not insulated, and, therefore, the heat flux is concentrated at this area. Figure 3-9 (b) shows the ground conductance with respect to thickness and depth, the results of which are consistent with Figure 3-9 (a). In particular, ground conductance decreases when *d* and *e* increase. Heat loss will path through the junction (for H < 0.3 m).

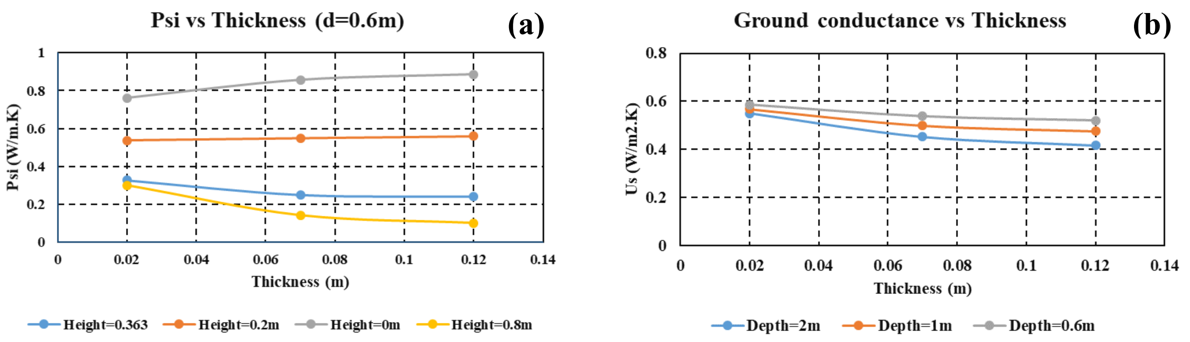

Figure 3-9: Linear thermal transmittance coefficient, (b) ground thermal conductance as a function of insulation thickness for different depths for vertical exterior solution type.

3.6.4.3. Vertical and horizontal exterior insulation

Different insulation thicknesses were studied at three insulation widths x: 0.5, 1, and 1.5 m (Figure 3-10).

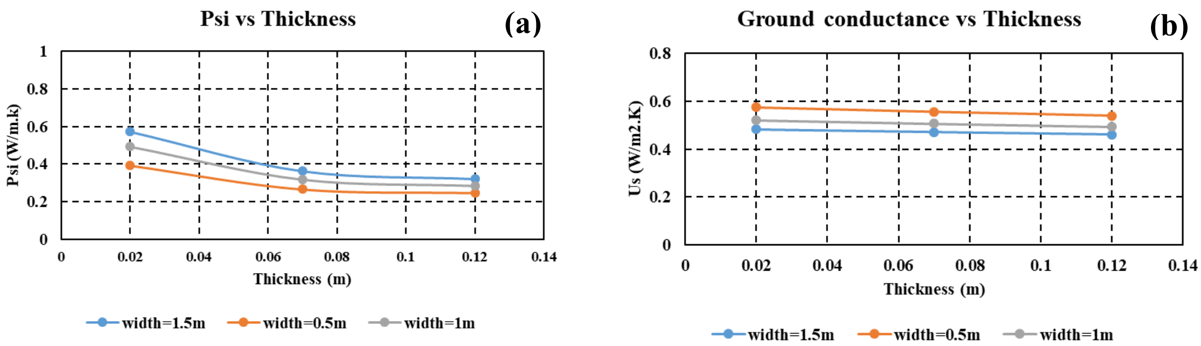

Figure 3-10: Linear thermal transmittance coefficient, (b) ground thermal conductance as a function of insulation thickness for different depths for vertical and horizontal exterior solution type.

For the L type, H was set to be 0.363 m. The linear thermal transmittance coefficient as a function of insulation thickness and length is shown in Figure 3-10 (a). The linear thermal transmittance coefficient decreases when the insulation length and thickness are increased. Similar to the previous case, the wall–slab junction is insulated (H > 0.3 m), and, therefore, the linear thermal transmittance coefficient is inversely proportional to depth and thickness.

3.6.4.4. Exterior inclined

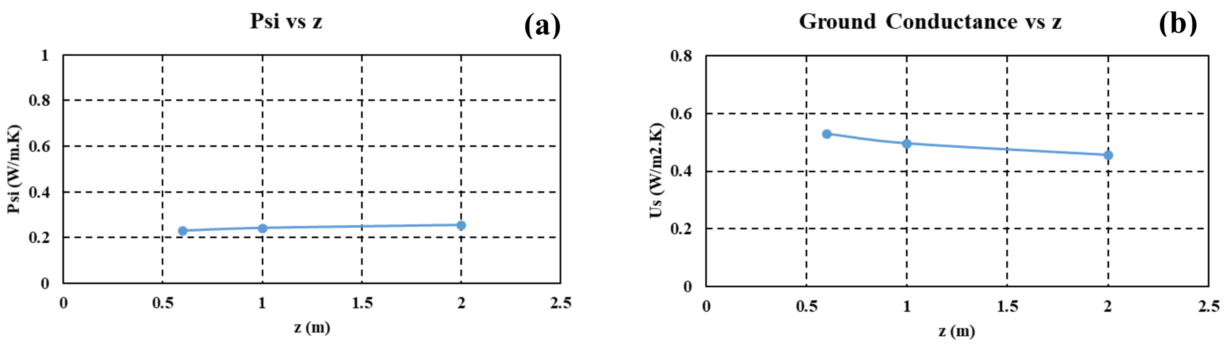

Figure 3-11: Linear thermal transmittance coefficient, (b) ground thermal conductance as a function of thickness for different depths for inclined exterior solution type.

Figure 3-11 shows the case of a diagonal insulation for H = 0.363 m and *e* = 12 cm, from which it is evident that the linear thermal transmittance coefficient increases when the length increases. Similar results are shown in Figure 3-11 (b), where ground conductance decreases if *z* increases (a larger *z* means that the insulation blocks more thermal flux to the soil). Therefore, the thermal loss from the interior to the exterior is concentrated at the slab–wall junction where no insulation exists (Ψ will increase).

3.6.4.5. Exterior conical

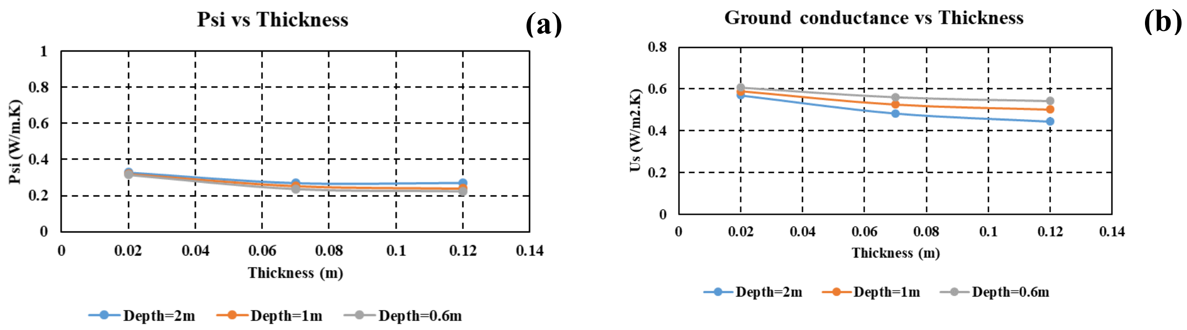

Figure 3-12: Linear thermal transmittance coefficient, (b) ground thermal conductance as a function of thickness for different depths for conical exterior solution type.

Figure 3-12 presents conical insulation for H = 0.363 m, from which it is evident that the linear thermal transmittance coefficient decreases when the thickness and depth both increase.

3.6.4.6. Exterior trapezoidal

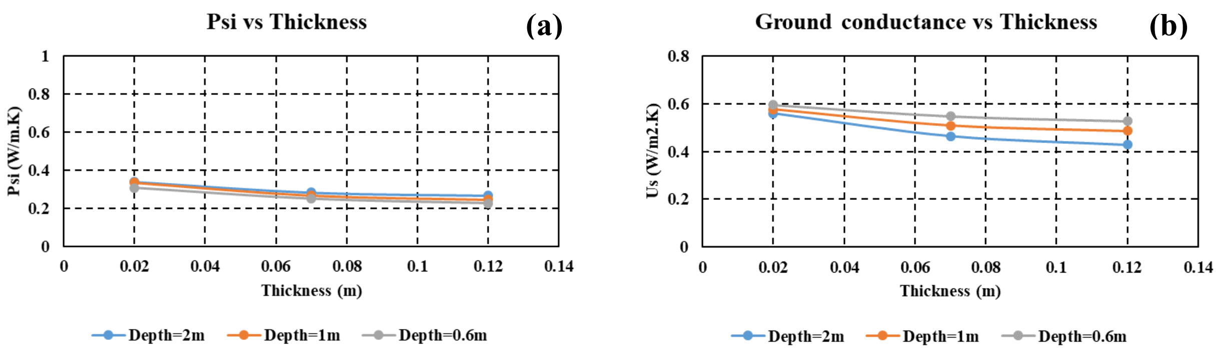

Figure 3-13: (a) Linear thermal transmittance,(b) ground thermal conductance as a function of thickness for different depths for trapezoidal exterior solution type.

Figure 3-13 shows vertical insulation for H = 0.363 m, from which it is evident that the linear thermal transmittance coefficient decreases when thickness and depth both increase.

3.6.4.7. Exterior trapezoidal (double insulation)

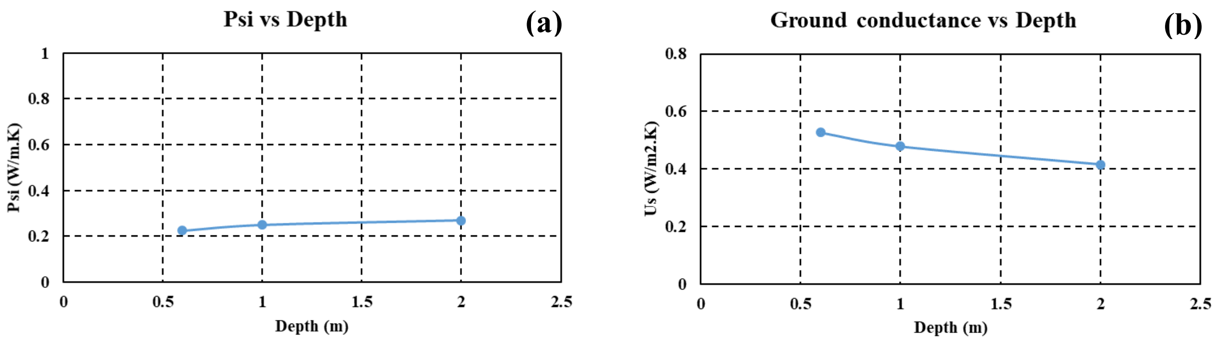

Figure 3-14: Linear thermal transmittance coefficient, (b) ground thermal conductance as a function of thickness for different depths for trapezoidal (double insulation) solution type.

Figure 3-14 shows trapezoidal insulation for H = 0.363 m, from which it is evident that the linear thermal transmittance coefficient increases when depth increases.

In light of these results, it is evident that improving insulation thickness does not necessarily reduce the TB effect. Moreover, heat flux and TB have different behaviors for different conditions:

For H > 0.3 m (or insulation height above the junction), the linear thermal transmittance coefficient is inversely proportional to insulation thickness for constant *d*. And, Ψ is inversely proportional to insulation depth when e is constant.

In contrast, for H < 0.3 m, (or insulation height below the junction), the linear thermal transmittance coefficient has opposing behavior with respect to H > 0.3 m. In particular, it is proportional to *e* when *d* is constant and proportional to *d* when *e* is constant.

An additional case was run where all insulation types are compared to no insulation case (Figure 3-4 (a)) using same insulation volume. The purpose here is to highlight thermal bridges reduction (Psi reduction) for every one of these solutions:

For I, conical, trapezoidal and trapezoidal double insulation H=0.363m, e=12 cm and d=1m.

For L and inclined solutions, H=0.363m, e=12cm, l=1m (L type) and z= 1m (inclined type).

Based on Figure 3-8 to Figure 3-14, the psi can be retrieved and the difference with respect to no insulation case for every insulation type can be calculated. Therefore, TB reduction are 57% (I), 54% (L), 60% (inclined), 61% (conical), 60% (trapezoidal), and 59.6% (trapezoidal double insulation).

Therefore the trapezoidal double insulation type is the best renovation type based on thermal efficiency.

Figure 3-15 (a and b) shows the temperature distribution diagram of the no-insulation case and for the I-type insulation (H = 0.363 m, *e* = 12 cm, and *d* = 0.6 m), respectively, from which it is evident that using suitable external insulation increases slab-surface temperature (mainly at the corner), which reduces condensation risk [133].

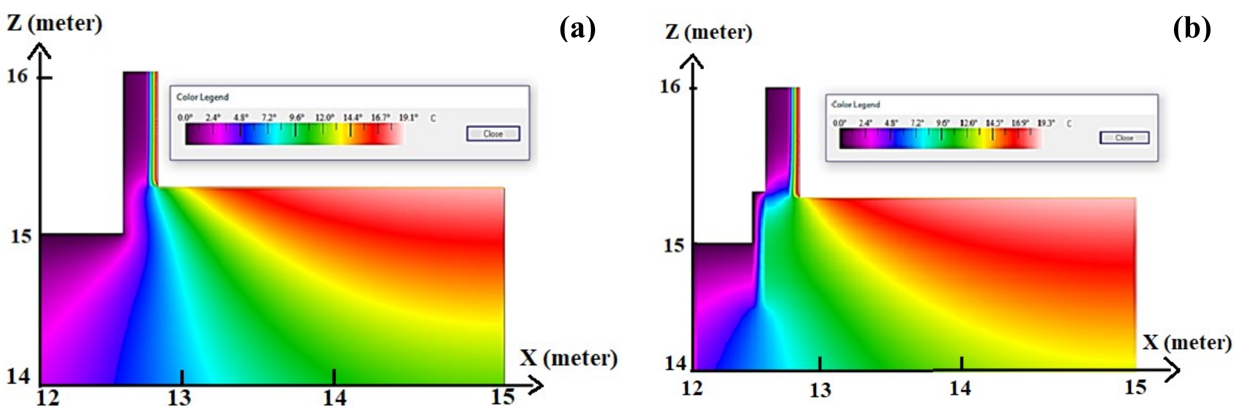

Figure 3-15: Temperature distribution diagram for (a) the no-insulation case, (b) for the insulation case.

The six types of insulation cases discussed herein have good potential to reduce TBs and thus heating consumption. However, for "I geometry", conical, trapezoidal and diagonal types, it is necessary to drill the soil, and, therefore, they cannot be applied for stony one (high drilling costs); moreover, some insulation requires additional protection to avoid moisture-caused degradation. The L type is the most practical, but all types of conditions should be considered in future studies to achieve generalizable results, e.g., climate, soil surface, feasibility with respect to actual and different cases (sidewalks around building), etc.

3.7. CONCLUSION

This study presents state-of-the-art research on thermal bridges focusing on slab on grade TB and highlights the importance of ground TBs for slab-on-grade house. The main results are outlined below:

- Different standards exist to describe TB calculation methods in accordance with countries' or regions' legislation framework. The ANSI/ASHRAE/IES standards are used in the United State of America, the NECB norms are used in Canada, and finally the ISO norms are mainly used in Europe.
- The main difference between these norms consist in taking into consideration by the American standard the interaction between adjacent TB, which is ignored by the European one.
- Several models exist to calculate TBs, in literature three main methods are widely used: 3D dynamic method, the U-value method, and the equivalent wall method. The 3D dynamic method can model the TB effect in all cases, the U-value method is suited for steady-state conditions with low-thermal-mass materials, and the equivalent wall method is recommended for transient state and simple geometries.
- Concerning ground thermal properties, the dependency of soil thermal conductivity on water content must be considered as well as its effects on ground thermal heat loss. As expected, with water content increase, thermal conductivity will increase leading to a growth in ground heat loss.
- In particular, the linear thermal transmittance coefficient is inversely proportional to soil thermal conductivity. Therefore, if soil thermal conductivity is decreased, soil is considered as a thermal insulation: ψ (ground TB) will increase. Neglecting soil effect can cause an important error (up to 50%) in slab on grade heat loss calculation during energy simulations.
- To reduce ground TBs and heat loss, a variety of insulation solutions are available for existing building: interior (vertical or horizontal) and exterior (vertical, horizontal/vertical, inclined, conical, trapezoidal, two insulations (trapezoidal)). Exterior insulation is strongly recommended because it is more practical than interior and can effectively reduce the TB effect (from 54% to 61%).

- Different exterior insulation techniques were examined thermally under different conditions. Improving insulation thickness and depth does not necessarily reduce the TB effect. It is related also to insulation height H (whether the junction is insulated or not). For example, for the I type H=0 m (Junction is not insulated): Psi (TB) is reduced for smaller depth (0.6m) and thickness (2 cm).
- Insulation is an important factor in thermal bridges simulation. Slab on grade insulation will reduce boundary condition impact on ground heat loss. It will decrease the difference between 2D and 3D calculation (3D corner flow and building geometry influence).
- The economical and feasibility aspects of retrofitting solutions should be considered. For example, for some types (I, conical, and trapezoidal) it is necessary to drill into the soil. Therefore, to choose the optimal solution, the insulation cost (drill), thermal efficiency (reducing TB effect), and feasibility (soil type) should be studied. In all types studied herein, the L type is optimal as it results in a 54% reduction in the TB effect; moreover, drilling is not necessary, and it can be applied on soil top edges.

Therefore, to fill the research gaps in this domain, many recommendations are suggested for future work:

  - Reliable experimental data must be obtained to further validate the results (e.g., ground temperature distribution or soil water content).
  - New insulation solutions should be proposed to reduce foundation thermal loss.
  - Soil type, feasibility, and costs study when choosing renovation solutions should be considered.
  - Slab on grade thermal bridges effect is not widely discussed with respect to whole building simulation. It is important to include its impact in future work.

- Finally, TB hygrothermal analysis is still a challenge due to following difficulties: moisture-dependent soil properties (conductivity) and computer run time. So, it is important to study hydrothermal effect of thermal bridges.

Chapter 3 studied two dimensional thermal bridges at grounds level. Therefore, Chapter 4 will improve this study by presenting a three-dimensional one. Next chapter will start by highlighting thermal bridges importance at whole building level and calculate 3D temperatures and heat fluxes in soil and slab level.

CHAPTER 4. NUMERICAL STUDIES OF GROUND THREE-DIMENSIONAL HEAT EXCHANGES

4.1. RÉSUMÉ EN FRANÇAIS:

Dans ce chapitre, le comportement du PT au niveau du sol et à l'échelle du bâtiment est étudié. Les conductivités thermiques, les conditions aux limites du sol et les solutions de rénovation sont considérées en utilisant un aspect tridimensionnel. De plus, une partie de cette étude concerne le transfert de chaleur et d'humidité dans le sol en utilisant deux matériaux de la dalle (béton et béton de chanvre).

Ce chapitre présente une analyse des transferts thermiques d'un bâtiment français sur terre-plein des années 1950. Les simulations sont effectuées avec le logiciel WUFI Plus qui utilise le modèle de Künzel pour prédire le transfert couplé de chaleur et d'humidité en 1D et peut calculer les ponts thermiques grâce aux "objets 3D" (transfert de chaleur en 3D).

Les résultats montrent que :

- Les déperditions de chaleur au niveau du sol augmentent entre 30 et 50 % lorsqu'on considère les PT pendant l'hiver entraînant une augmentation de 20% des consommations énergétiques par rapport à un cas sans ponts thermiques au niveau de la dalle. Dans ce cas, les échanges thermiques avec le sol vont augmenter le chauffage du bâtiment en hiver, et elles ont tendance à réduire son énergie de refroidissement en été.
- L'influence des conditions aux limites (CL) au niveau du sol augmente si le rapport surface/périmètre (dalle) augmente. De plus, les propriétés thermiques (conductivité thermique du sol) peuvent étendre l'influence des CL sur les résultats (pour des conductivités thermiques les plus élevées). A partir d'une profondeur du sol supérieure à 12 m, l'influence des CL est

négligeable et le problème est équivalent à une condition aux limites de type adiabatique (comme suggéré par la norme EN 10211).

- La consommation de chauffage est réduite de 3,1% lorsque le coefficient d'albédo passe de 1 à 0,15 alors que la consommation liée au refroidissement augmente légèrement.
- L'augmentation de la conductivité thermique du sol affecte les consommations énergétiques totales du bâtiment. Elles passent de 24421 à 25500 kWh (1079 kWh), ce qui est équivalent à 4,2% des besoins énergétiques annuels.
- La solution isolation verticale au niveau de la face extérieure des murs de soubassement peut diminuer les consommations totales d'énergie. Pour des isolations de 0,2 m et 0,5 m au-dessus de la surface du sol, les consommations d'énergie sont réduites de 3,5 % et 8,5 % par rapport au cas sans isolation.
- Le béton de chanvre réduit les pertes thermiques du sol de 30% et, par conséquent, les consommations annuelles d'énergie de 6,7% par rapport à une dalle en béton.

In this chapter, ground TB behavior at the building scale is studied. Soil thermal conductivities, ground boundary conditions and renovation solutions are considered using a three-dimensional aspect. In addition, a part of this study concerns ground heat and moisture transfer with two slabs materials (concrete and hempcrete).

4.2. INTRODUCTION:

An essential part of ground floored houses' heat losses is at slab level (Figure 4-1): 15% to 45% of annual heating load [134]. They are related to the constructive mode. Two constructive modes are widely used: floor on crawl space and floor on grade. The first is widely spread and well documented compared to the second one, which is primarily used in France. To overcome these losses, the ground is mainly subjected to continuous insulation under slab. Other solutions, such as horizontal and vertical floor periphery insulation, can be interesting for ground renovation since they take advantage of the inertia of the soil and limit summer overheating [34].

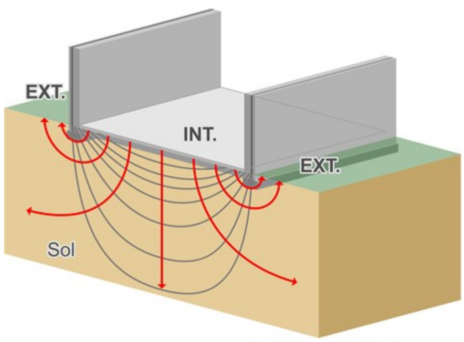

Figure 4-1: Heat loss at ground's level [135]

Modelling heat and moisture transfer through slab and soil in residential buildings is made possible with WUFI Plus. However, the desired platform will not consider thermal bridges at the slabs level. The 3D model (in WUFI) is used to calculate three dimensional heat transfer and consider TB behavior. At ground level, TB is expected along the perimeter between the external wall and slab interface. Therefore, the construction elements near the perimeter, which lead to thermal bridges, need to be described and defined (geometry).

Therefore, this chapter will present an extended study on ground heat loss calculation and energy consumption. A detailed three-dimensional heat transfer study is done using WUFI Plus. The purpose is to explain the effect of soil thermal properties, exterior thermal insulation, ground boundary conditions, insulation solutions, and seasonal variation on building calculations. In the same context, ground heat and moisture transfer calculations will be included in this work.

4.3. CASE STUDY

This paragraph shows a heat transfer analysis through a case study corresponding to a French building from the 1950th (Figure 4-2). The house disposes of a kitchen, a living room, two bedrooms, a toilet and loft space. For dynamic thermal simulations, we represent this house by two thermal zones of 8mx10mx3m:

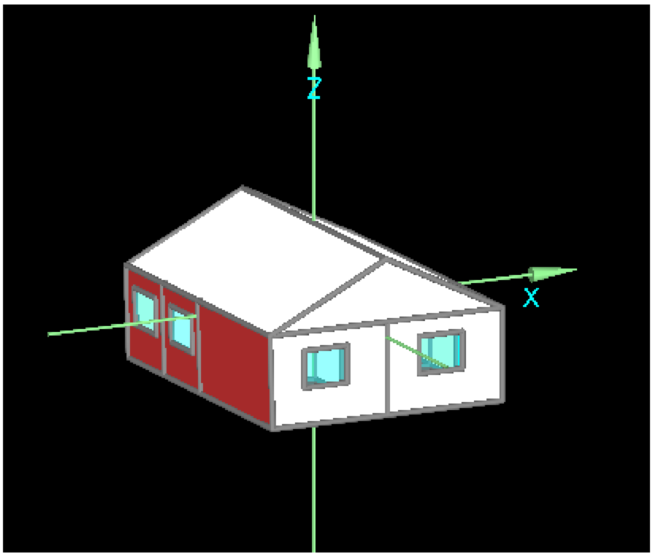

Figure 4-2: Slab on grade building.

Slab on grade zone and loft zone. Exterior wall composition from outside to inside is described in Table 4-1 (material properties are found in WUFI's library):

Table 4-1: Building construction components.

	Material layers (From outside to inside)	Thermal Conductivity (W/m.K)	Thickness (cm)
Exterior wall	Exterior plaster	0.87	1.5
	Concrete block	0.9	20
	Plaster brick	0.13	4
	Air layer	0.28	5
	Interior plaster	0.2	1
Interior wall	Interior plaster	0.2	1
	Plaster brick	0.13	4
	Interior plaster	0.2	1
Intermediate slab	Interior plaster	0.2	1
	Hardwood	0.16	5
Roof	Ceramic tile	2.2	1.5
	Wooden frame	0.16	2
Slab	Gravel	1.4	5
	Concrete	1.6	25
Foundation	Concrete	1.6	32
Windows	single glazed clear	0.9	0.6
Doors	Wood	0.16	5

The foundation depth is 0.6 m. Concerning external conditions, they are represented by the climate of Lyon city. All schedules are imported from WUFI's library for individual buildings case. Clay soil with 1.28 W/m.K thermal conductivity and building materials properties in Table 4-1 are set at 50% relative humidity. Ground upper surface heat transfer coefficients [96] [136] are presented in Table 4-2.

Table 4-2: Ground heat transfer coefficients.

	Radiative-Convective (RC) Convective (C) Coefficient ($W/m^2.K$)	**Short wave radiation (albedo) (-)**	**Long wave radiation (emissivity) (-)**
Ground in contact with exterior conditions	25-C	1	0.9
Ground in contact with interior conditions	8-RC	-	-

The internal convective condition is shown in Figure 4-3; it describes the convective heat being given off by two persons (and some electric equipment) in a zone.

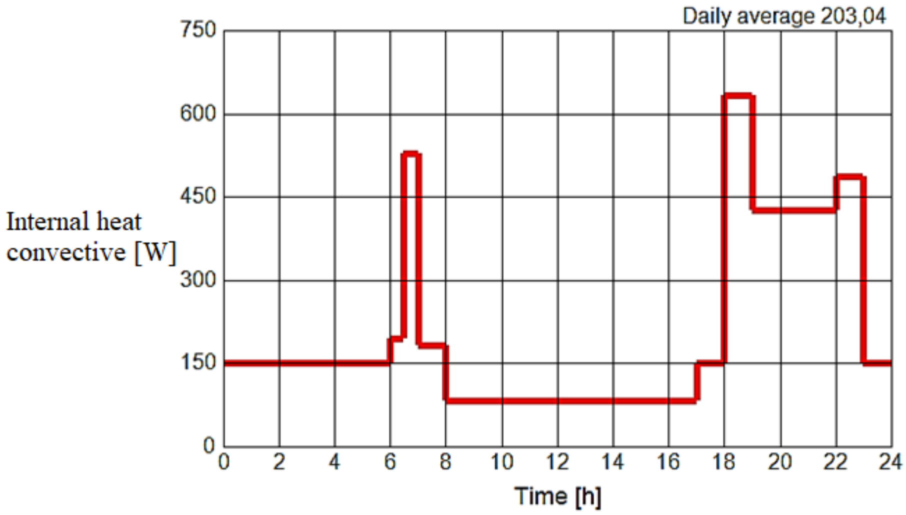

Figure 4-3: Internal heat convective schedule

The lighting schedule in this building is presented in Figure 4-4:

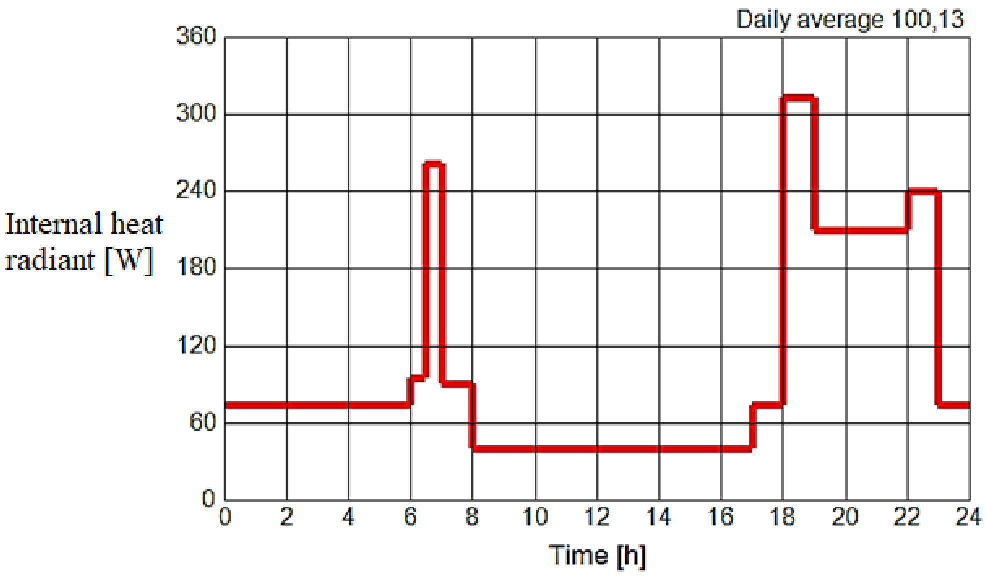

Figure 4-4: Internal heat radiant schedule.

And finally, the internal moisture production is as following (Figure 4-5):

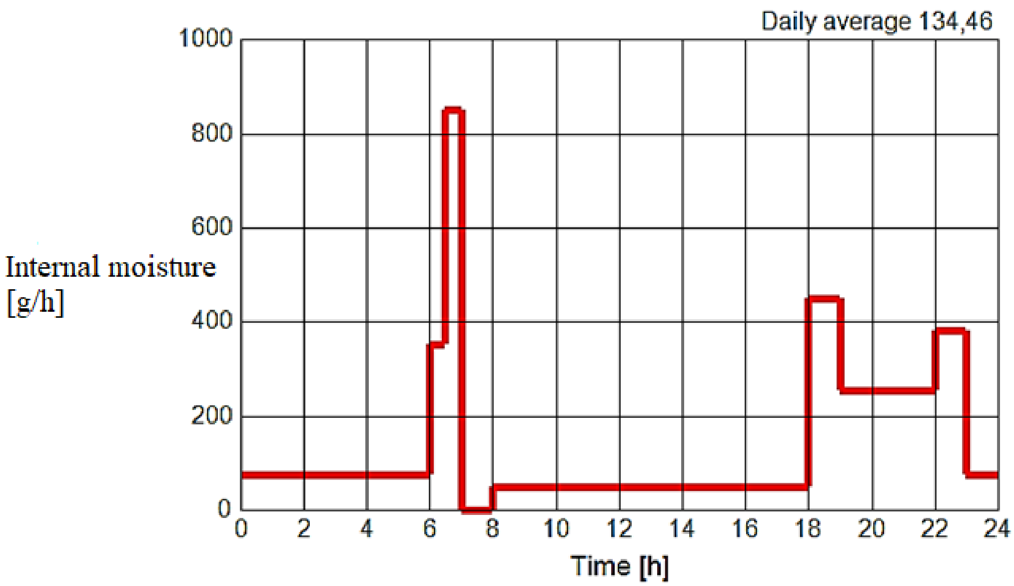

Figure 4-5: Internal moisture schedule.

The building loads are maximum from 06:00 a.m. to 07:00 a.m. and from 18:00 until 23:00. Internal gains are maximum during these periods due to different activities like cooking, showering, washing, and watching tv.

Table 4-3: Heating, cooling setpoint and ventilation rate.

Hour	**Heating set point**	**Cooling set point**	**Mechanical Ventilation**
	°C	**°C**	**1/h**
0	16	26	0.3
6	19	28	0.5
18	16	26	0.3

Also, the heating and cooling set point and ventilation flow rate are represented in Table 4-3[137] [143]. The infiltration flow rate is 0.6 ACH. The simulation run period is one year. Finally, the calculation was initialized for two years with 12°C as initial temperature (Average soil temperature from Lyon climate file) .

4.3.1. Methodology

4.3.1.1. Software and model used for calculations: WUFI Plus

WUFI Plus [111] is a whole building Heat, Air and Moisture transfer calculation software. It was developed to simulate the energy consumption of buildings under different climate conditions by considering coupled heat and moisture transfer. WUFI uses Künzel's model (Künzel 1995). It provides the possibility to predict 1D coupled heat and moisture transfer and can calculate 3D thermal bridges by the "3D objects". It uses the finite volume method to calculate 3D thermal bridges based on the thermodynamic law of energy conservation.

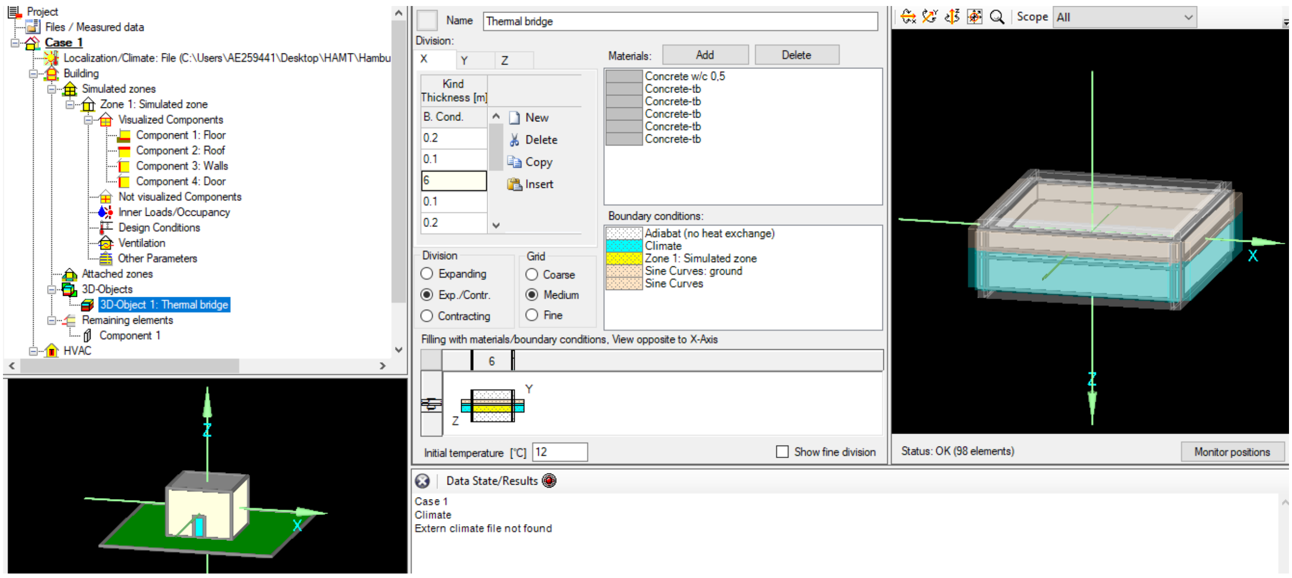

Figure 4-6: 3D object interface in WUFI Plus software.

Using the 3D heat transfer object in WUFI Plus, the first step is to define the TB geometry. This can be done by providing the system's x, y and z coordinates. The second step is to enter the materials' thermal and hydric properties (from WUFI library) for each geometric part. Finally, the boundary conditions for each surface, such as internal, external, and ground, should be defined. All these steps are summarized in Figure 4-6.

The soil deep ground is at 12 m with an adiabatic boundary condition. Moreover, the far-field boundary (15 m) is also adiabatic. These boundaries and depths are considered based on the European norm 10211 and literature (chapter 3) and their effect is discussed in section 4.5.

4.4. RESULTS AND ANALYSIS:

4.4.1.1. Ground thermal effect on whole building calculations

Thermal bridges effect:

The first purpose is to calculate the ground thermal bridges and then highlight the impact of soil and ground thermal heat loss on the whole building calculations. First, the 3D soil with and without TB was created (Figure 4-7 and Figure 4-9).

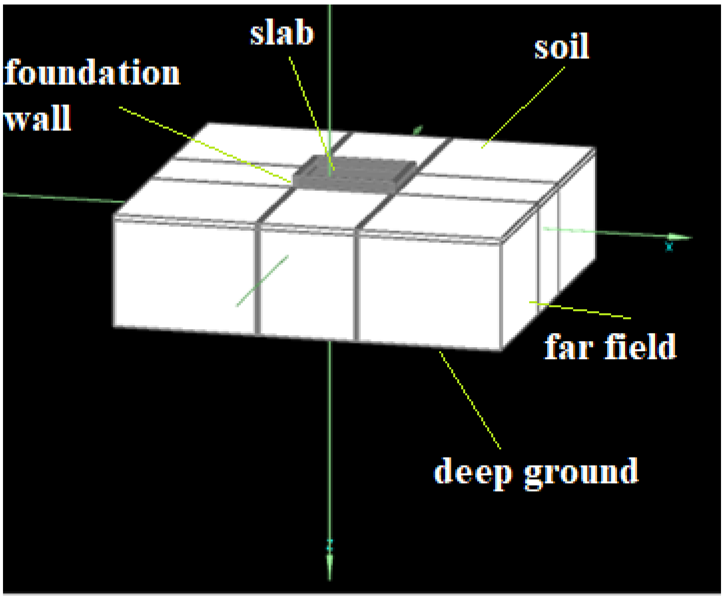

Figure 4-7: 3D soil, slab and foundation model.

Then, these cases are compared: the first one (Figure 4-7) represents a case with the 3D slab soil and foundation walls model (Figure 4-8).

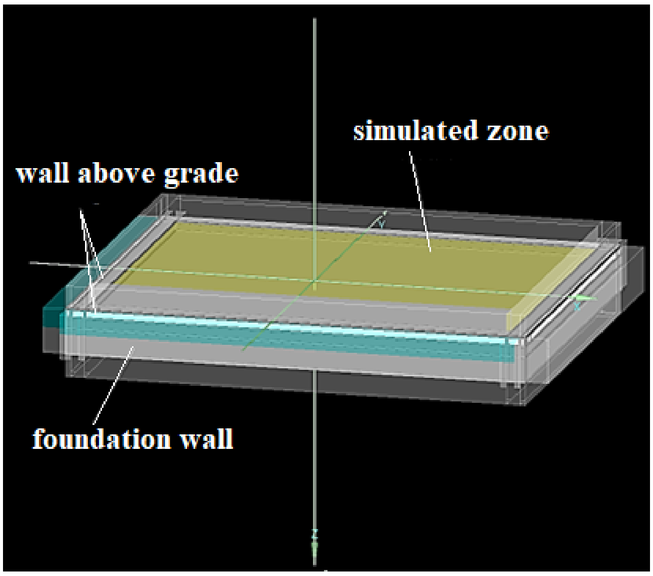

Figure 4-8: Foundation and slab model.

However, the other case (Figure 4-9) is represented by soil and slab layer: without any representation of slab-wall junction.

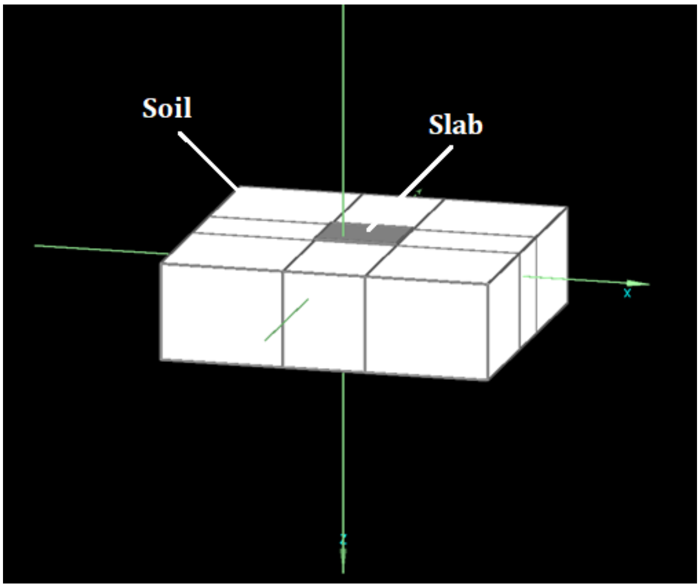

Figure 4-9: 3D soil and slab model.

The first results describe the difference between the two cases. A case without thermal bridges will underestimate the annual energy consumption by 20 %: 25500 kWh and 20619 kWh (Figure 4-10).

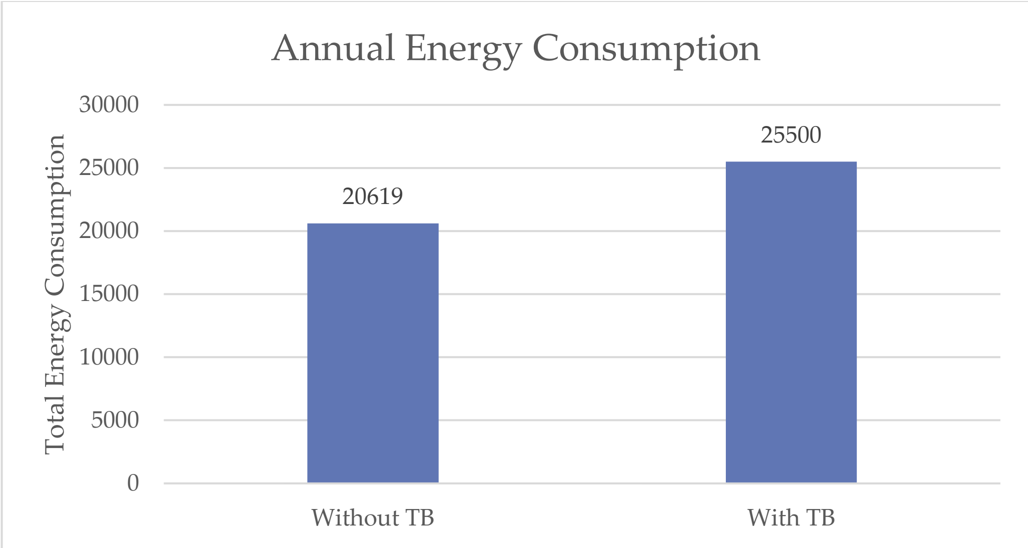

Figure 4-10: Annual energy consumption.

Figure 4-11 and Figure 4-12 show the exterior air temperature for the winter period between 15 and 22 February 2021 with the lowest exterior temperature, and the summer period between 1 and 8 July 2021 with the highest exterior temperature.

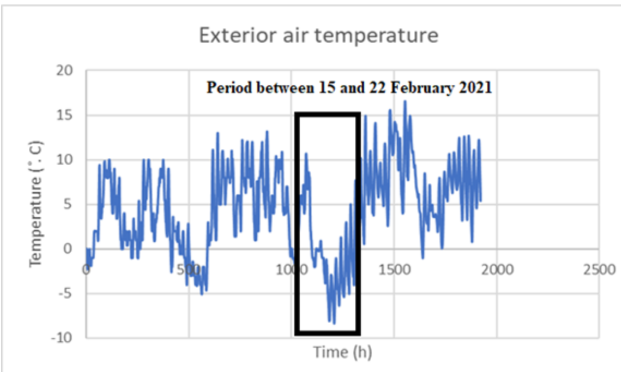

Figure 4-11: Exterior air temperature between 01 January 2021 and 21 Mars 2021.

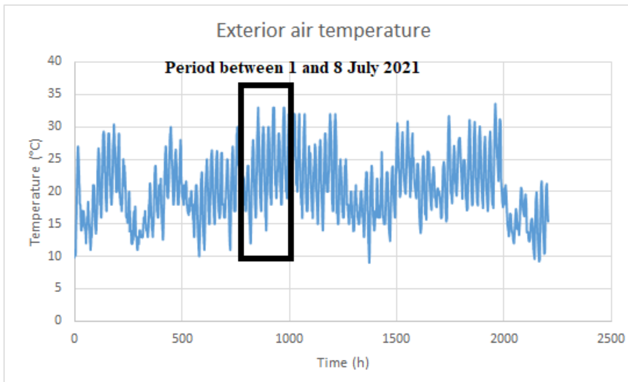

Figure 4-12: Exterior air temperature between 01 Juin 2021 and 01 September 2021.

During winter, heat is transferred from the inside (higher temperature, maintained between 16 and 19° C during this period (Figure 4-11)) to the outside (lower temperature).

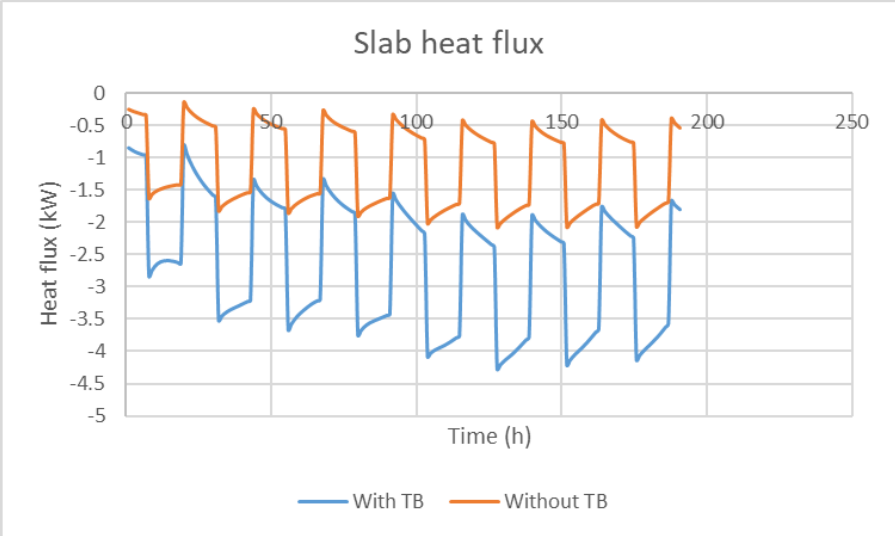

Figure 4-13: Average slab heat fluxes with and without TB (winter period).

Heat fluxes are smaller without thermal bridges (Figure 4-13). The heat losses will increase between 30% and 50% when considering TB during this period. Therefore, the 20% difference in energy consumption is justified. It should be mentioned that the heat flux decreasing aspect is due to the decreasing aspect from the exterior air temperature (Figure 4-11).

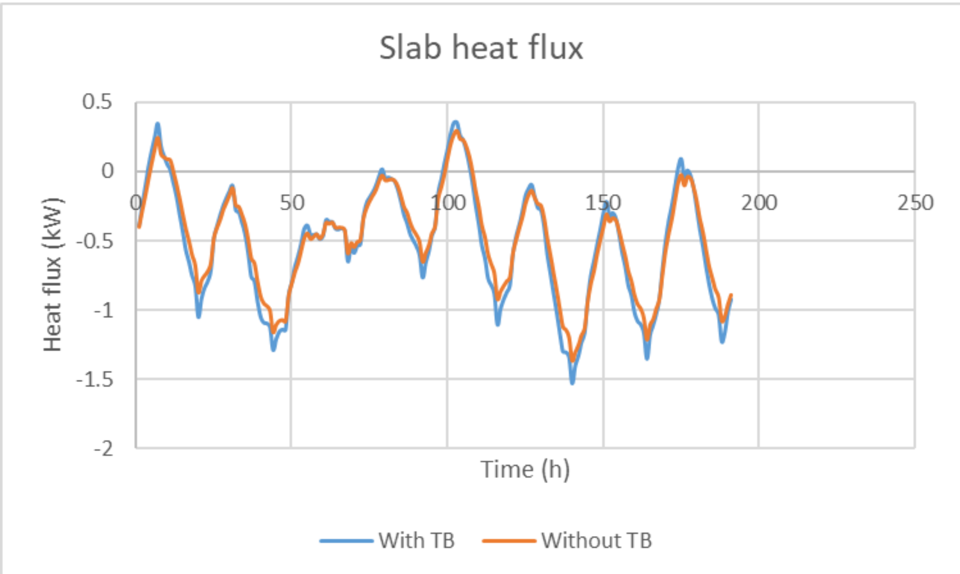

Figure 4-14: Average slab heat fluxes with and without TB (summer period).

During summer, heat exchange with the ground is smaller than winter period. It varies from an average magnitude of 2.2 kW in winter to 0.6 kW in summer. It is shown that heat is transferred from the ground to the building (positive heat flux) during the day. Heat losses to the ground (negative heat flux) are due to the low outside temperatures during the night (Figure 4-12).

Building heat losses:

Figure 4-15 illustrates the building heat flows at different levels. The 3D object represents the slab, the foundation and the soil. It shows that higher heat losses are related to opaque partitions (walls, roofs) and 3D object. Ground heat losses will decrease from winter to summer. They represent an average of 25 % of the total heat flux during winter; this percentage will be reduced to 5 % during summer. In this case, ground heat losses increase building heating energy in winter, and they tend to reduce its cooling energy in summer.

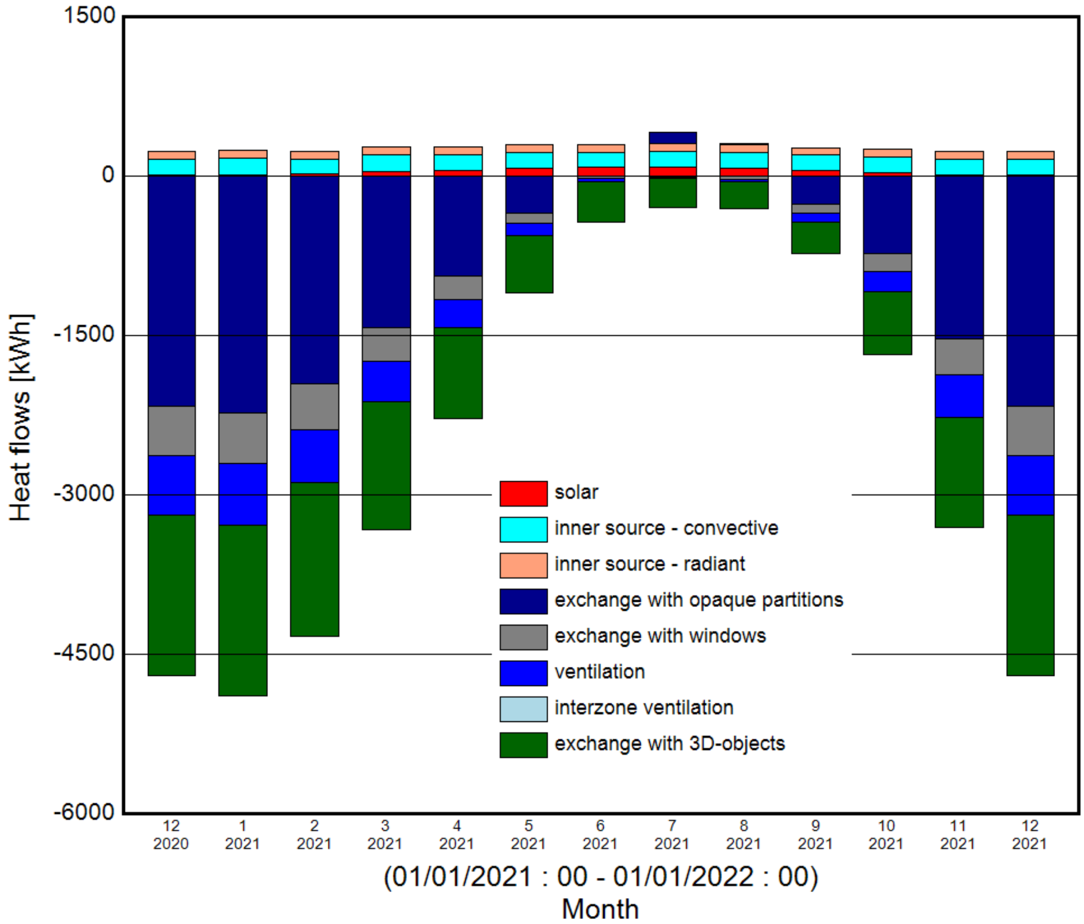

Figure 4-15: Different building heat flows.

This paragraph shows the effect of a ground thermal bridge on annual whole-building energy consumption and heat loss. Therefore, it is essential to study ground thermal performance and variation during this period.

4.4.1.2. Seasonal ground temperature distribution

Ground temperature distribution varies during different periods of the year. Soil thermal behavior fluctuates from season to season due to the dynamic variation between the temperatures inside the building and the ground surface. During winter, high heat flux region forms at the slab perimeter. During summer, perimeter heat flux is not substantially different from those near the centre.

Winter:

Figure 4-16 represents the soil and slab domain temperature distribution on 26 January 2021 (3:00 p.m).

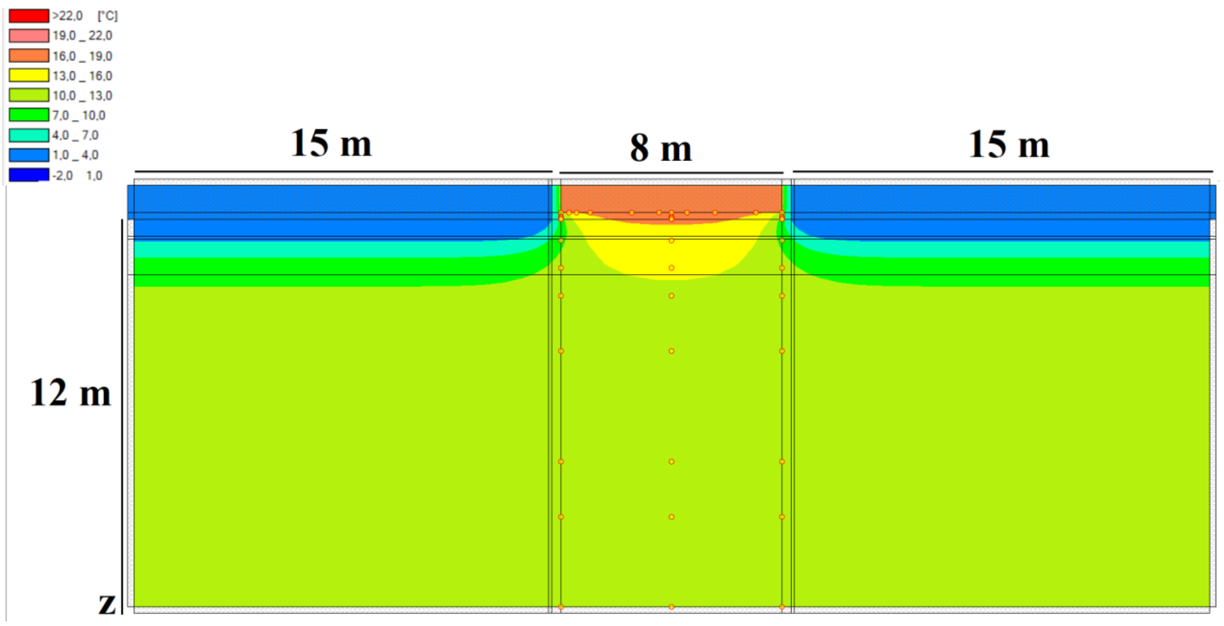

Figure 4-16: Temperature distribution via soil and slab on 26 January 2021 at 3:00 p.m.

Isotherms are tightly arranged and almost horizontal on a winter day near the perimeter. The low temperature starts from the foundation to the ground in contact with the outdoor conditions (between 1 and 4 °C). Heat is transferred from the high-temperature region (floor) to the lower one (ground and outdoor). The indoor and outdoor conditions affect the upper two meters of the ground and the slab. The extensive soil mass is responsible for the relative stability of its temperature below these 2 meters. Soil can be a thermal tank that stores heat and affects indoor conditions.

Spring:

Figure 4-17 represents the temperature distribution in the soil and slab domain on 02 March 2021 (3:00 p.m).

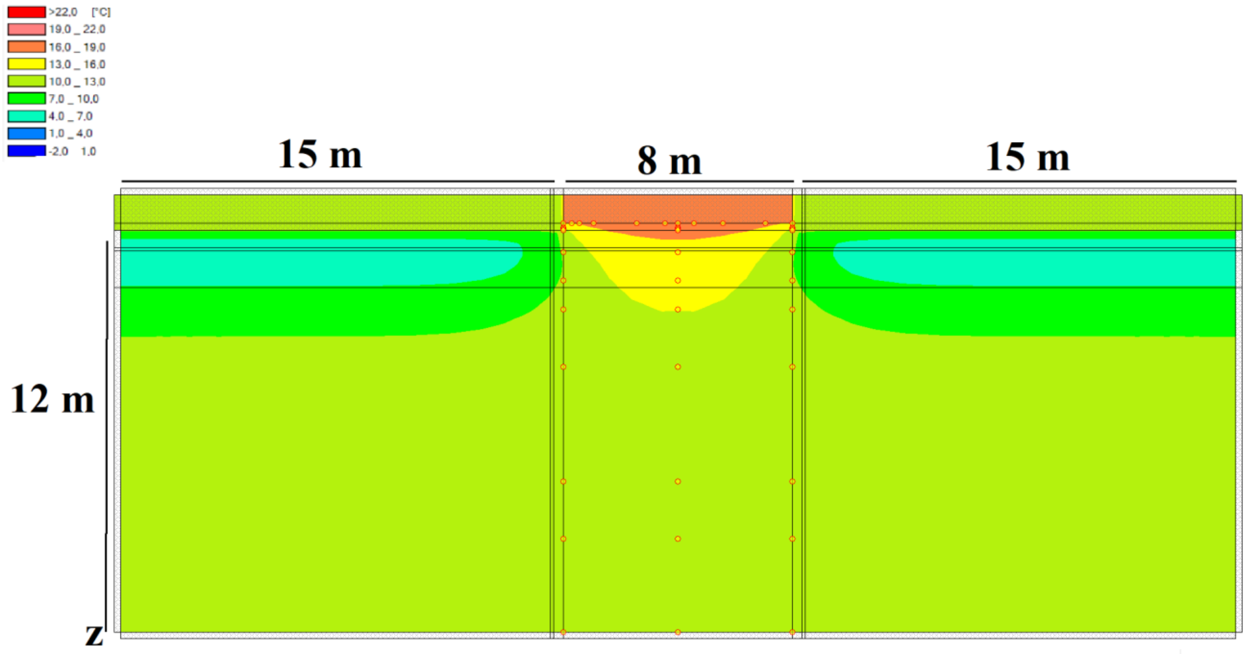

Figure 4-17: Temperature distribution via soil and slab on 02 Mars 2021 at 3:00 p.m.

During a spring day, the temperature difference near the surface is small (negligible), and the isotherm below the house is quite horizontal. However, a low-temperature region is observed. This is due to the cold dissipation from the winter period.

Summer:

Figure 4-18 represents the soil and slab domain temperature distribution on 09 Juin 2021 (3:00 p.m). The low-temperature region from Figure 4-17 disappears during the summer days. It is homogenized with the soil temperature (soil temperature is increasing). Isotherms below the slab become horizontal, and the core and edge floor temperatures are almost identical.

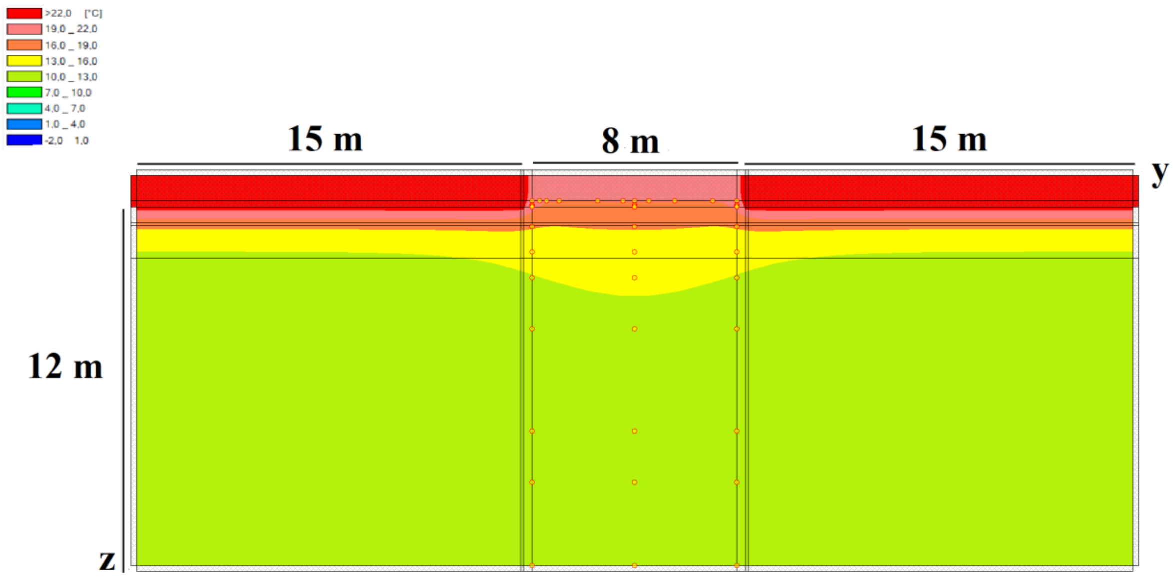

Figure 4-18: Temperature distribution via soil and slab on 09 Juin 2021 at 3:00 p.m.

During night time (Figure 4-19), indoor air and slab surface temperatures are less than the outdoor. Therefore heat will pass from interior to exterior during night time. This result can explain the 5% heat losses during summer from Figure 4-15.

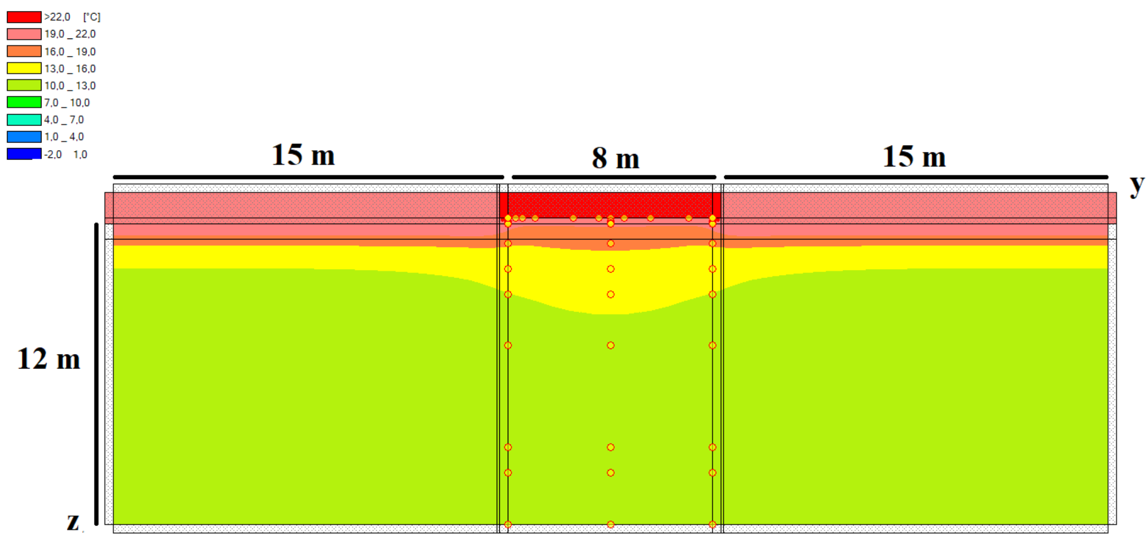

Figure 4-19: Temperature distribution via soil and slab on 09 Juin 2021 at 3:00 a.m.

Fall:

Figure 4-20 represents the soil and slab domain temperature distribution on 25 September 2021 (3:00 p.m).

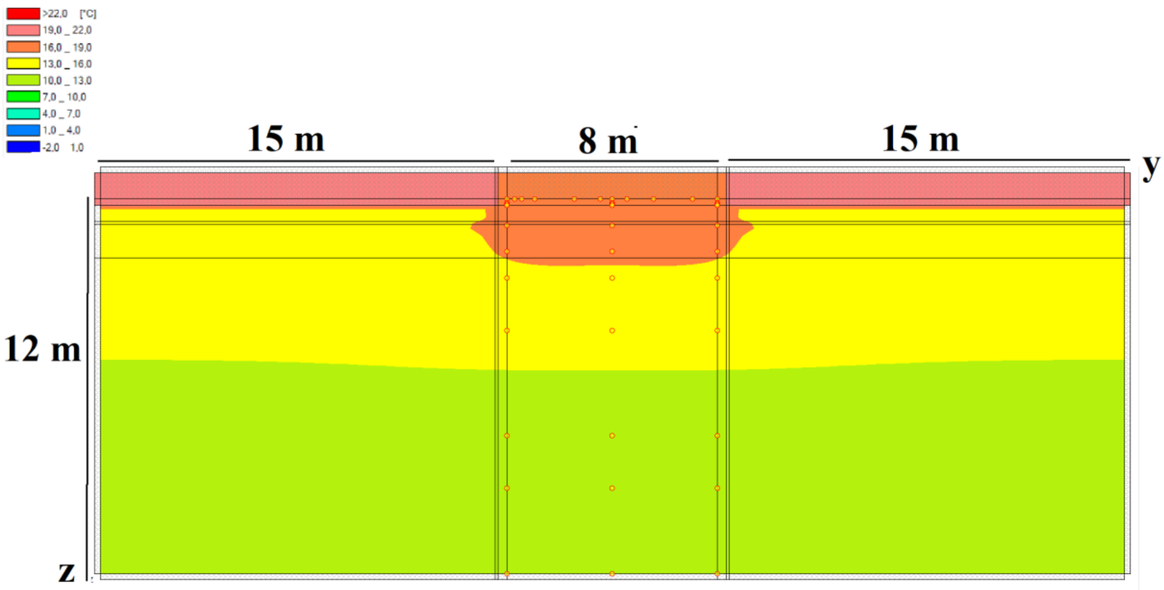

Figure 4-20: Temperature distribution via soil and slab on 25 September 2021.

It shows that the winter temperature distribution reappears, and the fall weather reduces the ground surface temperature. Seasonal variation affects the soil temperature to a 5 m depth (yellow region). Therefore, it can be concluded that: during winter, when the temperature gradient is large between indoors and outdoors, a significant heat loss occurs at the floor perimeter. During summer, heat flux at the slab perimeter is similar to those at the different slab positions (all slab surfaces will contribute equally to the heat loss). During seasonal variation, indoor and outdoor conditions affect a region of two to five meters of soil depth. However, the remainder of the soil depth is not affected due to the boundary conditions effect and ground thermal mass. This effect will be discussed in the next section (paragraph 4.34.5.1).

4.5. PARAMETRIC STUDY:

In this section, many parametric studies were performed. The effect of the ground depth, the deep ground temperatures, the ground surface albedo, the climate, the soil and the floor area are included.

4.5.1. Effect of deep ground boundary conditions

Different cases were studied to highlight the influence of deep boundaries on the final results:

4.5.1.1. Effect of temperature and adiabatic boundary conditions:

Constant temperature is applied at the deep ground when a water table exists. This temperature equals the annual average outdoor air temperature [139] [140].

For a ground depth of 12 m, different temperatures and adiabatic boundary conditions are applied: 9°C, 12°C, and 15°C. Table 4-4 shows the different results for the different cases.

Table 4-4: Results at different temperature and adiabatic conditions (80 m^2).

Boundary condition	Yearly average ground heat flux (W)	Total energy consumption (kWh)
Adiabatic	1145	25500
9°C temperature	1166	25611
12°C temperature	1146	25501
15°C temperature	1124	25392

It is clearly shown that the change in the deep ground boundary conditions has a small effect on the ground heat flux and the total energy consumption for this case of study (80 m^2 slab). If the temperature increases from 9°C to 12°C and 15°C, the average ground heat flux will decrease by 1.5% and the total energy consumption by 0.5%. An adiabatic boundary condition is similar to 12°C temperature for this case of study.

4.5.1.2. Effect of depth:

Different depths are applied for a 12°C deep ground temperature: 5 m, 12 m, and 15 m. Table 4-5 shows the results.

Table 4-5: Results at different depths (80 m^2).		
Depth	**Yearly average ground heat flux (W)**	**Total energy consumption (kWh)**
5 m	1163	25623
12 m	1145	25501
15 m	1144	25498

Similar to the previous case, the deep ground depth variation will slightly affect the final results. For a constant temperature (12 °C), the ground heat flux and the energy consumption will decrease (by 1 and 0.1%, respectively) as depth increases. A negligible effect is shown between 12 m and 15 m cases.

4.5.1.3. Effect of surface

The slab surface is increased from 80 m^2 (8mx10m) to 1440 m^2 (36mx40m). This dimension is chosen, so the area-to-perimeter ratio is 9.5 > 2.2 (80 m^2).

At a ground depth of 12 m, temperatures and adiabatic boundary conditions were applied: 9°C, 12°C, and 15°C (Table 4-6).

Table 4-6: Results at different temperature and adiabatic conditions (1440 m^2).		
Boundary condition	**Yearly average ground heat flux (W)**	**Total energy consumption (kWh)**
Adiabatic	7063	254455
9°C temperature	7729	257003
12°C temperature	7314	255140
15°C temperature	6900	253294

It is found that the change in deep ground temperature has a higher effect (with respect to the 80 m^2 case) on the ground heat flux and the total energy consumption. If the temperature increases from 9°C to 12°C and 15°C, the average ground heat flux will decrease by 6% and the total energy consumption by 1%. For this case, the difference between adiabatic boundary conditions and temperatures will rise for a larger building perimeter and floor (heat flux will be greater by 4% with respect to the 12°C case). For the floor area (1440 m^2), different depths are applied for a 12°C deep ground temperature: 5 m, 12 m, and 15 m. Table 4-7 shows the different results for the different cases.

Table 4-7: Results at different depths (1440 m^2).

Depth	Yearly average ground heat flux (W)	Total energy consumption (kWh)
5 m	8276	259983
12 m	7314	255140
15 m	7229	254893

If depth increases from 5 m to 12 m, the average ground heat flux will decrease by 11.6% and the total energy consumption by 2%. From 12 m to 15 m, the heat flux will decrease slightly by 1% and the energy consumption by 0.1%.

4.5.1.4. Effect of soil thermal properties:

Now for a similar condition as in Table 4-7, but with high soil thermal conductivity (2.2 W/m.K), Table 4-8 shows the new results.

Table 4-8: Results at different depths with high soil thermal conductivity (1440 m^2).

Depth	Yearly average ground heat flux (W)	Total energy consumption (kWh)
5 m	9874	269503
12 m	8385	261053
15 m	8213	260343

Similar behavior with respect to the previous one is shown when the depth increases. The average ground heat flux will decrease by 15% and the total energy consumption by 3.1%. Moreover, a negligible effect is found when the depth increases from 12 m to 15 m.

As a conclusion, a higher effect on ground heat flux and energy consumption is found for larger slab areas and perimeters. It is related to the ground floor area to perimeter ratio (A/P). Therefore, if the area to-perimeter ratio increases, the deep ground boundary condition influence increases. BC position causes a larger effect on the results than the boundary condition variation. In addition, the soil thermal properties (thermal conductivity) can extend the influence of the deep ground BC on the final results (for high soil thermal conductivities). Finally, an adiabatic boundary condition at 12 m of depth (based on EN 10211) will be a good application in this work.

4.5.2. Effect of ground cover:

It is important to include the soil surface cover in the whole building calculations to study the effect of the outdoor conditions on the final results. Therefore, many surface solar radiation reflection coefficients (albedo α_{soil}) are presented: 1(Totally reflected), 0.9 (snow), 0.6 (concrete), 0.4 (vegetation), and 0.15 (bitumen).

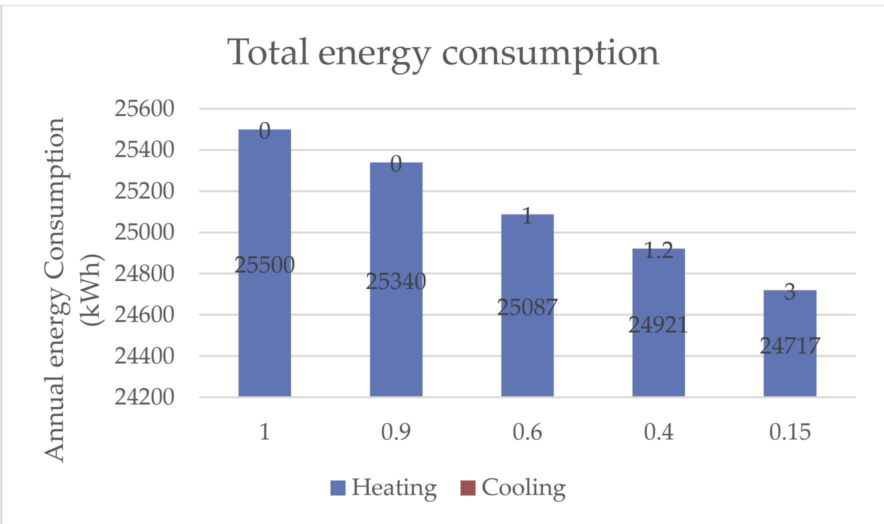

Figure 4-21:Total energy consumption for different solar reflection coefficient.

Figure 4-21 represents the annual total energy consumption for the five cases. It is shown that the energy consumption will be reduced when the reflection coefficient decreases from 1 to 0.15, and the energy consumption is decreased by 3.1%. The cooling consumption is negligible in all cases. However, cooling will increase slightly in the Lyon climate (in 2021) when this coefficient decreases. To better understand this effect on the final results, the ground temperature is shown in Figure 4-23. Ground temperature is represented by the yearly average temperature at monitor points (x=5, y=4 and z is a variable depth) (Figure 4-22). The monitor position is defined to retain 3D results like the temperature and the heat fluxes.

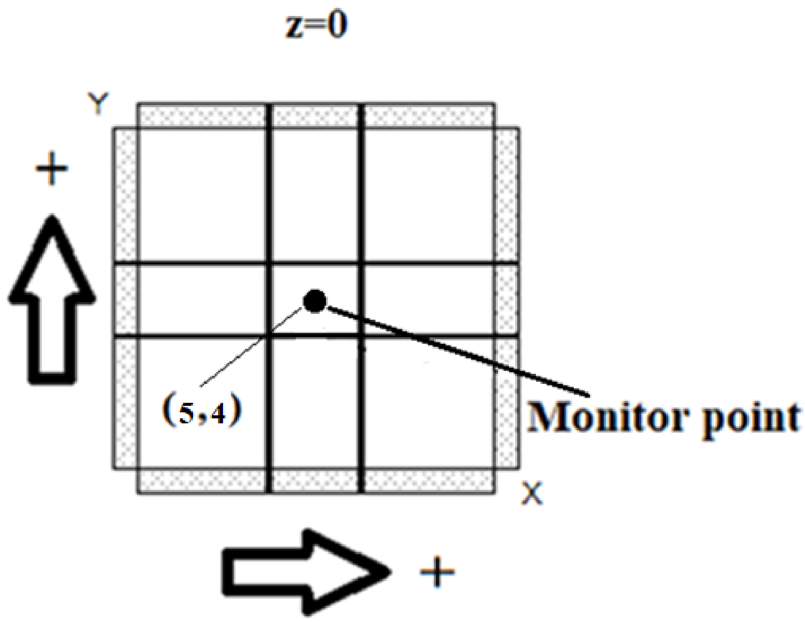

Figure 4-22: Monitor point at x= 5m and y= 4m.

The soil temperature increases when α_{soil} decreases. If the albedo is reduced, the soil will absorb the solar radiation and starts to be warmer. This variation will significantly affect the soil temperatures at a depth between 3 m and 12 m (under the slab): it will increase by 1.5°C from α_{soil}=1 to α_{soil}=0.15. The indoor conditions highly influence the first three meters of depth, so the ground temperatures for different albedo are very close.

Therefore, this coefficient should be considered in the whole building calculations. Finally, an α_{soil}=1 will be considered in this study, in which no absorbed radiation will affect the final results.

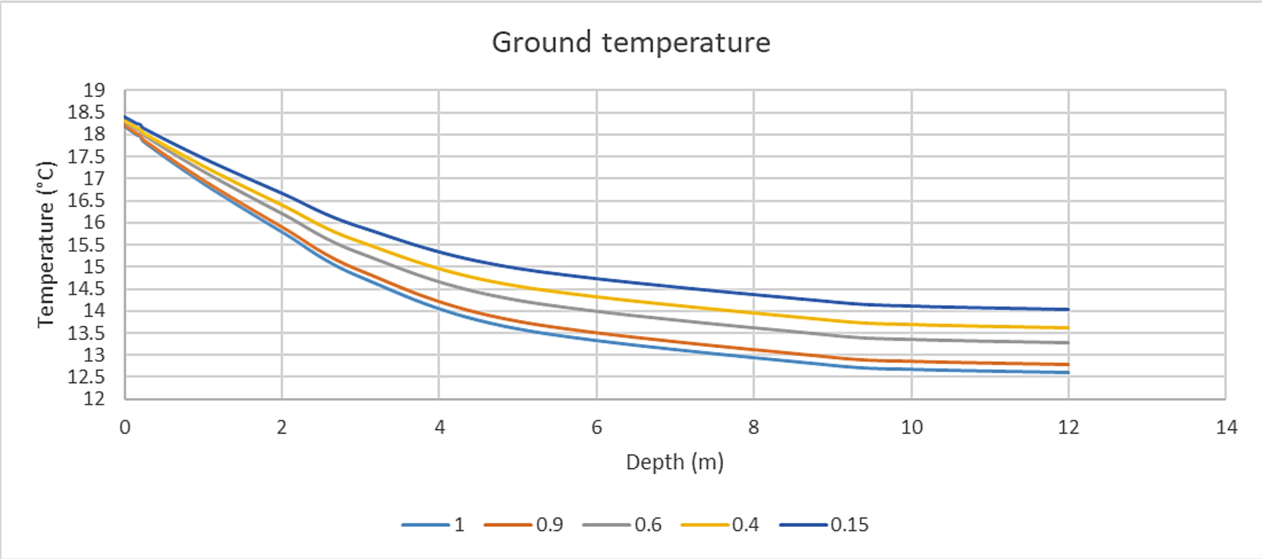

Figure 4-23: Yearly average ground temperature as a function of depth for different solar reflection coefficients.

It has been shown that the effect of the ground boundaries and thermal properties on the final results are not negligible. These properties can directly affect the thermal bridges calculation and energy consumption.

4.5.3. Effect of soil thermal properties:

The clay soil was simulated for thermal conductivities at 0 and 50% relative humidity to highlight the soil impact on the whole building calculations. Therefore, the two thermal conductivities are 0.288 W/m.K and 1.28 W/m.K. The total energy consumption is affected by the soil properties (Figure 4-24): A variation of the soil moisture content leads to a variation of the soil thermal conductivity from 0.288 to 1.28 W/m.K (0 to 50% RH). Moreover, increasing ground thermal conductivity affects the total building energy consumption (Figure 4-24). It will rise from 24421 to 25500 kWh (1079 kWh), equivalent to 4.2% of the annual energy needs.

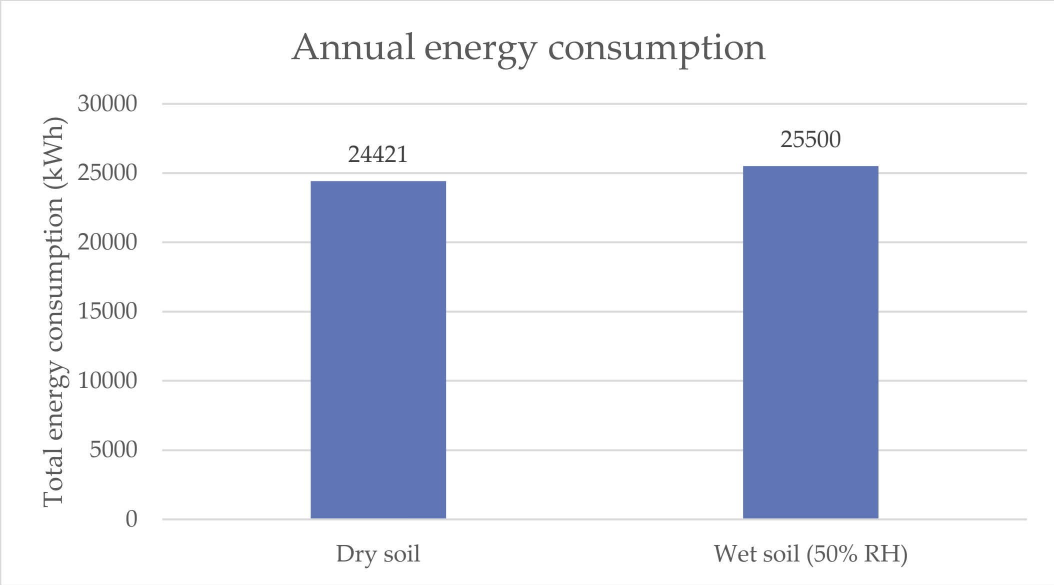

Figure 4-24: Total energy consumption as a function of soil type.

The two cases of clay conductivities were applied to the uninsulated floor.

The average indoor slab surface temperatures are calculated for wet and dry clay. They are presented in Figure 4-25 and Figure 4-26 for winter and summer, respectively.

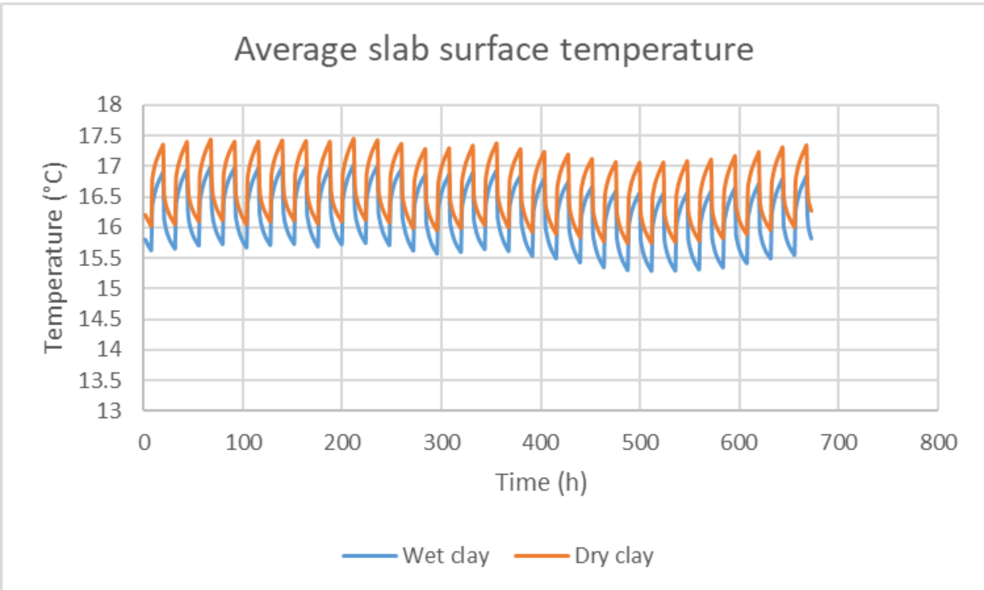

Figure 4-25: Average slab temperature for wet and dry clay (winter case).

Figure 4-25 presents the period between 1 and 28 February. For a lower thermal conductivity (dry soil), the ground heat flux is reduced during winter, and the slab surface temperature is warmer for dry soil (0.7°C).

Figure 4-26 presents the period between 1 and 31 July. Slab surface temperature is reduced between 0.1 and 1°C from dry to wet soil. These results reveal the essential role of ground on whole building calculations. Based on summer curves, it is seen that for a low thermal conductivity, slab surface temperature will increase, and therefore an overheating risk will occur.

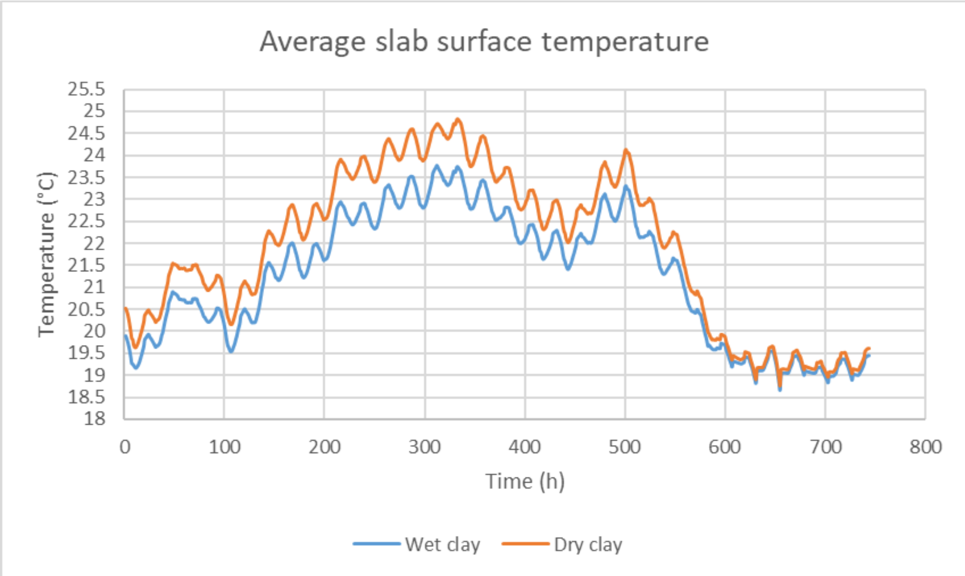

Figure 4-26: Average slab temperature for wet and dry clay (summer case).

Figure 4-25 and Figure 4-26 show a direct effect of the thermal conductivity on the ground thermal inertia. For a low λ of 0.288 W/m.K, the dry soil temperatures and the heat fluxes will phase lag the wet one by 1 hour.

It has been shown from previous sections that the thermal bridges and the losses are mainly concentrated at the slab-foundation wall junction and the perimeter (mainly in the winter period). Therefore, good insulation of foundation walls and junctions will offer several advantages. External insulation can reduce the thermal bridges effectively, mainly through the floor-wall connection. Treating the thermal bridges becomes very important on these walls exposed to cold and humidity because any bad installation of internal insulation could increase the condensation risk and mould growth.

4.5.4. Effect of thermal bridge external insulation:

External vertical insulation of 0.6 m depth and 12 cm thickness was applied (polystyrene: Figure 4-27). The insulation is installed on the outer side of the foundation and above the ground (0.2 m and 0.5 m) (Figure 4-27). The slab surface temperatures are calculated based on these cases.

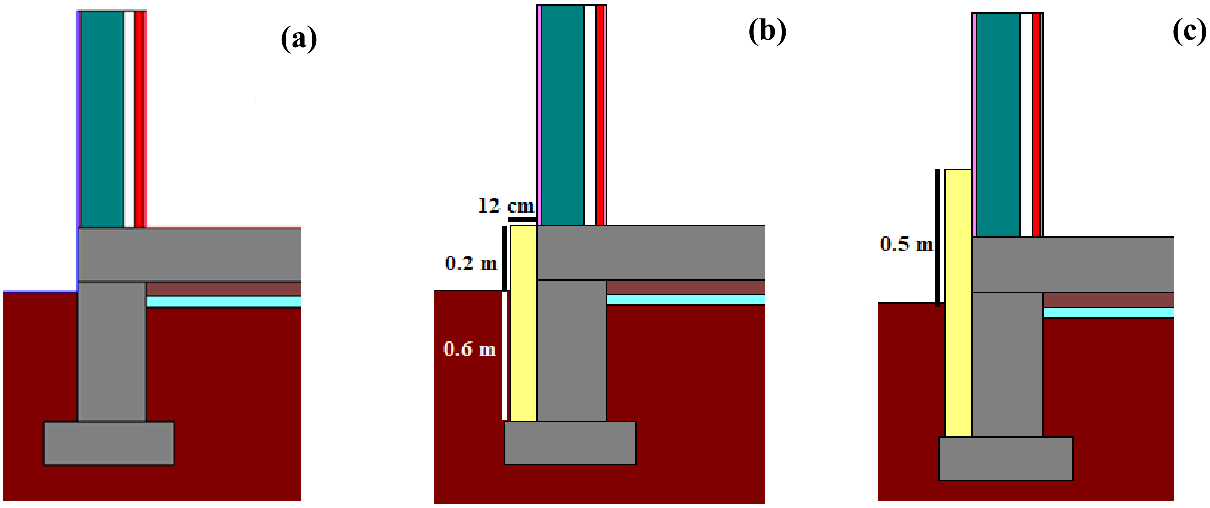

Figure 4-27: Three cases: (a) no insulation case, (b) 0.2 m exterior vertical insulation (Polystyrene), (c) 0.5 m exterior vertical insulation (polystyrene).

4.5.4.1. Total energy consumption:

Total energy consumption for three cases are presented in Figure 4-28. It is found that the vertical solution at the external foundation wall can decrease the total energy consumption. For 0.2m and 0.5 m insulations above ground, the energy consumption is reduced by 3.5 % and 8.5% with respect to the no insulation case. It is concluded that the energy consumption will decrease as a function of the insulation volume. Also, it is shown that if the wall-slab junction is insulated, the percentage of energy reduction will extend.

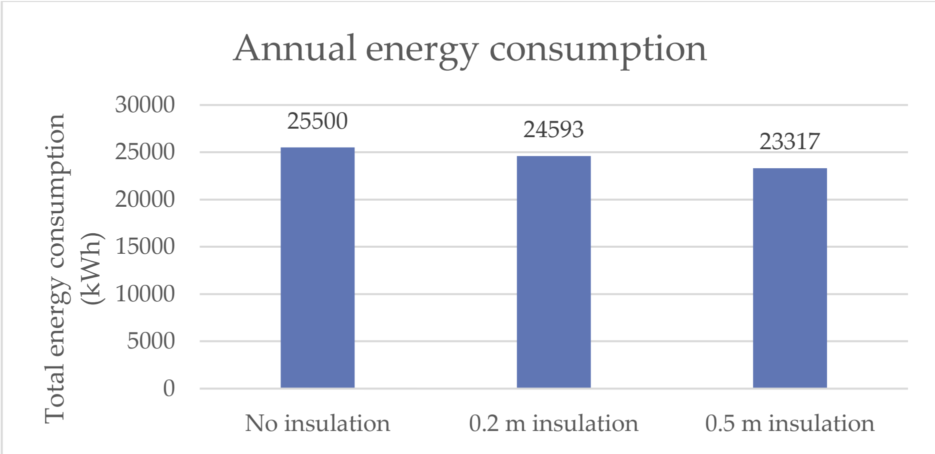

Figure 4-28: Total energy consumption as a function insulation height above ground.

Figure 4-29 represents the monitor points. It is chosen to be at the slab's perimeter (5,0,0) and the corner (0,0,0).

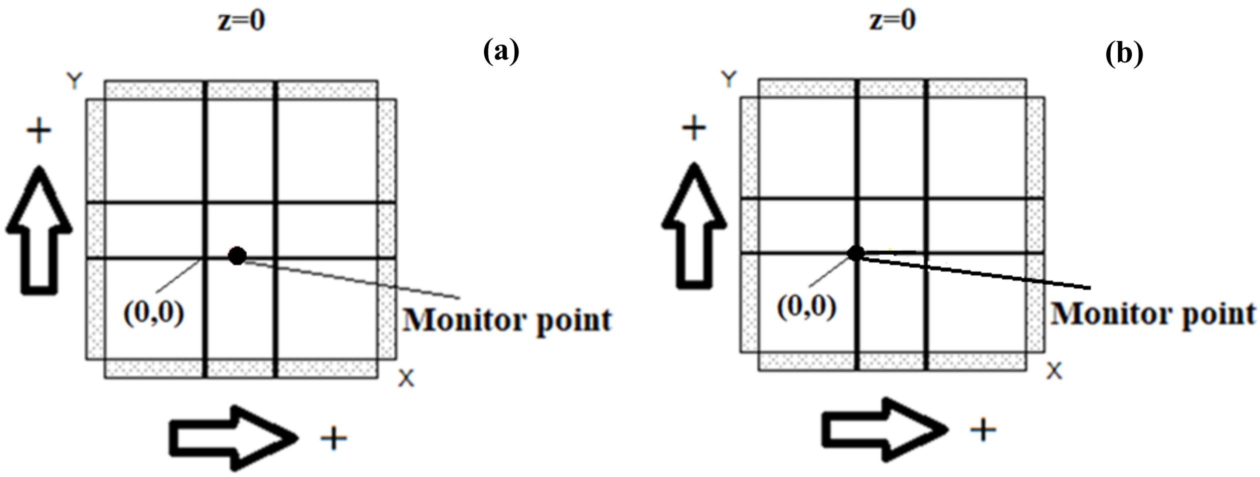

Figure 4-29: Ground upper face with monitor points (a) and (b).

The purpose here is to highlight the effect of such solutions on the slab surface temperature and to confirm the importance of this insulating technique in reducing the winter losses. Figure 4-30 to Figure 4-33 represent the slab surface temperatures with and without insulation at the slab's edge (5,0,0) (a) and the corner (0,0,0) (b) (in winter and summer).

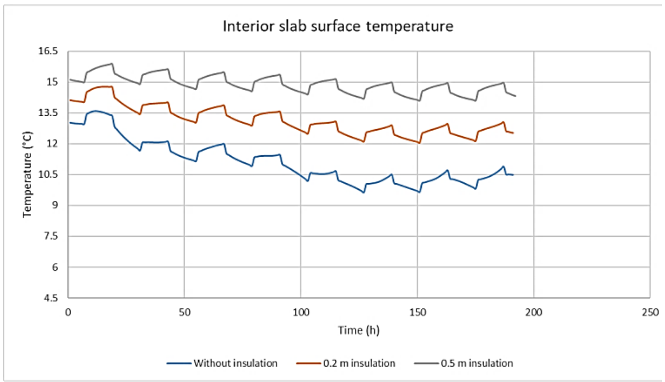

Figure 4-30: Slab surface temperature with and without insulation at monitor point (5,0,0) (winter case: 15 until 22 February 2021).

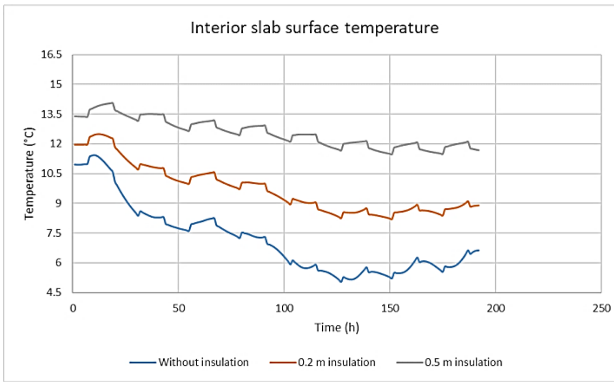

Figure 4-31: Slab surface temperature with and without insulation at monitor point (0,0,0) (winter case: 15 until 22 February 2021)

These figures reveal that during winter, the external insulations would increase the slab edges and the corner temperature up to 4°C (0.2 m insulation) and 8°C (0.5 m insulation) with respect to the no insulation case.

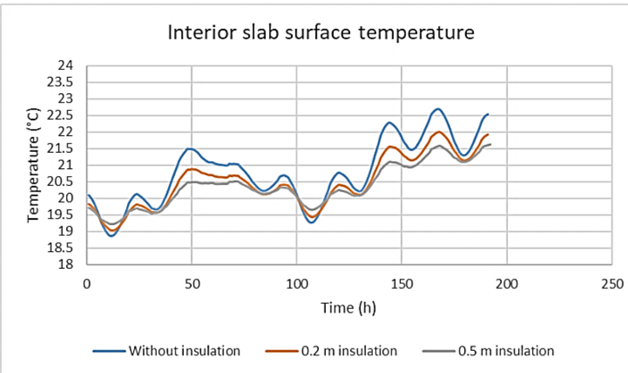

Figure 4-32: Slab surface temperature with and without insulation at monitor point (5,0,0) (summer case: 1 until 8 July 2021).

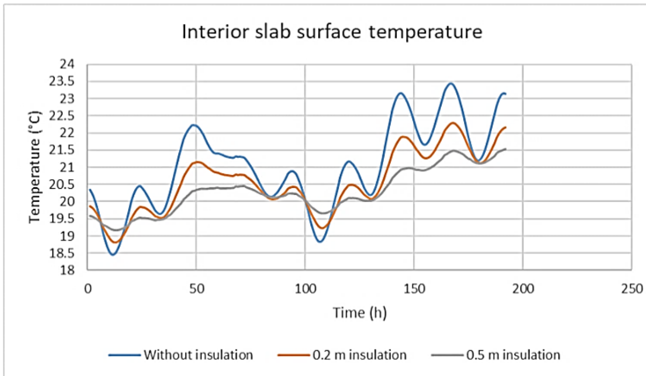

Figure 4-33: Slab surface temperature with and without insulation at monitor point (0,0,0) (summer case: 1 until 8 July 2021).

Conversely, this type of insulation in summer will decrease the slab surface temperatures but with a lower impact between 0 and 0.7°C.

Compared to the monitor point at (x=5, y=0, z=0), the thermal bridges' impact will increase at the corner (x=0, y=0, z=0). Based on Figure 4-30 and Figure 4-31 for the no insulation case (winter), the edge temperature will vary between 9.5 and 13°C. However, this temperature will vary between 5 and

11°C at (0,0,0). The corners' and edges' temperatures will increase, and the condensation risk will decrease using external vertical insulation.

Insulating the slab-wall junction (0.5m insulation) is essential. The corner temperature is raised up to 8°C with respect to the no insulation case. This temperature is increased up to 4°C using a 0.2 m solution. During summer (Figure 4-31 and Figure 4-32), the difference between the corners and the edges is shallow (edge temperature is greater by 0.5°C). This is because the heat fluxes during this period are not only concentrated at the perimeter and edges (winter case) but they will also be found at the slab core (Figure 4-18).

Finally, typical insulations (polystyrene) do not impact the thermal inertia with respect to the case without insulation (no time shift).

4.5.4.2. Slab surface temperature

Figure 4-34 and Figure 4-35 represent the monthly mean indoor slab surface temperatures for winter (February) and summer (July) periods at the different y positions (x=5m, z=0 m). The temperatures are studied for three different cases: 0.2 m, 0.5 m insulation and no external insulation case. A comparison of these cases reveals some interesting qualitative effects:

During winter, the perimeter insulation will create a larger region of rising horizontal temperature (Figure 4-34): the insulation effect is up to 2m wide (from the slab edges). As a result, the slab surface temperatures are increasing by 1.5 °C and 3°C for y=0m with respect to the no insulation case (for 0.2 m and 0.5 m solutions).

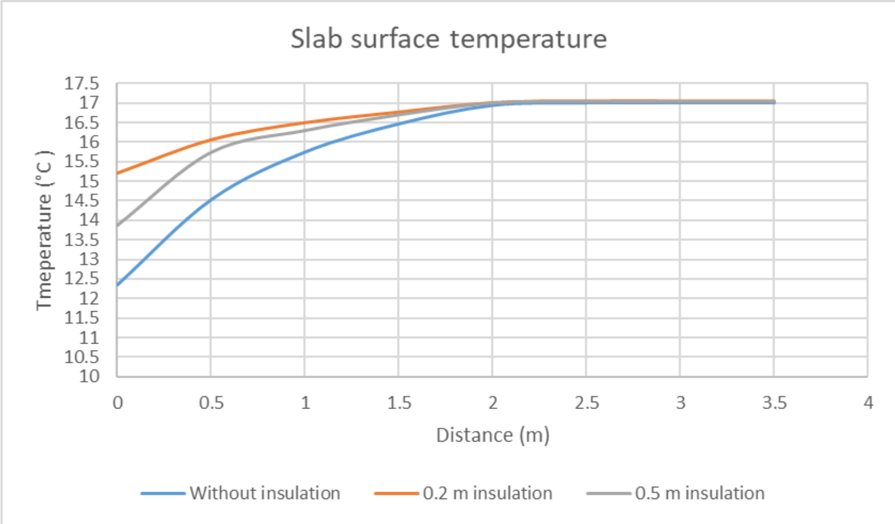

Figure 4-34: Monthly mean slab surface temperature as a function of distance from perimeter with and without insulation (February).

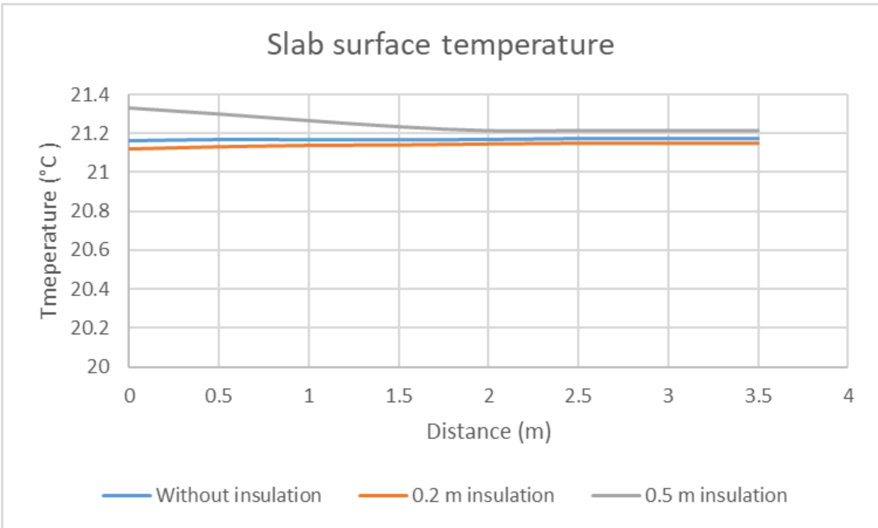

Figure 4-35: Average slab surface temperature as a function of distance from perimeter with and without insulation (July).

In summer, the external insulation will have a lower effect on the slab surface temperature (Figure 4-35). It is clear that the polystyrene has a lower impact during this period: Temperature is reduced between 0.05 and 0.3 °C with respect to the no insulation case. Therefore, it is concluded that the no slab overheating problem will happen using this renovation technique.

4.5.4.3. Thermal behavior in a hot climate

The purpose is to study the ground thermal behavior and the overheating risk under Malaga hot climate. The external temperature will fluctuate during summer between 23 and 40°C (Figure 4-36). However, the albedo is considered as an average value of 0.6, due to the direct effect of ground covering radiation in such climates.

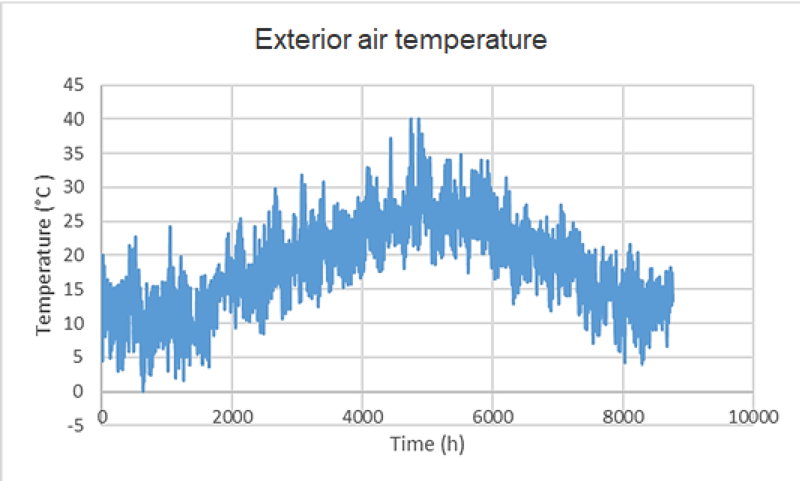

Figure 4-36: Exterior air temperature for Malaga climate.

Two cases were studied: 0.5 m insulation and no insulation case. Figure 4-37 represents the annual heating and cooling consumption.

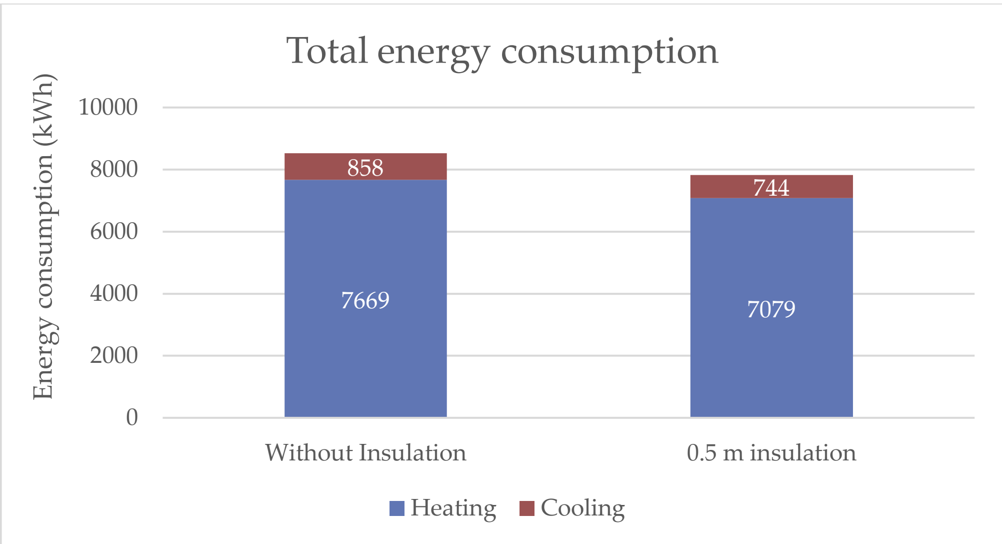

Figure 4-37: Total energy consumption for Malaga climate.

For Malaga climate, the cooling energy represents 10% and 9.5% of the annual energy consumption for the no insulation and the insulation cases, respectively. The cooling energy consumption is reduced by 114 kWh using the polystyrene (0.6 m depth, 12 cm thickness and 0.5 m height above ground) with respect to the no insulation case.

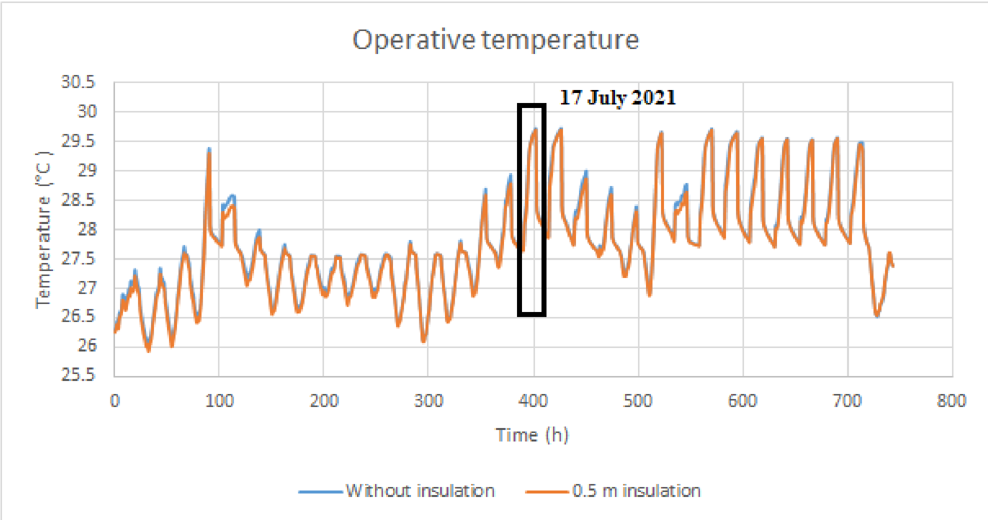

Figure 4-38: Operative temperature variation with and without insulation case during July 2021.

The zone operative temperature in Malaga is represented in Figure 4-38. The outside peak temperature can reach 40°C during the day and 23°C during the night (Figure 4-36). The two curves almost overlap during the hottest period.

In this part, it was shown that the use of external insulation has a negligible effect on the zone temperature variation under summer conditions. During this period, the zone is overheated for the two cases: The maximum zone operative temperature will exceed 28°C. The internal operative curves overlap: The external insulation will not increase the overheating risk because it is combined with mechanical ventilation.

In order to reduce greenhouse gas emissions and high energy consumption, different thermal regulations and labels are imposed in France: RE2020, RT2012 and BBCA (low-carbon building) label. These regulations impose greenhouse gas emissions and energy consumption using different solutions like bio-based materials. Hence there is an interest in using hemp concrete in construction since it has low embodied energy. In the next section, hempcrete will be applied at the slab level to study its effect on the final results. The ground heat and moisture transfer model will be used in these calculations.

4.5.5. Effect of soil heat and moisture transfer:

WUFI Plus uses Kunzel model to calculate heat and moisture transfer through building materials. This model is presented in Chapter 2 (eq. 2-28 and 2-29). Kunzel model was used for ground calculations and validated against the Annex A of EN 15026:2007 [141] for heat and moisture transfer in a semi-infinite region. The case study used in this calculation is the same used previously. This section applies 1D heat and moisture transfer to the soil since WUFI 3D cannot take into account moisture transfer. Concerning TB, they will be considered as a linear thermal transmittance coefficient, integrated in WUFI model. The next sections will discuss the TB calculation method.

Soil and slab properties:

Initial and boundary conditions:

Initial ground moisture conditions are retrieved from [142] and [15] for clay soil (Figure 4-39). Soil initial conditions are presented for the first 5 m of depth. The soil will be saturated at this level ($z=z_{max}$, RH=100%).

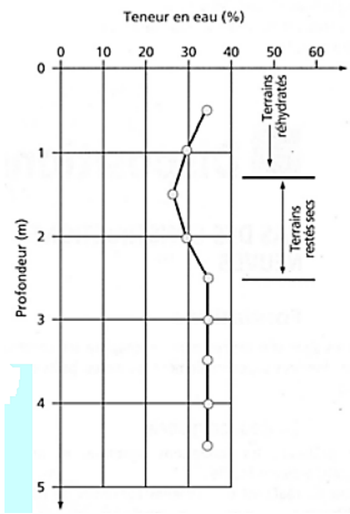

Figure 4-39: Initial moisture condition for clay soil [142].

At z=0, for slab surface in contact with interior air: moisture conditions can be represented by this equation [33]:

$$g = 7.10^{-9}.h_c(p_{v,ambient} - p_{v,surface}) \quad 4\text{-}1$$

Where g is the vapor flux at slab surface, h_c is the surface convective coefficient, $p_{v,ambient}$ is the ambient water vapor pressure and $p_{v,surface}$ is the surface water vapor pressure. The convective heat transfer coefficient is set to be 5.5 W/m^2.K [143].

Slab materials:

Two types of slabs are studied: The first one is with traditional concrete and the second one with hempcrete. Hempcrete slab is often used in renovating floors of old houses or in eco-construction. Two properties distinguish the hempcrete slab with respect to the traditional concrete: it insulates, stores, and-releases humidity. The following paragraph will explain the importance of this material.

Hempcrete:

Hemp concrete is an environmentally friendly material made from renewable plant-based aggregates that can store carbon [144]. It is one of few constructive systems whose GHG release is negative. In addition, it has good mechanical and acoustic properties [145]. Hemp concrete is lighter than traditional building materials and has excellent thermal insulation properties due to its low thermal conductivity [146]. This size depends on the material composition. Since the binder is the most conductive, increasing the binder portion leads to high thermal conductivity. The density of the material can also influence the thermal conductivity of hemp concrete. In fact, the more the density increases, the more the thermal conductivity increases [147]. Concerning the hydric properties, hemp concrete has many advantages. It has an excellent moisture buffering capacity (MBV) [148]. This allows to maintain the quality of the indoor air.

Furthermore, it is very porous structure makes it capable of absorbing large quantities of water. Moreover, hemp concrete has a high permeability to water vapor, and the property of substantially moderating the relative humidity variations. It can generally reduce daily changes in indoor relative humidity by absorbing and returning moisture, reducing energy consumption, and maintaining hygrothermal comfort in buildings [149]. For a soil application, binder content is higher compared to other type with lower mechanical properties. Due to the lack of hempcrete moisture properties for soil application, hempcrete density is considered as 450 kg/m^3, water vapor resistance factor as 10 and 0.1 W/m.K as thermal conductivity (wall property).

Hempcrete and concrete properties are shown in Table 4-9 ([150]):

Table 4-9: Slab on grade layers from outside to inside.

	Hempcrete slab			Concrete slab		
	Layers	Thickness (cm)	Thermal conductivity (W/m.K)	Layers	Thickness (cm)	Thermal conductivity (W/m.K)
Slab	Gravel	5	1.4	Gravel	5	1.4
	Hempcrete	15	0.1	Polystyrene	6	0.04
	Lime	4	0.7	Concrete	25	1.7
	Floor finishing	1.5	1.66			

All slab's thermal and moisture layers properties can be retrieved from WUFI's library. The two types of material are set at 50% relative humidity as an initial moisture condition. Initial material temperatures are at 20°C. Also, the calculation is initialised for 10 years. It should be mentioned that no heat and moisture transfer is considered in walls and roofs.

Thermal bridges calculation:

To include thermal bridges calculation for the heat and moisture transfer model, the linear heat transmittance coefficient ψ is integrated in WUFI Plus. Therefore, the two slab types are created in THERM software (Figure 4-40 and Figure 4-41).

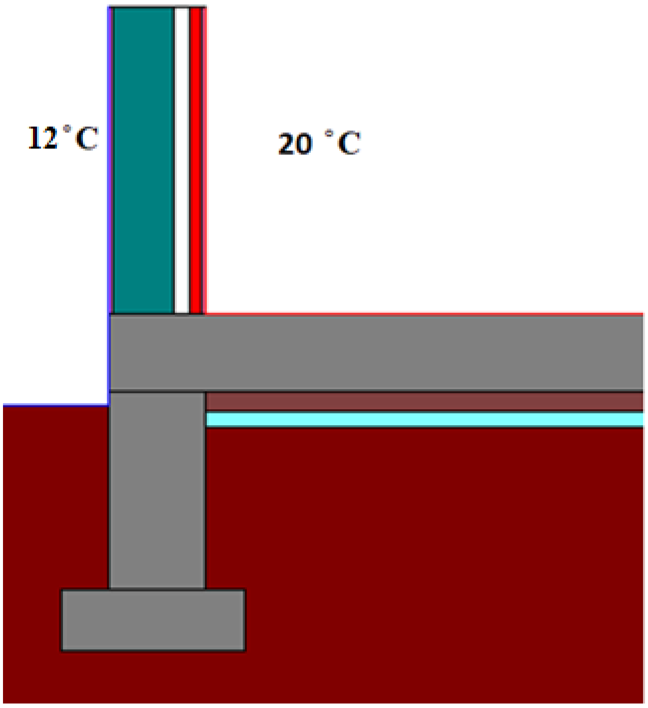

Figure 4-40: Slab-wall junction in THERM software (concrete case).

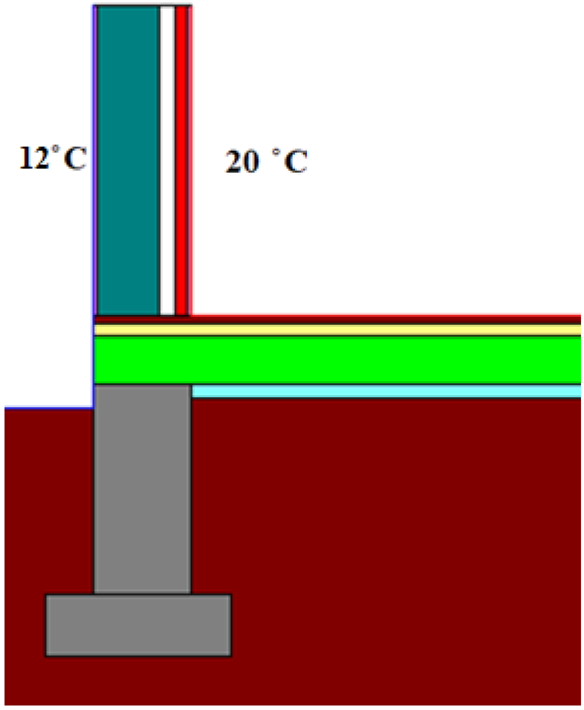

Figure 4-41: Slab-wall junction in THERM software (hempcrete case).

ψ is calculated using equation 3-14 based on the European norm 10211. Psi is 0.5 W/m.K for the concrete case, and case is 0.1 W/m.K for the hempcrete. Heat flux from TB is included in WUFI Plus using the following equation: °

$$Q_{TB} = \sum_{i=1}^{N} \psi_i . l_i (T_{attachement,i} - T_{zone}) \qquad \text{4-2}$$

Where ψ_i is the linear heat transfer coefficient [W/m.K], l_i is the thermal bridge length [m] and $T_{ttachment, i}$ is the attached temperature for the thermal bridge (outdoor temperature or surface temperature) [°C], and T_{zone} is the zone temperature [°C]. ψ_i results for concrete and hempcrete cases are calculated using THERM software.

4.5.5.1. Soil and slab with and without heat and moisture transfer:

Two cases with and without heat and moisture transfer are compared in a building with a concrete slab. The main goal is to highlight the effects of ground heat and moisture transfer on ground heat loss and indoor conditions. For heat and moisture transfer cases, thermal conductivity is initially considered at 50% relative humidity (Table 4-9).

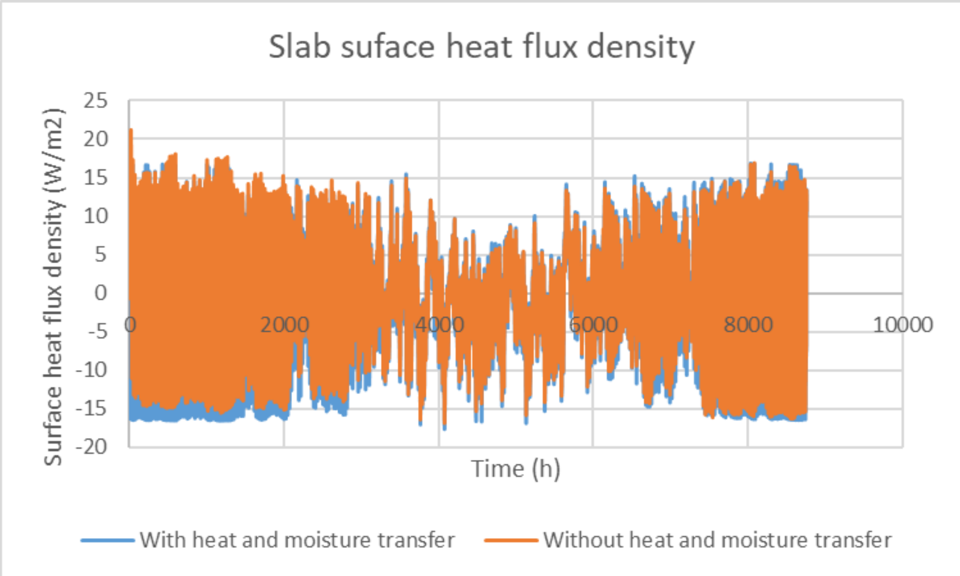

Figure 4-42: Yearly slab on grade heat flux density for heat and coupled heat and moisture transfer case (concrete slab).

From Figure 4-42, it is clearly shown that the heat and moisture transfer affects the ground heat loss. For an almost saturated soil during winter, the heat loss for a case considering ground moisture transfer is higher than a heat transfer case. Heat loss is greater by an average of 2.5 W/m^2, equivalent to 10% of the total ground heat flux density. This is because the ground thermal conductivity increases with moisture content and achieves a value higher than a dry case. Also, based on equations (2-28 and 2-29), the heat storage, transport and generation are related to the moisture-dependent thermal conductivity k_w, relative humidity and water vapor saturation pressure. Therefore, considering moisture transfer in the heat storage and transfer correlations will produce new mechanisms for heat transfer and storage.

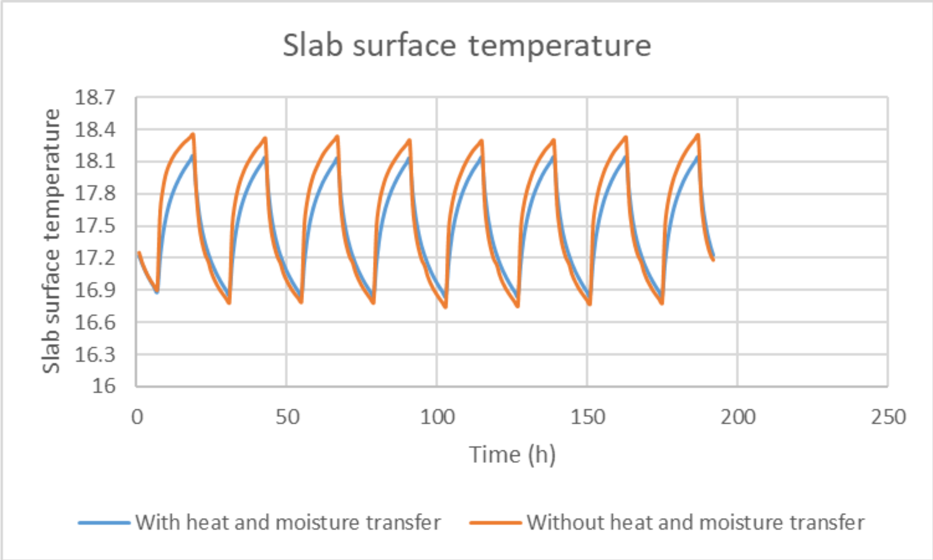

Figure 4-43: Concrete slab on grade temperature for a heat and coupled heat and moisture transfer case (from 15 till 22 February 2021).

Figure 4-43 illustrates the slab interior surface temperature for the period between 15 and 22 February 2021. The purpose of this figure is to show the ground moisture effect on the slab surface temperature during the winter period. It is concluded that for the heat transfer case, the temperature is higher from the heat and moisture one by 0.3 ˚C. Concerning the total energy consumption, thermal bridges are applied for the two cases (Psi=0.5W/m.K). Therefore, a difference of 320 kWh exists, where the heat transfer case has a lower consumption (15400 kWh). This difference is related to the increase in the slab surface temperature related to thermal bridges calculation (equation 4-2).

4.5.5.2. Effect of slab materials

Hempcrete and concrete slab:

In this paragraph, hempcrete is compared to the concrete slab to study the effect of such material on the ground heat loss and the thermal bridges.

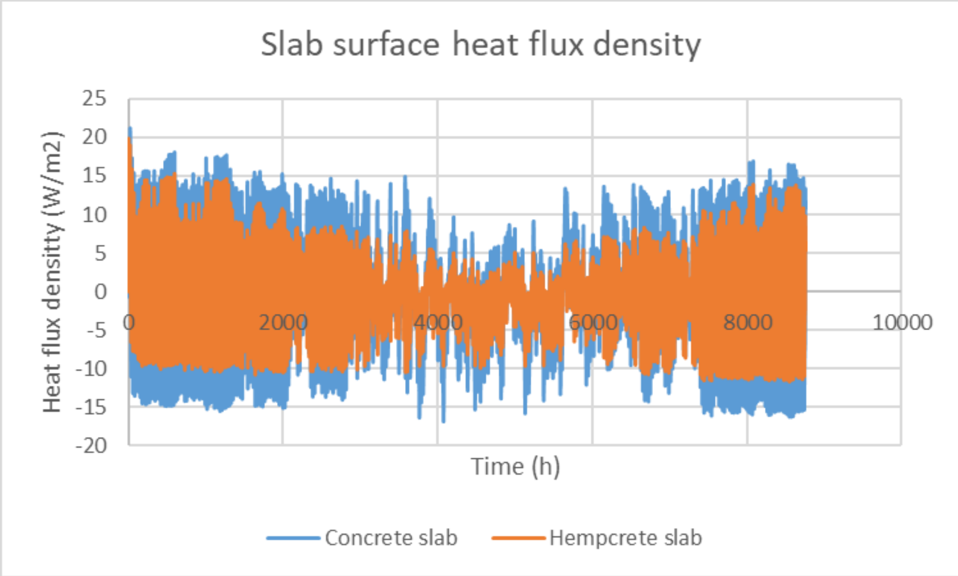

Figure 4-44: Yearly slab on grade heat flux density for a hempcrete and concrete slab.

The two types have a similar slab thermal resistance. Hempcrete is a permeable material with a low thermal conductivity compared to concrete. It plays a role in damping and controlling temperature and relative humidity.

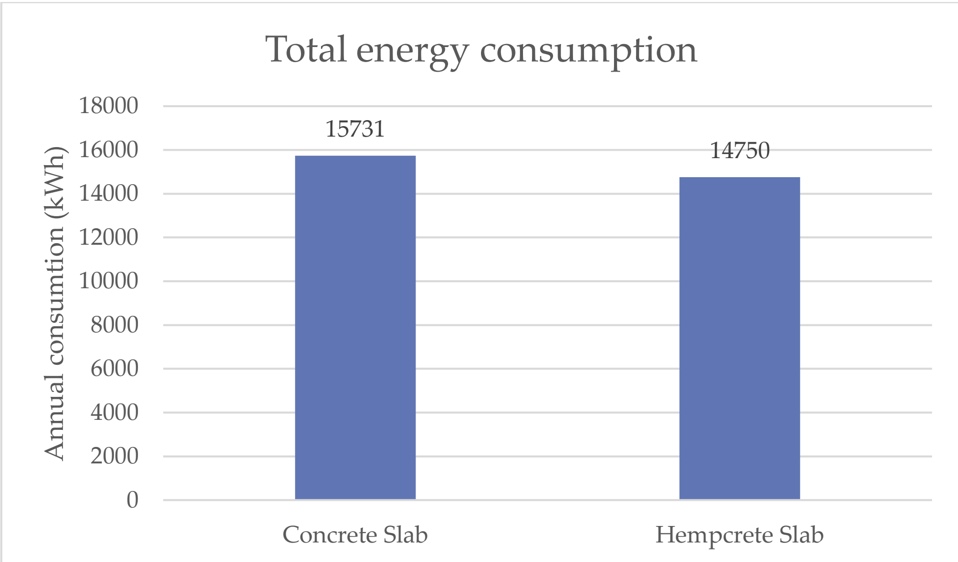

Figure 4-45: yearly total energy consumption for hempcrete and concrete slab buildings case.

Therefore from Figure 4-44, it is seen that hempcrete will reduce the ground thermal heat loss by 30% and, therefore, the annual energy consumption by 6.7% (Figure 4-45).

Compared to the total energy consumption in section 4.4 (25500 kWh), there is a 10000kWh difference with respect to Figure 4-45: This difference is due to the internal insulation (6 cm polystyrene) used under the slab (concrete slab), in addition to the 3D effect of thermal bridges calculated in section 4.4 and ignored in this paragraph.

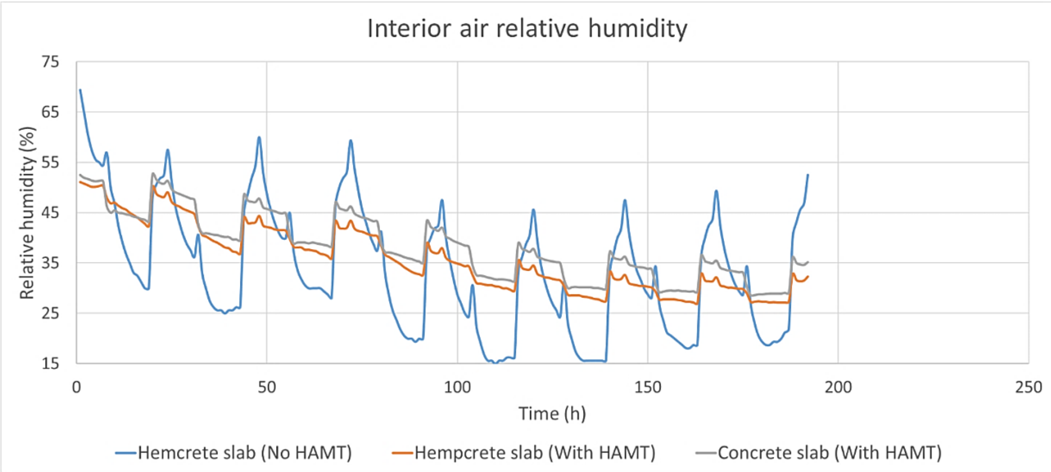

Figure 4-46: Interior air relative for different cases: hempcrete and concrete slab (15 to 22 February 2021)

Figure 4-46 represents interior air relative humidity during winter (15 to 22 February 2021). To highlight slab effect on interior RH, heat and moisture transfer is considered only at soil and slab level (walls and roofs are impermeable).

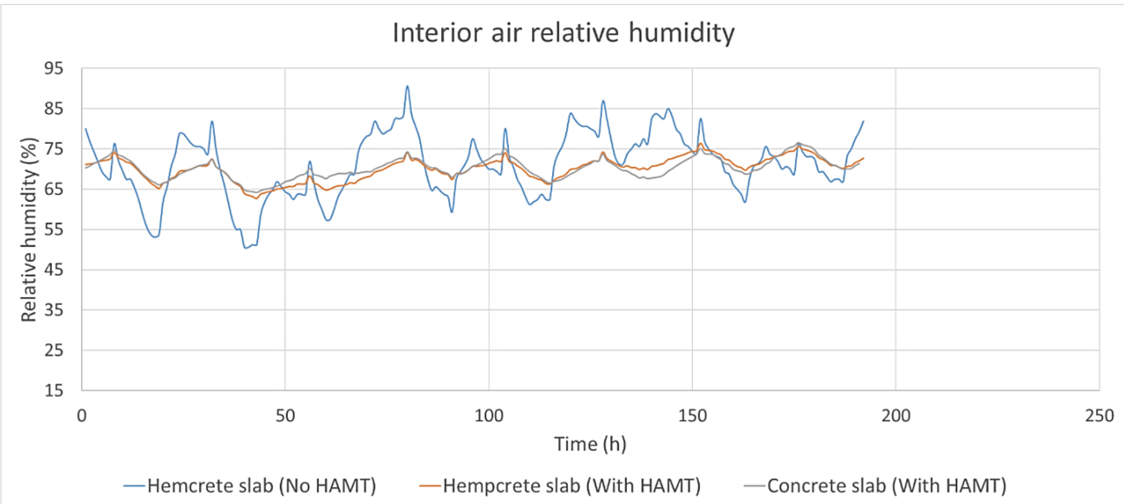

Figure 4-47: Interior air relative for different cases: hempcrete and concrete slab (1 to 8 July 2021)

Three cases are compared: hempcrete slab with and without moisture transfer and concrete with HAMT. It is concluded that the slab plays a role in controlling and damping relative humidity. Moreover, it is also seen that hempcrete can slightly reduce RH more than concrete (3% RH reduction) during winter.

Similar performance is found under summer conditions (Figure 4-47) (for high interior relative humidity). The difference between the two slab types is small because of ventilation rate. In addition, it should be noted that for slab applications, hempcrete is applied with a floor tile (Table 4-9) which is resistant to moisture transfer.

4.6. CONCLUSION

This chapter presents a 3D heat transfer calculation through slab, foundation and soil to highlight the importance of a detailed model for ground analysis. In addition, a 1D heat and moisture transfer model was used with thermal bridges. Simulations were done for a french buildings from the 1950th under the Lyon climate.

The first results showed the importance of considering the ground thermal bridges in heat loss. The total energy consumption is underestimated by 20% if TB is not considered. Moreover, for seasonal variation: heat fluxes are mainly concentrated at the perimeter during winter and equally distributed at the slab surface during summer. Ground heat losses increase building heating energy in winter, and they tend to reduce its cooling energy in summer.

Ground heat fluxes are affected by deep boundary conditions and ground cover. For deep ground boundary conditions, the soil depth and thermal conductivity causes an important effect on larger slab area and perimeter (adiabatic and temperature BC). The ground depth where a small effects is recorded is up to 12 m.

Concerning ground cover, the albedo variation leads to indoor conditions variations. Energy consumption is reduced by 3.1% when the albedo decreases from 1 to 0.15. Also, this variation increases ground temperature up to 2°C (3m to 12 m depth)

In addition, the soil's thermal conductivity can increase the influence of these boundary conditions: a higher variation in the thermal conductivity of the soil means a higher boundary effect.

Also, it is necessary to include soil thermal effect on ground heat transfer calculation. An increase of soil thermal conductivity from 0.28 W/m to 1.28 W/m.K leads to an increase of slab surface temperature (up to 0.7°C during winter and summer).

Under moisture transfer, the ground heat flux increased by 10% with respect to the heat transfer case (concrete slab). For hempcrete, it was shown that ground heat fluxes are reduced by 30% when it is used as slab material. Due to its low thermal conductivity, hempcrete slab decreases thermal bridges (Psi=0.1 W/m.K) with respect to the concrete case (0.5 W/m.K). Therefore, the total energy consumption is reduced by 1000 kWh/year (equivalent to 6.7% of the total energy consumption). Moreover the two cases have similar moisture performace for slab application.

Renovation presents a good solution to reduce energy consumption. Vertical external insulations are proposed (0.6 m depth and 12 cm thickness) with 0.2 m and 0.5m height above the ground. These insulations could reduce the slab surface temperature between 4°C and 8°C (at slab edges and corners). Under a hot climate (Malaga), external insulation has a negligible effect on the temperature variation under summer conditions. It will not increase the overheating risk because it is combined with mechanical ventilation.

The next chapter will follow this study by proposing different ground renovating techniques. An optimization study is applied to include thermal and economical calculations with different renovation solutions.

CHAPTER 5. OPTIMUM SOLUTIONS FOR RENOVATING SLAB ON GRADE BUILDING

5.1. RÉSUMÉ EN FRANÇAIS:

Ce chapitre contribue à réduire les PT (au niveau du sol) en proposant plusieurs techniques de rénovation. Ces solutions de rénovation sont comparées sous différentes conditions afin de choisir la solution optimale.

Pour une étude d'optimisation, WUFI Plus ne peut pas être utilisé car le temps de la simulation est élevé (entre 2h et 48h pour une seule simulation) et il ne peut être couplé à d'autres outils de simulation. Pour lancer ce calcul, c'est EnergyPlus qui est utilisé avec KIVA (pour le calcul de transfert de chaleur 2D dans le sol). Il est couplé avec un logiciel d'optimisation "GenOpt".

Le bâtiment étudié dans cette partie est le cas d'un bâtiment français datant des années 1950 : le même cas et conditions (climatiques, scénarios) de la partie précédente. Les types d'isolation étudiés sont: l'isolation extérieure verticale (type I- polystyrène), l'isolation extérieure verticale (type I - polyuréthane), l'isolation extérieure horizontale et verticale (type L - polystyrène), l'isolation extérieure verticale avec différentes épaisseurs (type q- polystyrène), et l'isolation extérieure trapézoïdale (polystyrène).

Les paramètres qui varient dans cette étude d'optimisation sont : la profondeur, la hauteur, l'épaisseur, et la largeur de l'isolant. La fonction objet à minimiser c'est le temps de retour sur investissement qui représente le nombre d'années au bout duquel le cout d'énergie économisée va compenser celui de l'investissement initial (coût de l'isolation et de la main d'œuvre).

Nos résultats suggèrent que:

- Les types L et trapézoïdale sont recommandés pour la rénovation : ils présentent le temps de retour le plus faible.

- Le deuxième type (géométrie I-polyuréthane) n'est pas recommandé car le prix de l'isolant est élevé ce qui augmente le temps de retour sur investissement (de l'ordre de 20 ans).
- Le quatrième type (géométrie q) assure la plus grande réduction de consommations énergétiques mais son cout est élevé.
- Les délais de rentabilité pour les cas du sol rocheux sont plus importants que ceux du sol argileux.
- Le délai de rentabilité diminue quand le taux d'infiltration diminue. Ce résultat s'explique par le fait que les consommations énergétiques sont proportionnelles au taux d'infiltration.

Literature research on ground thermal bridges at the whole building simulation level does not discuss renovation solutions' economic and thermal performance. This chapter contributes to filling these gaps by proposing several exterior ground renovating techniques. Different aspects related to soil, insulation material, insulation installation types and infiltration rates, as well as the energy consumption needs, are included in the calculation. A comparison is done between several renovating solutions under different conditions to choose the optimum one for each case.

5.2. INTRODUCTION

Dynamic variables such as electrical energy price, investment cost and climate change over building lifetime introduce uncertainty. This leads us to the studies that increase simulation number (to be carried out) and computation time. However, energy buildings modelling nowadays aim to reduce the calculation time and find the best design by using a particular model: optimization. Building performance optimization is a dynamic and complex phenomenon in which the researcher usually uses a dynamic simulation model for the desired objectives. For example, reduction of energy consumption, reduction of environmental impact, optimization of costs, etc.[151].

Best alternative solutions have been identified for building environmental impact by using the life cycle analysis principle and considering many economic and environmental criteria [152]. An example of optimization problems in literature: Carreras et al. [153] minimize both the cost and the environmental impact linked to energy consumption in the operational and construction phases. Wu et al. [154] minimize life cycle costs and greenhouse gas emissions by simultaneously optimizing the building's energy system and its redevelopment with heat pumps and renewable energy systems. Penna et al. [155] consider energy savings, cost and thermal comfort to estimate the optimal total energy on a building, including the energy systems and the envelope.

Most of the research on building optimization used the single-objective approach [156]. In the optimization study we propose here, we used GenOpt software to study a French building coupled with

EnergyPlus software. GenOpt is a generic single-object optimization tool that could be linked with any program reading input text files and producing results as text files. We can therefore use GenOpt to achieve our single-object optimizations with EnergyPlus.

The originality of this environment is to offer an integration of different optimization functions with a single-objective optimization method. This chapter will start by comparing the 2D KIVA heat transfer model in EnergyPlus to the three dimensional one in WUFI Plus. KIVA is validated for our case study. Then this section is followed by an introduction on optimization with the GenOpt tool which will be coupled to EnergyPlus via KIVA. Different insulation techniques are presented and compared. And finally, the optimum solutions are found and discussed from a thermal and economic point of view.

5.3. METHODOLOGY

5.3.1. KIVA model

It is very important to use WUFI Plus for detailed ground and building studies. However, if the research aims to reach a large number of simulations and therefore realize an optimization study, WUFI Plus cannot be used due to its moderate to slow simulation time (between 2h to 48h for a single simulation). Also, it is considered as a commercial black-box software: it can't be coupled to other tools like GenOpt (for optimization).

In this section, KIVA results in EnergyPlus and the 3D dynamic model in WUFI Plus will be compared to show the ability of KIVA to predict ground heat transfer and thermal bridges in our case.

A similar case study from section 4.3.1 is applied. Due to ground model comparison, the two examples will be compared without any windows, heating, cooling and ventilation (Figure 5-1): To ensure that the two models are compared for similar conditions and aspects.

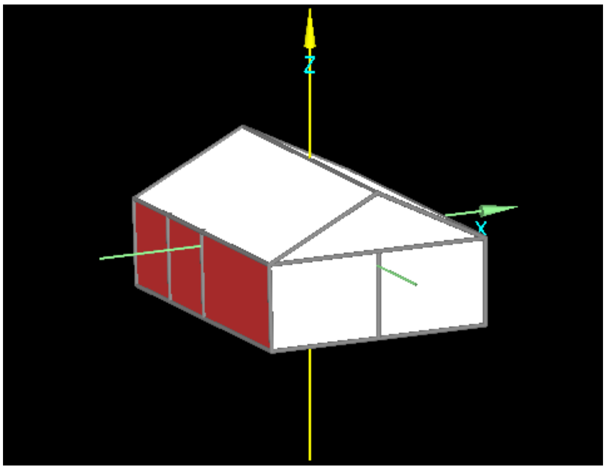

Figure 5-1: Building model in EnergyPlus and WUFI.

KIVA is a 2D coupled heat transfer model between building, slab, foundation and soil. KIVA model uses heat equation (3-12), but it estimates the 3D aspect (corner flow) using a simplified correlation [119]. It is also able to predict temperature profiles through the ground surface.

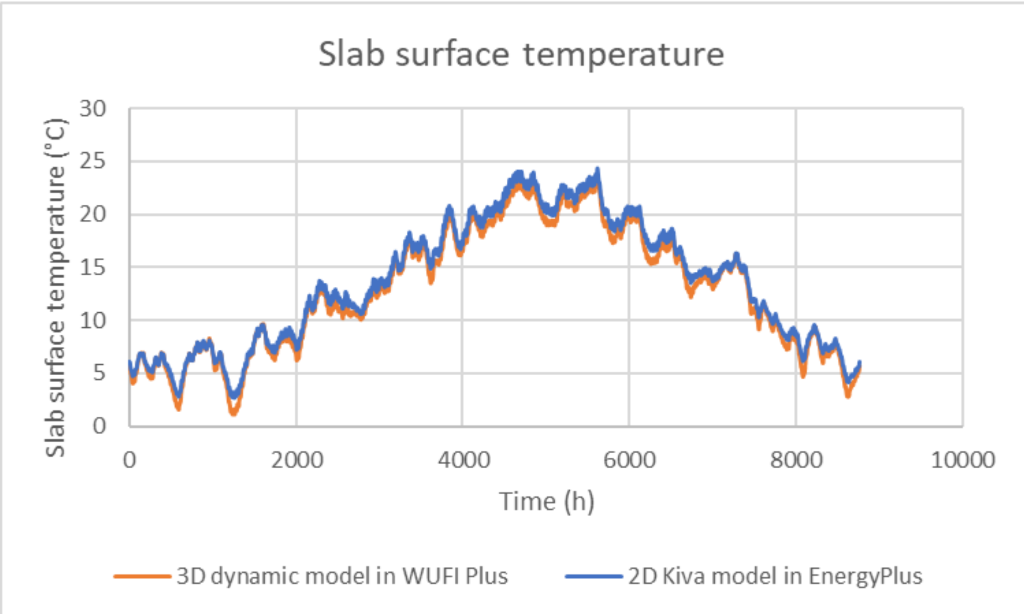

Figure 5-2: Average interior slab surface temperature calculated by the 3D model in WUFI Plus and 2D model in EnergyPlus.

Figure 5-2 represents the yearly interior slab surface temperature. 3D dynamic heat transfer model in WUFI Plus and 2D dynamic heat transfer are compared. The two models have similar conditions:

climate, exterior condition, heat transfer coefficients, and no solar radiation. It is shown from this figure that the two graphs are very close during the year.

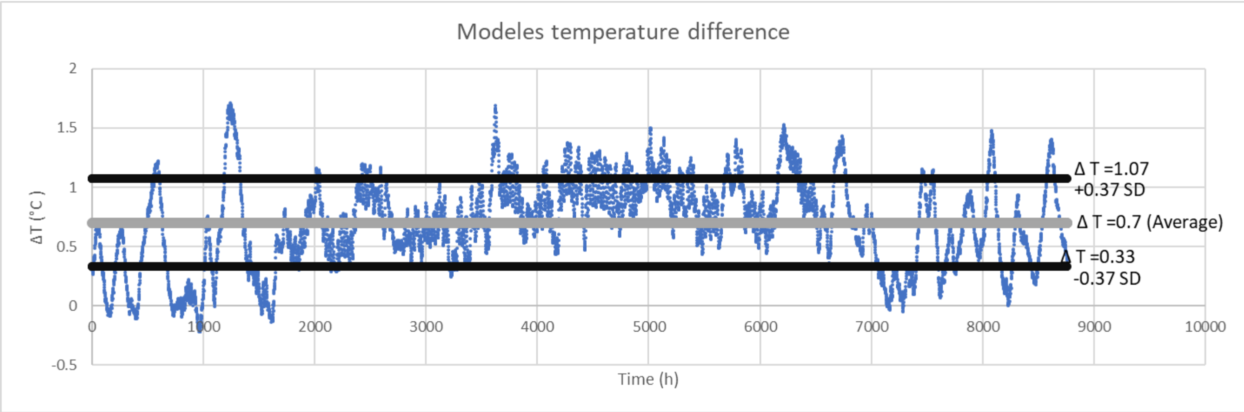

Figure 5-3: ΔT between KIVA and 3D model.

Figure 5-3 represents the temperature difference ΔT of KIVA with respect to the 3D model. The average ΔT is 0.7 °C, and the standard deviation SD is ±0.37°C. It is shown that most of the points lie between the black lines 1.07 °C and 0.33 °C (68% of the total points).

Higher ΔT (above 1.07 °C line) exists during the summer (16% of the total points) due to the imposed radiation: Radiation is considered negligible in the two cases. However, it is not possible to set 0 radiation coefficients in EnergyPlus. Then, these coefficients are set to be very small.

Also, KIVA can calculate most of 3D aspects using simple correlation (corner flow, geometry effect), but it will not perfectly predict the 3D calculations. Lower ΔT exists under winter conditions, where the three-dimensional TBs are remarkable during heating periods.

Therefore, these results show the ability of KIVA to predict ground heat transfer in our whole building calculation case of study. The next step is to couple EnegyPlus and KIVA with an optimization software “GenOpt”.

5.3.2. GenOpt

The GenOpt software [157] allows the use of many optimizations and parametric study algorithms. The choice of an appropriate optimization algorithm depends in particular on the type of variables presented (continuous, discrete or both) and the type of function to be minimized. Note that several optimization algorithms may be suitable for studying the same problem. Many algorithms are used like GPSHookeJeeves, GPSPSOCCHJ and a parametric study algorithm.

5.3.3. Coupling EnergyPlus with GenOpt:

To realize an optimization study between EnergyPlus and GenOpt, several files must be created:

- The initialization file "*optWinXP.ini*": contains the definition of the objective functions and the paths to locate and make the connections between the optimization and simulation files.
- Command file "*command.txt*": contains the parameters to be optimized with their variation intervals and their initial values, and the optimization method used (The method is already implemented in the software and will be described in the next paragraph).
- Running E+ file "*RunEP.bat*": file calling the simulation software (EnergyPlus).
- EnergyPlus template file "*template.idf*": input file, containing the variables; it will be rewritten for each simulation by GenOpt, in order to launch EnergyPlus.

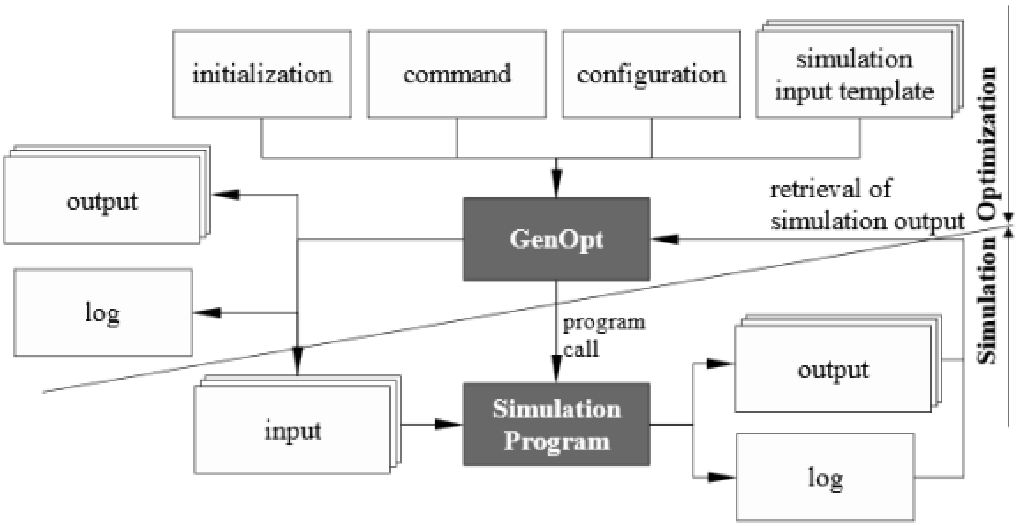

Figure 5-4: Different steps and files needed to run GenOpt [158].

Briefly, coupling steps (Figure 5-4) can be explained as follow:

Step1: Transform the EnergyPlus input.idf into a template file (template.idf), by replacing the parameters that we want to vary (which still have a fixed numerical value), by the name of the variables associated, according to the following convention :% variable_name%

Step 2: Define variables and choose optimization algorithm (command.txt)

Step3: Define objective functions in OptWinXP.ini.

Once the files are correctly configured, the simulations is launched:

The %variable_name% (template.idf file) are replaced by the values defined in command.txt.

The process runs over a large number of iterations, until the algorithm completes

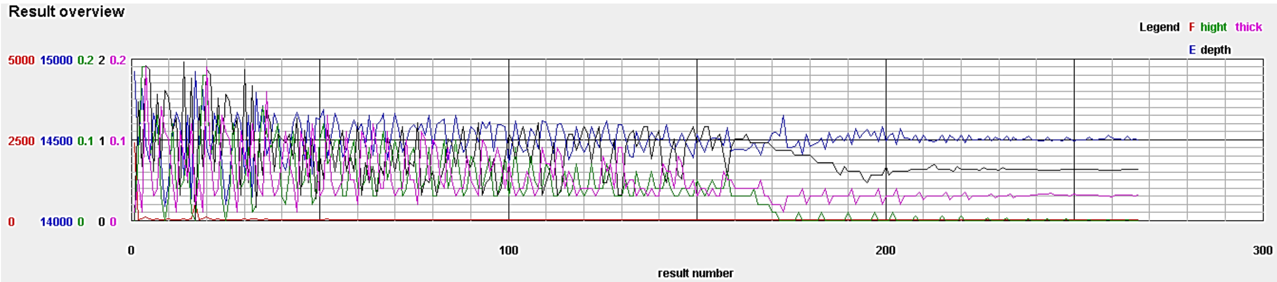

Figure 5-5: GenOpt interface.

When the simulation ends, the objective function results are presented at the GenOpt interface (Figure 5-5).

5.3.4. Optimization methods

In general, no optimization algorithm is suitable for all problems. Each one has its limits and application conditions. GenOpt therefore offers several optimization methods such as: the Nelder-Mead method, the generalized model search algorithm (GPS), Hooke-Jeeves algorithm, PSO type optimization algorithms etc. A brief description of these algorithms is given below.

5.3.4.1. Hooke-Jeeves (HJ) algorithm:

It is an optimization method [159] that calculates all possible solutions before deciding which one is the best. Hooke-Jeeves does not follow a single line in the direction of research: it predicts rather discrete steps according to the possible directions.

Three parameters must be set for the algorithm to work: a scalar ϵ which serves as a stop criterion for the method, an initial point: x_1, and the size of the pattern.

The procedure is then summarized in two repetitive movements:

- A first exploratory search evaluates the value of the cost function in x_1, then tests are made with discrete steps following directions $\{v_j\}$. The value of the function in each direction f $(x_1 + v_j)$ is then compared to the current point x_1 and only the value verifying $f(x_1 + v_j) < f(x_1)$ will be taken into account. This movement then ends up in one of the following two situations: either it finds a new point x_2 with a better value of the cost function, or it fails. In this case, the size of the pattern will be reduced and then a new exploratory movement will be carried out at the same point x_1. However, if this is successful, the algorithm does not move to the new point to explore again but will initiate a pattern search movement with the search direction $i = x_1 - x_2$.
- The second search uses the direction and values found in the previous exploratory movement. The algorithm is experimenting with the new search direction of the new center $x_c = x_1 + 2i = x_2 + i$. If this process is failed, a new exploratory movement will be initiated with the value x_2 in the center.

5.3.4.2. The Generalized Pattern Search (GPS) type optimization algorithm:

Several modified versions of the method are being developed to address a larger number of issues. All of the GPS models are based on mesh construction in a problem space. Each model has its own law to choose the finite number of points of its mesh. If a mesh point has a value lower than the initial one, the search for the optimum continues with the same mesh size. Otherwise, the mesh will be refined with a reduced size factor and the procedure is repeated.

5.3.4.3. Nelder-Mead (NM) algorithm:

The Nelder-Mead method [160] is based on a numerical method that seeks to minimize a continuous function in a space with several dimensions. The algorithm exploits the simplex concept, a prototype of N + 1 vertices in an N-dimensional space. Starting from a simplex, it undergoes transformations, deforms, moves and progressively reduces until these vertices approach a minimal point. It is well known that this method can fail and converge towards a fixed point, especially if the number of variables is high. However, it is commonly used.

5.3.4.4. Particle Swarm Optimization (PSO) type optimization algorithms:

The Particle Swarm Optimization (PSO) algorithm [161] is inspired by our world such as the movement of a group of birds or fish.

The particles can converge towards a local optimum from simple movements in space. It is more particularly suitable for spaces of continuous variables. To apply the PSO, it is necessary to define a search space made up of particles and an objective function to be optimized. Each particle is endowed with:

- A position
- A speed that allows the particle to move
- A neighborhood, a set of particles that interact directly with the particle
- A best visited position.
- At each iteration, the particles move by taking into account their best position (egotistical displacement) but also the best position of its neighborhood (panurgian displacement).

Finally, a hybrid method that combines the GPS, PSO and Hooke-Jeeves is used in our work. The Particle Swarm Optimization PSO is a global optimization method. However, the Hooke-Jeeves is a local one: HJ algorithm finds local minimum (that is not global). Therefore, a hybrid method was used to combine the PSO global feature with the provable GPS convergence properties. The following paragraph will discuss the case study and functions applied with this method.

5.3.5. Case Study:

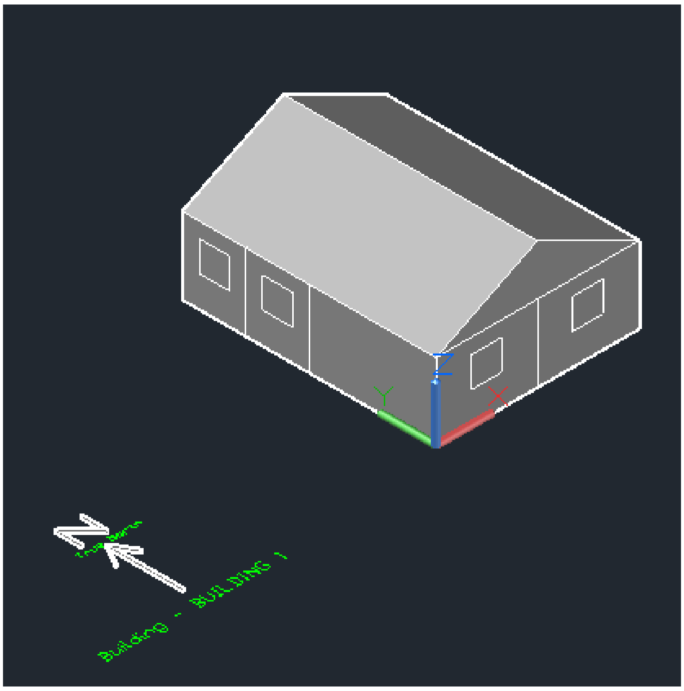

Figure 5-6: Slab on grade building.

It is the case of a french older building from the 1950th (Figure 5-6): the same case from chapter 4. It is considered as a two thermal zone house 8mx10mx3m: Slab on grade zone and loft zone. Exterior wall composition from outside to inside and all building details can be found in chapter 4 (material properties are found in WUFI's library). The simulation run period is one year.

Two infiltration flow rates are studied 0.1 ACH and 1 ACH. Results are compared to highlight the effect of this parameter on this calculation. Finally, different exterior insulations are presented:

5.3.5.1. Exterior Insulation types:

Different Insulation types will be studied (Figure 5-7):

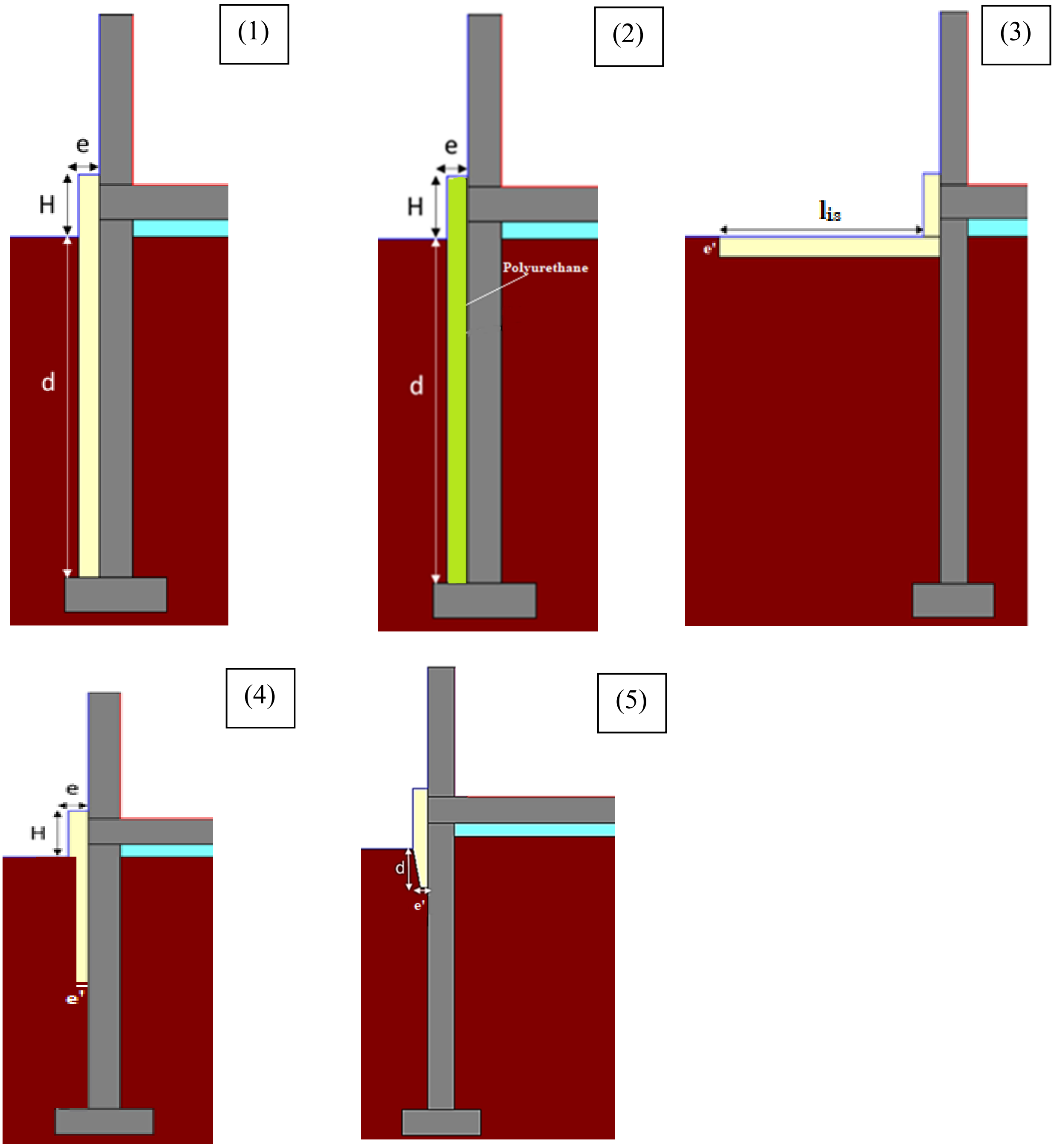

Figure 5-7: Different insulation types.

(1): is the vertical exterior insulation (I type- polystyrene).

(2): is also vertical exterior insulation (I type- polyurethane).

(3): is the horizontal and vertical exterior insulation (L type- polystyrene).

(4): is also vertical exterior insulation with different thicknesses (q type- polystyrene).

(5): is the trapezoidal exterior insulation (polystyrene).

It should be mentioned that for a base case (no insulation), the total energy consumption per year is presented in Table 5-1:

Table 5-1: Total energy consumption for base case without any insulation

	Total energy consumption (kWh)	
	0.1 ACH	**1 ACH**
Clay soil	9314	13377
Stony soil	9294	13473

For Lyon city, the heating consumption is dominating. On the other hand, the cooling one represents 2% of the total energy. Therefore, energy reduction is represented mainly by the heating case.

5.3.5.2. Insulations price and labor cost:

Exterior slab on grade insulations are: polystyrene and polyurethane. The costs of these insulations are represented by Figure 5-8:

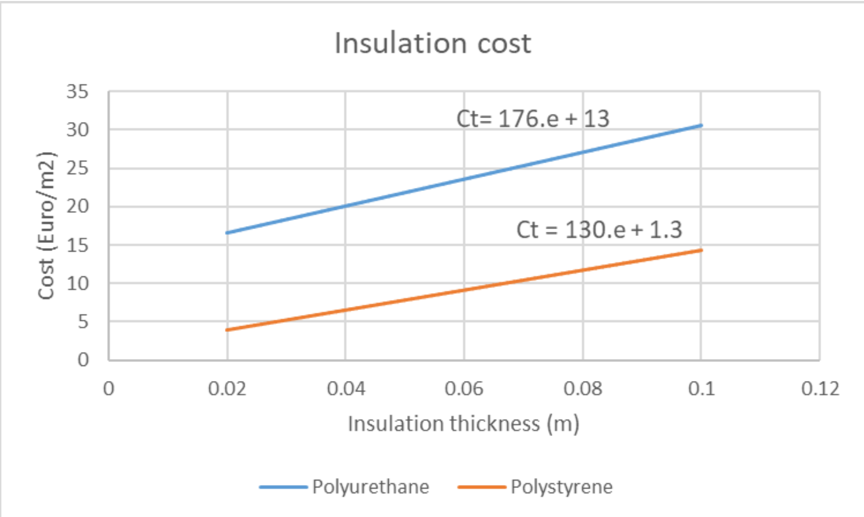

Figure 5-8: Polystyrene and polyurethane costs.

Labor and equipment costs depend on excavation volume and soil type (Table 5-2):

Table 5-2: Labor and equipment costs.		
Excavation type	**Average cost (non-rocky soil) €/m³**	**Average cost (rocky soil) €/m³**
Traditional (Labor)	30	60
With equipment	8	10

5.3.5.3. Variables:

The paramete rs that vary in this optimization study are represented in Table 5-3:

Table 5-3: Optimization variables.					
Variables (insulatiom)	**d (m)**	**H (m)**	**e (m)**	**e' (m)**	**x (m)**
Definition	**depth**	**height**	**thickness**	**thickness**	**length**
Initial value	0	0	0	0	0
Minimum-Maximum	0-2	0-0,2	0-0,2	0-0,2	0-2
Step	0,05	0,01	0,01	0,01	0,05

The parameters that vary in this optimization study are: the depth, the height, the thickness, and the width of the insulation.

5.3.6. GenOpt Functions:

Different equations are needed to find an optimum point as a function of total building energy consumption and insulation installation cost. Therefore, the first function is the total energy consumption:

$$E_t = E_{heating} + E_{cooling} \tag{5-1}$$

Where $E_{heating}$ is the building heating energy [kWh], $E_{cooling}$ is cooling energy [kWh] and E_t is the total energy consumption for every insulation type [kWh].

Insulations costs are given by:

$$\text{Polystyrene: } Ct_1 = (130.e + 1.3).A \qquad 5\text{-}2$$

$$\text{Polyurethane: } Ct_2 = (176.e + 13).A \qquad 5\text{-}3$$

Where Ct_1 is the polystyrene cost [€], Ct_2 is the polyurethane cost [€], e is the insulation thickness [m], and A is the insulation area [m^2].

Concerning Labor and equipment cost (to drill soil), it is represented as follow:

$$Ct_3 = 200 + (\text{cost per } m^3).\mathrm{V} \qquad 5\text{-}4$$

Where Ct_3 is the labor cost [€] and is the insulation volume [m^3].

Finally, the payback period "F" will be expressed as a function of the above equations:

$$F = \frac{Total\ cost}{Electric\ power\ Cost} = \frac{Insulation\ cost + Labor\ or\ Equipement\ cost}{\frac{(E_{ni} - E_t)}{C.O.P} * 0.18} \qquad 5\text{-}5$$

Where E_{ni} is the total energy consumption [kWh] with no insulation (base case), E_t is the total energy consumption for every insulation type [kWh], C.O.P [-] is the coefficient of performance of the system (heating and cooling), and 0.18 [€] is the cost of 1 kWh of electricity in France. The C.O.P is considered 3, it represents a reversible heat pump.

5.4. RESULTS

5.4.1. For 1 ACH infiltration rate:

5.4.1.1. Clay soil with traditional excavation:

Table 5-4 shows optimization points for every insulation type for clay soil with traditional excavation.

Table 5-4: Optimum points for different insulation types (Clay soil with traditional excavation).

Type	F (year)	d (m)	H (m)	e (m)	e' (m)	l_{is} (m)	Reduction (kWh)

(1)	15	0.57	0.2	0.032	-	-	385
(2)	23.6	0.26	0.2	0.023	-	-	303
(3)	14.5	0	0.2	0.05	0.02	0.4	377
(4)	17.3	0.47	0.2	0.2	0.02	-	484
(5)	14.2	0.43	0.2	0.051	0.021	-	401

Several graphs comparing the five insulation strategies were presented:

Energy reduction for different insulation methods:

Based on Table 5-4, the annual energy savings (compared to no insulation case) are presented in Figure 5-9 that summarizes the whole-building energy reduction data.

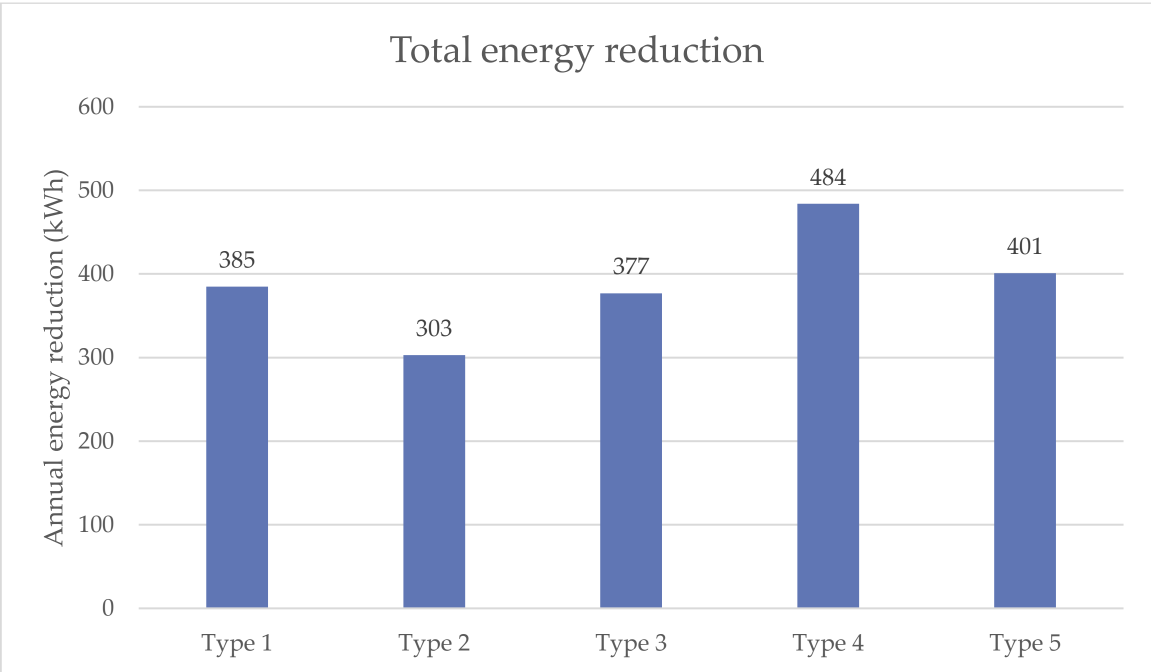

Figure 5-9: Energy reduction for different insulation types (Clay soil with traditional excavation).

It is clearly shown that type 4 (q type) has the highest energy reduction. Type 2 (I-polyurethane) has the lowest one. Types 1, 3 and 5 have almost similar reductions. The high energy reduction of 4 is due to the increased insulation thickness (0.2m) at the wall-slab junction. This junction is in contact with the exterior, where temperatures are very low during winter period.

Payback period for different insulation methods:

Figure 5-10 represents the economic study for those types. The payback period is shown in this figure. It represents the period required for the investment to recover its initial outlay in terms of energy savings.

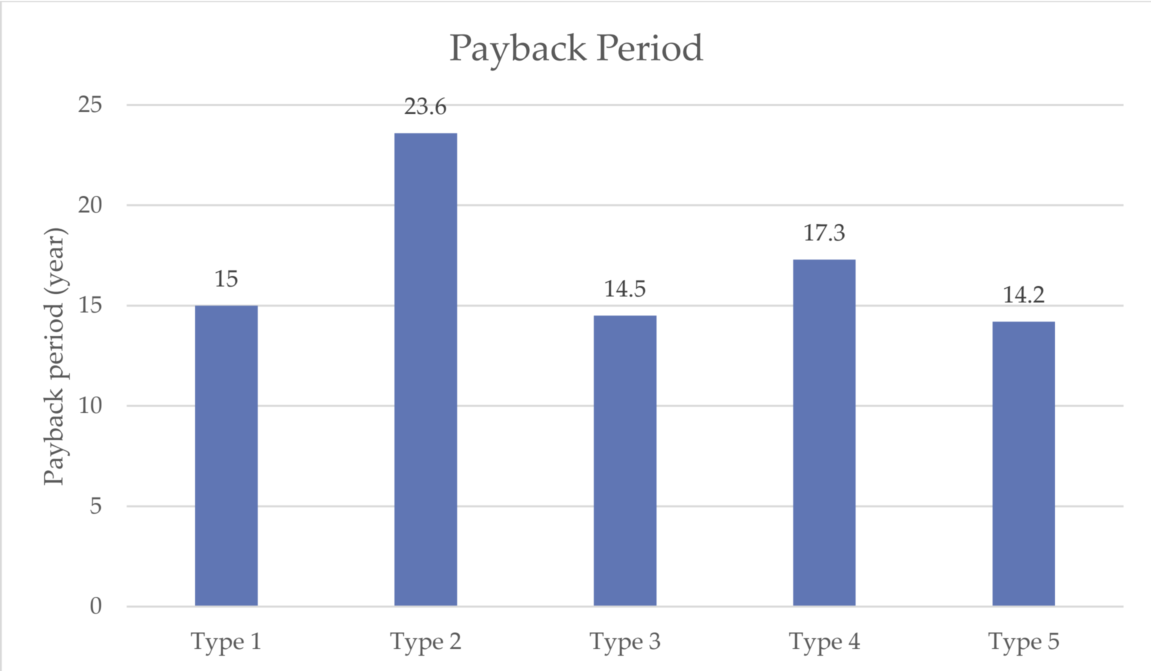

Figure 5-10: Payback period for different insulation types (Clay soil with traditional excavation).

The 3 and 5 types (L and trapezoidal geometry) have the lowest payback periods. 2 and 4 have the highest one. 1 is between these two categories. Type 2 represents polyurethane insulation. This material is more expensive than polystyrene (1, 3, 4 and 5 cases), which is why it has a higher payback period. Type 4 also has a high F, Table 5-4 shows that the fourth case has the largest insulation volume and the highest insulation and excavation costs.

Therefore, based on Table 5-4, Figure 5-9, and Figure 5-10 for clay soil with traditional excavation, types 3 and 5 are the best from a thermal and economic point of view.

5.4.1.2. Clay soil with equipment excavation:

This case is similar to the previous one; the only difference is the excavation method. The soil is drilled using equipment. Optimum results are shown in Table 5-5:

Table 5-5: Optimum points for different insulation types (Clay soil with equipment excavation).							
Type	**F (year)**	**d (m)**	**H (m)**	**e (m)**	**e' (m)**	**l_{is} (m)**	**Reduction (kWh)**
(1)	14.3	0.63	0.2	0.033	-	-	405
(2)	22.9	0.26	0.2	0.046	-	-	307
(3)	14.5	0	0.2	0.05	0.02	0.4	377
(4)	17	0.53	0.2	0.2	0.022	-	500
(5)	13.9	0.44	0.2	0.051	0.023	-	410

The above table shows that the best energy reduction is for the fourth type. However, to choose the best one from an economical and thermal point of view, the F factor should be compared: the trapezoidal one (5) has the lowest payback period.

5.4.1.3. Stony soil with traditional excavation:

Table 5-6 shows optimization points for every insulation type for Stony soil with traditional excavation. The differences with resect to previous simulations is the soil thermal properties and excavation costs.

Table 5-6: Optimum points for different insulation types (Stony soil with traditional excavation).							
Type	**F (year)**	**d (m)**	**H (m)**	**e (m)**	**e' (m)**	**l_{is} (m)**	**Reduction (kWh)**
(1)	16.6	0.84	0.2	0.024	-	-	397
(2)	27.9	0.56	0.2	0.028	-	-	379

(3)	16.5	0	0.2	0.045	0.019	0.56	347
(4)	18.4	0.7	0.2	0.2	0.018	-	501
(5)	15.3	0.64	0.2	0.048	0.018	-	413

Two histograms for the new soil type will describe the results for the energy reductions and payback periods.

Energy reduction for different insulation methods:

Based on Table 5-6, the annual energy savings (compared to no insulation case) are presented in Figure 5-11.

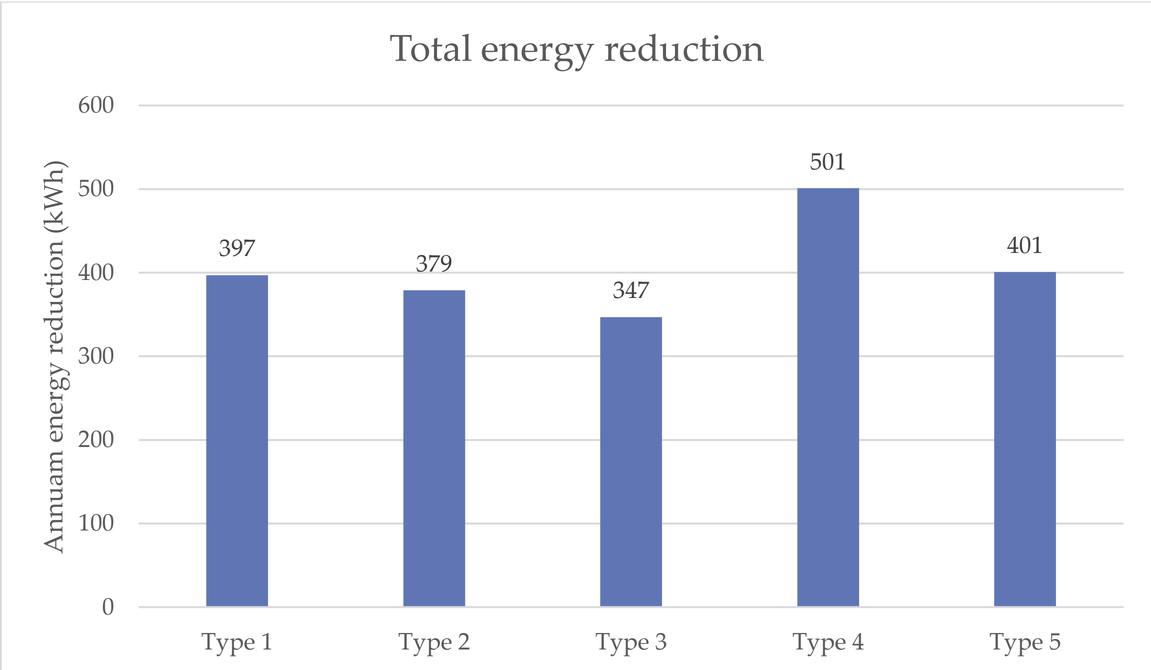

Figure 5-11: Energy reduction for different insulation types (Stony soil with traditional excavation).

It is clearly shown that type 4 (q type) has the largest energy reduction. Type 2 (I-polyurethane) has the lowest one. Types 1, 3 and 5 reductions are between 2 and 4. Similar as previous, the high energy reduction of 4 is due to the increased insulation thickness (0.2m) at the wall-slab junction.

Payback period for different insulation methods:

Figure 5-12 represents the payback period for these types. It should be mentioned here that this factor is depended on excavation, insulation costs and energy savings.

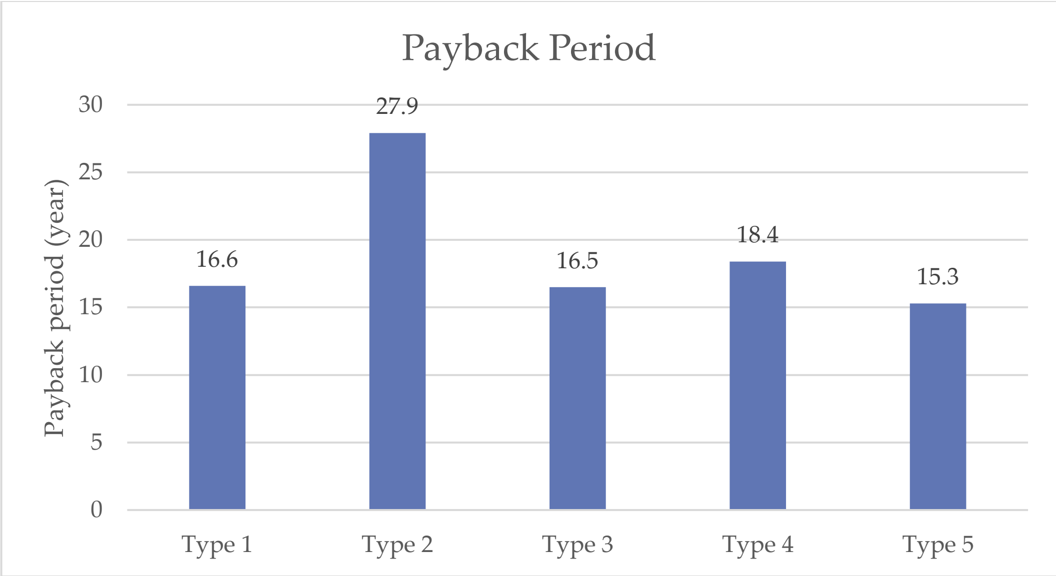

Figure 5-12: Payback period for different insulation types (Stony soil with traditional excavation).

The 3 (L geometry) have the lowest payback period. 1, 2, and 4 have the highest one. Therefore, based on Table 5-6, Figure 5-11, and Figure 5-12 for stony soil with traditional excavation, type 3 is the best from a thermal and economic point of view. For the L type (3), no excavation is needed. The installation costs are decreased, and then the payback period is reduced.

5.4.1.4. Stony soil with equipment excavation:

Equipment is used to drill stony soil. Optimum results are shown in Table 5-7:

Table 5-7: Optimum points for different insulation types (Stony soil with equipment excavation).

Type	**F (year)**	**d (m)**	**H (m)**	**e (m)**	**e' (m)**	**l_{is} (m)**	**Reduction (kWh)**
(1)	14.9	0.9	0.2	0.028	-	-	435
(2)	26.5	0.56	0.2	0.03	-	-	388
(3)	16.5	0	0.2	0.045	0.019	0.56	347
(4)	17.4	0.86	0.2	0.2	0.022	-	547
(5)	14.3	0.78	0.2	0.048	0.021	-	456

The best energy reduction is also for the fourth type. The lowest payback period is for: the trapezoidal one (5).

It is shown from the four cases: clay soil with labor excavation, clay soil with equipment excavation, stony soil with labor excavation, and stony soil with equipment excavation that:

1. For all cases, the L and trapezoidal types are recommended to be used. This is because they have the lowest F factor.
2. The second type (I geometry-polyurethane): It is not recommended to use such material for these cases, it has a high insulation cost and, therefore, a high payback period (order of 20).
3. The fourth type (q geometry) has larger energy reduction with higher cost: More insulation means more fees.
4. The payback periods for the stony soil cases are increasing with respect to the clay soil case.

5.4.1.5. Soil parametric study:

A case with no insulation is considered to highlight the effect of soil thermal properties on ground thermal bridges calculation. As a result, soil thermal conductivity and heat capacities are varied as a function of total energy consumption. Figure 5-13 represents a surface curve describing these parameters:

It can be seen from this figure that soil thermal properties have an impact on the whole building calculation. Total energy consumption will vary between 12000 and 14500 kWh (17%): if the specific heat and the thermal conductivity vary: from 300 to 2500 J/kg.K and 0.3 to 2.5W/m.K, respectively. Also, it is concluded that the energy consumption is proportional to soil thermal conductivity.

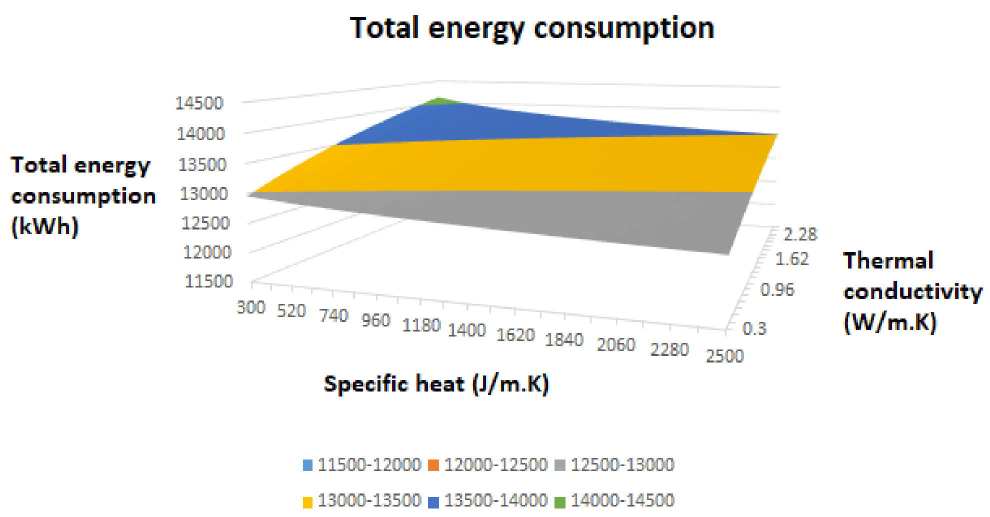

Figure 5-13: Total energy as a function of soil thermal conductivity and heat capacity.

5.4.2. For 0.1 ACH infiltration rate:

The following results will compare the two cases 0.1 and 1 ACH. As shown from previous part, the payback period for all cases will decrease using equipment excavation. Therefore, the following comparison will include clay and stony soil under traditional one.

5.4.3. Comparison

5.4.3.1. Clay soil with traditional excavation

First of all, the payback periods are compared for the five insulation types. The results are presented in Figure 5-14. It is clearly shown that the new infiltration rate will not widely affect final results: The 3 and 5 types (L and trapezoidal geometry) have the lowest payback periods. 2 and 4 have the highest one. Type 2 represents the polyurethane insulation, with a high payback period. Although, type 4 also has a high F, it is shown that the fourth case has the most significant insulation volume and, therefore, the highest insulation and excavation costs.

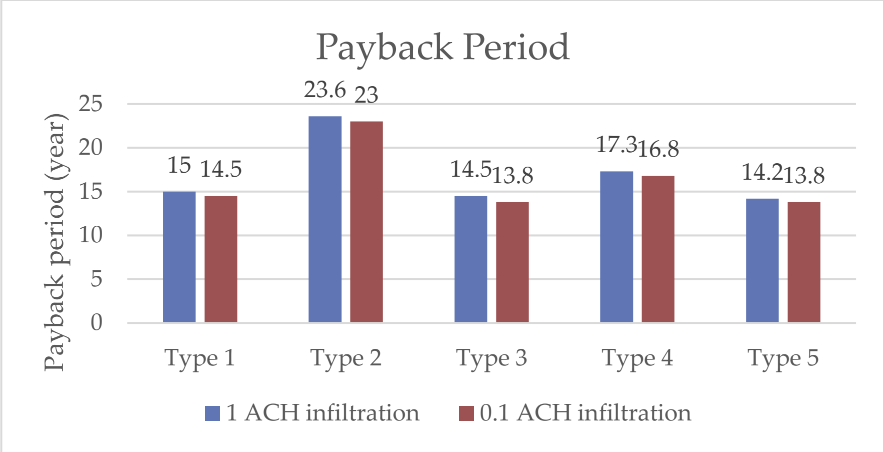

Figure 5-14: Payback period for different insulation types and different infiltration rate (Clay soil with traditional excavation).

By comparing the 0.1 ACH infiltration rate to the previous one (1ACH), it is found that the payback period will decrease for an average of 0.5 years (from 1 ACH to 0.1 ACH). These results are explained by the fact that energy consumption is proportional to infiltration rate; therefore, if we reduce infiltration, energy consumption and F will decrease.

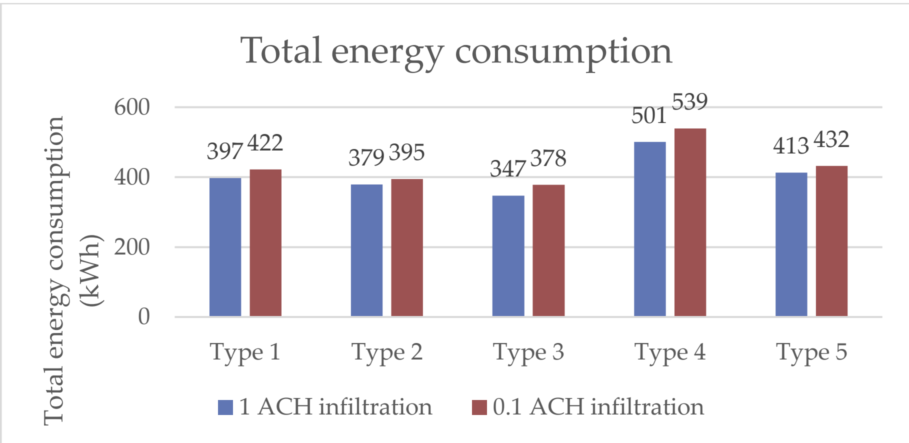

Figure 5-15: Total energy consumption for different insulation types and different infiltration rate (Clay soil with traditional excavation).

Also, based on Figure 5-15, clay soil with traditional excavation, types 3 and 5 are the optimum from a thermal and economic point of view.

5.4.3.2. Stony soil with traditional excavation

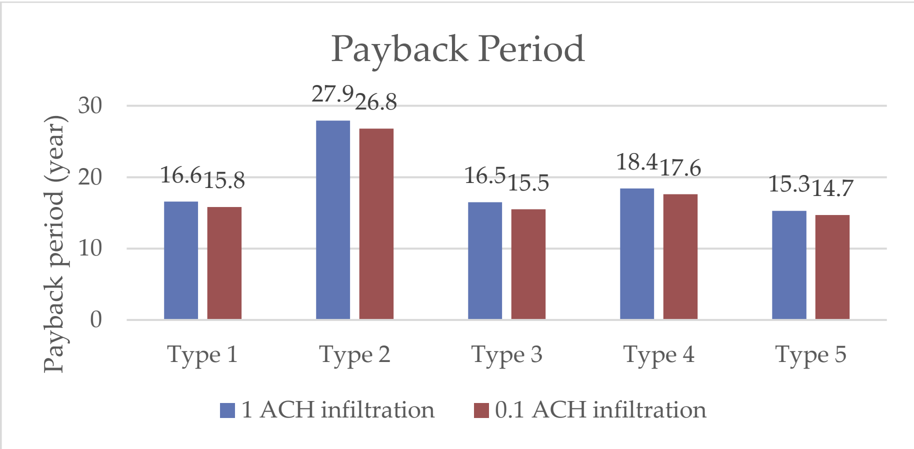

Figure 5-16: Payback period for different insulation types and different infiltration rate (Stony soil with traditional excavation).

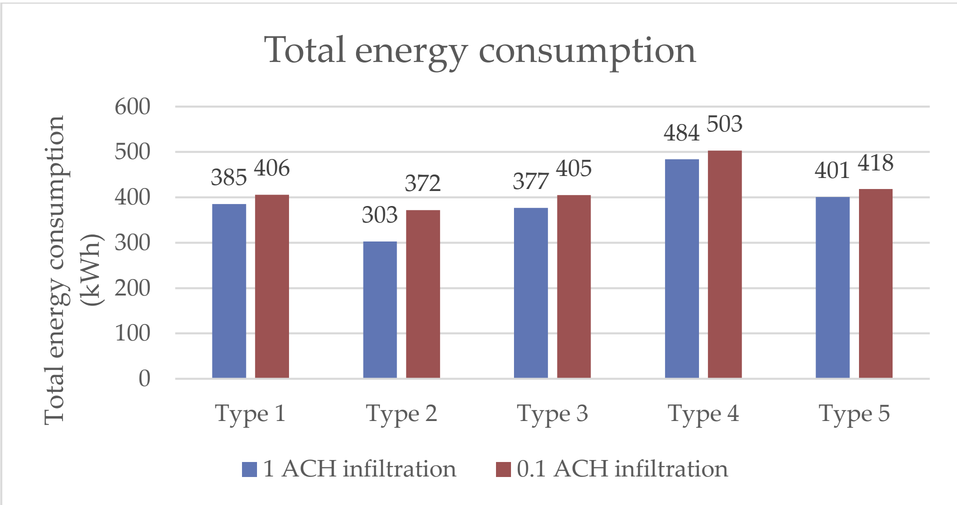

Figure 5-17: Total energy consumption for different insulation types and different infiltration rate (Stony soil with traditional excavation).

Figure 5-16 and Figure 5-17), insulations performances are similar to clay: Types 2 and 5 have the largest and lowest payback period. However, type 1 has equivalent performance as 3. Therefore, 1, 3 and 5 is chosen to be our optimum solutions for this case.

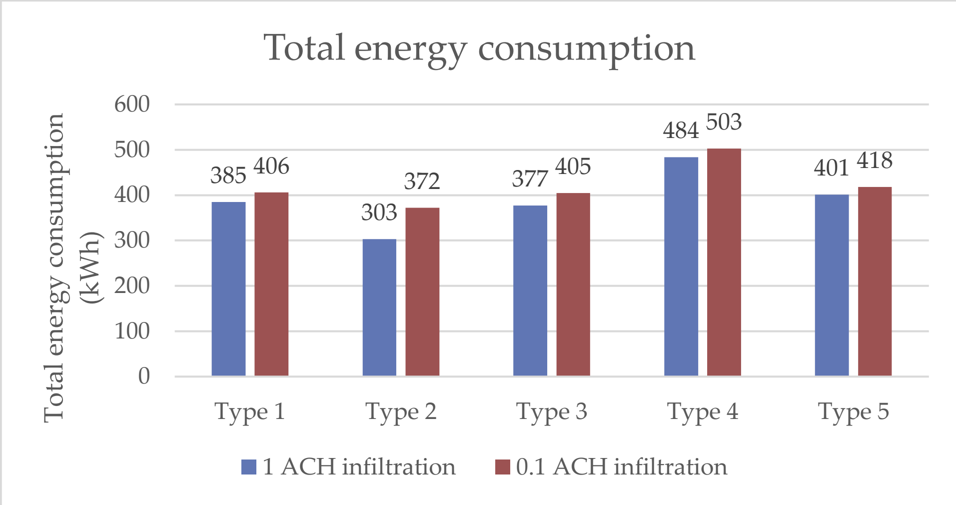

As a good agreement with the payback period, total energy reduction for 3 and 1 are similar. Type 5 has high energy reduction with respect to the five cases. It is deduced that these three types are thebest to be used.

By comparing the two soil types (for 0.1 ACH and traditional excavation), it is clearly shown also that energy reduction is decreased (due to the high soil thermal conductivity), and therefore, the payback period is increased.

5.5. CONCLUSION

This study is focused on calculating 2D dynamic ground thermal bridges with many exterior insulation types and soil for a slab on grade French building (1950). An optimization study was done to find optimum results for renovation. Thermal bridges were calculated using the KIVA model within EnergyPlus Software, and the optimizations data were simulated with GenOpt.

The objective of this chapter was to conduct an optimization analysis as a function of thermal and economic performance. Therefore, five types of exterior insulation were considered: (1) is the vertical exterior insulation (I type- polystyrene), (2) is the double insulation (I type- polyurethane), (3) is the horizontal and vertical exterior insulation (L type- polystyrene), (4) is also vertical exterior insulation with different thickness (q type- polystyrene) and (5) is the trapezoidal exterior insulation (polystyrene). These types are applied for two soil materials (clay, stony) and two excavation techniques (traditional and equipment).

It was found that the "L" and trapezoidal installation method (polystyrene) are the best insulation types to be used for renovating slab on grade building in Lyon city (1 ACH). Results are considered for:

a. Clay soil with traditional excavation, F=14.2 year and 14.5 year (trapezoidal and L type, respectively)
b. Clay soil with equipment excavation, F=13.9 year and 14.5 year.
c. Stony soil with traditional excavation, F=15.3 year and 16.5 year.
d. Stony soil with equipment excavation, F=14.3 year and 16.5 year.

However, L is strongly recommended for c and d cases where no soil drilling is needed.

The I type-polyurethane is not recommended due to high insulation cost and payback period. The q geometry has the higher energy saving at a higher cost.

F increased by an average of 0.5 years when the infiltration rates is reduced (from 1 ACH to 0.1 ACH). Then the ventilation and infiltration should be considered when syudying and choosing these solutions.

Soil thermal properties affect total energy simulation, an increase of 17% in energy consumption is calculated (ʌ will vary between 0.3 W/m.K and 2.5 W/m.K). Therefore, the soil is an essential factor when calculating ground thermal bridges and should be included in the calculation.

CHAPTER 6. GENERAL CONCLUSION AND PERSPECTIVES

6.1. RÉSUMÉ EN FRANÇAIS:

6.1.1. Conclusions :

Les normes et réglementations thermiques ont adopté des mesures en fonction des efficacités énergétiques des bâtiments neuves et rénovés. Par conséquent, pour optimiser le confort et réduire les coûts de chauffage et de climatisation, il faut bien prédire les fuites de chaleur à chaque paroi. Les efforts de recherche dans le domaine de la construction sont nombreux, mais peu d'études se focalise sur l'effet de la dalle et des fondations à partir desquelles, maintenant, une grande partie de la chaleur est perdue.

Après une présentation des phénomènes physiques de transferts de chaleur et d'humidité dans le sol, un état d'art sur les ponts thermiques au niveau de la dalle est présenté.

Par la suite, le travail a été orienté vers deux parties numériques : une première partie qui consiste à étudier les transferts à l'échelle d'un bâtiment sur terre-plein via le logiciel WUFI 3D et une seconde partie qui consiste à proposer des solutions de rénovation qui peuvent être appliqué au niveau de la dalle. Ces solutions sont évaluées par une étude d'optimisation (EnergyPlus et GenOpt) sous différents critères thermiques et économiques.

Une analyse des pertes de chaleur vers le sol sous le climat de Lyon est présentée pour le cas d'un bâtiment français (sur terre-plein) de 80 m^2 datant des années 1950. Cette étude montre un effet direct des conditions aux limites, du climat (chaud et froid, variations saisonnières), des isolations thermiques, ainsi que les propriétés hydriques et thermiques du sol et de la dalle sur les consommations énergétiques.

Une étude d'optimisation est réalisée en se basant sur les performances énergétiques et le coût de l'isolant. Cette étude montre que les solutions en "L" et trapézoïdale (polystyrène) sont les types d'isolation optimaux pour la rénovation des bâtiments sur terre-plein.

6.1.2. Perspectives :

Cette thèse ouvre vers plusieurs perspectives. Le modèle WUFI 3D présente des limites concernant le transfert de chaleur et d'humidité. Des améliorations supplémentaires pourront compléter ce travail :

- Un modèle 2D de chaleur et d'humidité peut être utilisé pour considérer le comportement hygrothermique dynamique des ponts thermiques. Il serait également important d'inclure l'effet de la pluie et de l'évapotranspiration sur les propriétés thermiques du sol et les pertes de chaleur.
- Des nouveaux matériaux de la dalle peuvent être proposé dans le futur comme les matériaux biosourcés.
- En plus, un manque significatif des données expérimentales dans le sol existe dans la littérature. Par conséquent, toutes nouvelles données expérimentales amélioreront ces études (pour valider les résultats numériques obtenus à ce niveau) : profil de la température ainsi que la teneur en eau en fonction de la profondeur du sol et pour différents types de sol.

Il existe de nombreuses difficultés lors de la rénovation des bâtiments sur terre-plein en utilisant une isolation par l'intérieure, les solutions utilisant une isolation extérieure sont plus intéressantes. Il serait utile de proposer plusieurs études à ce niveau, par exemple : étudier l'effet de la position de la liaison dalle-mur par rapport à la surface du sol et l'isolant (extérieure). Comme l'excavation présente un obstacle à ce niveau, il serait intéressant de se focaliser sur des solutions indépendantes de l'installation comme le type L: en fonction du type d'isolant et sous différentes conditions extérieures et couvertures du sol. Enfin, il serait également important de combiner ces techniques avec d'autres solutions et systèmes de rénovation des bâtiments (revêtement des murs intérieurs et extérieurs, ventilation....).

6.2. CONCLUSIONS

Public authorities have adopted new measures on energy efficiency for new and renovated constructions. Therefore, building thermal behavior and energy consumption have been a concern for optimizing comfort and reducing heating and air conditioning costs for years. Building research efforts in the field are numerous, but few focus on the effect of slab and foundation from which, now, a large part of the heat is lost via thermal bridges.

The first objective of this thesis is to highlight the importance of ground heat losses and thermal bridges on global building energy calculations by using a validated numerical model and software (WUFI Plus). This allows the development of new knowledge on ground heat transfer in slab-on-grade buildings.

Afterwards, the work was oriented towards two parts: The first is applying the developed model under insulation (slab and soil materials and boundary conditions) which are not widely discussed for global-building analysis. The second is to propose renovation solutions that can be applied at this level. Moreover, these solutions were evaluated in an optimization study that considers building thermal performance at different climates, soil and installation technics.

To begin with, a state-of-the-art on different physical parameters of soil and coupled heat and moisture transfer were done. Then, a description of the numerical model used by presenting ground phenomena and equations was presented.

In addition to that, special attention was paid to thermal bridge calculations methods in the literature and possible solutions to reduce it. Therefore, as a first step, the static calculation method was applied to a concrete slab-wall junction TB using THERM software: it was found that this calculation is strongly related to soil thermal properties, and insulations technics:

- The change in soil thermal conductivity can cause an important variation (up to 37%) in slab on grade heat linear thermal transmittance calculation.

- Exterior ground insulation is strongly recommended to reduce heat losses at this level, because it is more practical than interior one and can effectively overcome the TB effect on ground heat flux (from 54% to 61%). Improving insulation thickness and depth without insulating junction does not necessarily reduce the TB.

To continue this work, the dynamic effect of ground TB was applied at a building level. Several case studies were evaluated. An analysis of ground heat losses under Lyon climate is presented for an 80 m^2 slab-on-grade French building (1950^{th}) and the following observations were retained:

- A case without thermal bridges underestimates the total annual energy consumption by 4881 kWh compared to a case with thermal bridges, which is equivalent to 20% of the total energy consumption. The total heat loss increases between 30% and 50% when considering TB during the year. Ground heat losses increase annual heating energy in winter and reduce its total cooling energy in summer. The impact of thermal bridges is increased at corners due to three-dimensional thermal bridges compared to edges thermal bridges (corner temperature was found to be lower by 2 °C than the edge).
- For a seasonal variation study, it was found that: during winter, a more considerable heat loss forms at the building perimeter due to a higher temperature gradient between the interior and the exterior surfaces. On the other hand, during the summer, all slab surfaces will contribute equally in heat loss. It was also detected that the soil depth affected by the exterior and the interior climates is between 2 m and 5 m. However, the remainder of the soil depth is not affected. This is in good agreement with the thesis results (on deep boundary conditions effect) where total floor area directly affects this depth.
- For deep ground boundary conditions, its depth position causes an important effect on a larger slab area and perimeter. However, at a soil depth greater than 12 m, the influence is negligible. The difference between adiabatic and temperature conditions is minor for lower floor areas while it was noticeable for larger surfaces.

- In addition, the soil's thermal conductivity can increase the influence of these boundary conditions: a higher variation in the thermal conductivity of the soil means a higher boundary effect.
- Ground cover directly affects the global building calculations: if the albedo decreases from 1 to 0.15, total heating consumption is reduced by 3.1%, and cooling consumption increases slightly.
- The thermal losses for different soil thermal properties are also studied. The main differences were found to be caused by soil water content variations, which implies different soil thermal conductivities. For a dry clay, interior slab surface temperature increases in the winter period and decreases in the summer compared to wet clay case. Annual energy consumption increases by 4.2% when the thermal conductivity of the soil increases from 0.28 W/m.K to 1.28 W/m.K.
- To renovate and reduce thermal bridges, it is essential to use exterior insulation on foundation walls. The exterior renovation will increase corner temperatures up to 8°C (slab junction is insulated). Moreover, total energy consumption would be decreased by 8.5% for no insulation case. This solution will increase the slab surface by 2 m wide (from the edges). Also, it has a small effect under summer conditions (0.7°C reduction of slab surface temperature). During this period, no overheating risk exists due to insulation use (under the hot climate in Malaga). Combining exterior insulation with mechanical ventilation can decrease summer overheating and ensure occupant comfort.
- Using a heat and moisture transfer model, it was shown that the thermal conductivity of the soil and heat losses increase with moisture content. Compared to a concrete slab, a hempcrete slab can reduce ground thermal heat loss by 30% and the annual energy consumption by 6.7%. However, they have similar moisture performance under winter and summer conditions.
- Finally, KIVA can predict ground and foundation heat loss compared to a 3D detailed calculation (WUFI Plus). An optimization study using this model (in EnergyPlus) is based on

energy performance and insulation cost. It shows that the “L” and trapezoidal solution method (polystyrene) are the optimal insulation types for renovating slab-on-grade buildings under different conditions.

- It should be mentioned that the cooling and heating system is represented by a reversible heat pump (C.O.P=3) which is considered as a reference for such system in France (Thermal regulation, low electricity consumption). In addition, the ventilation and infiltration rates are important factor to be considered in such optimization studies.

6.3. PERSPECTIVES

The thesis opens several perspectives. The WUFI 3D model has limitations concerning heat and moisture transfer and boundary conditions. Further improvements could complete this work as for example:

- A 2D heat and moisture model can be applied to consider the dynamic hygrothermal behavior of thermal bridges. Also, it would be important to include the rain effect and evapotranspiration on soil thermal properties and heat losses.
- New slab materials can be included in future work, like bio-based materials, where detailed heat and moisture studies could be done at this level: temperature profile as well as water content via soil depths and types.

In addition to that, a significant lack of experimental ground data exists in the literature. Therefore, any new experimental data will improve these studies (to validate the numerical results obtained at this level): temperature profile as well as water content via soil depths and types under different boundary conditions.

There are many difficulties when renovating slab on grade buildings using interior insulation, however exterior solutions are more interesting. It would be useful to propose several studies at this level, for example: studying the position effect of the slab-wall junction with respect to the ground surface and the insulation. Since exterior excavation presents a difficulty at this level, it would be interesting to study renovation solutions independent of this type of installation: type L with different insulation materials and under outdoor conditions and ground cover. Finally, combining these techniques with other building renovation solutions and systems (interior and exterior walls covering, ventilation….) would also be interesting for future work.

REFERENCES

[1] "Énergie dans les bâtiments," *Ministère de la Transition écologique et solidaire*, 2016. https://www.ecologique-solidaire.gouv.fr/energie-dans-batiments (accessed May 11, 2020).

[2] "Chiffres de la construction 2019," *Ministère de la Cohésion des territoires et des Relations avec les collectivités territoriales*. https://www.cohesion-territoires.gouv.fr/chiffres-de-la-construction-2019 (accessed May 11, 2020).

[3] Z. Zhong and J. E. Braun, "A simple method for estimating transient heat transfer in slab-on-ground floors," *Building and Environment*, p. 10, 2007.

[4] N. Simões and C. Serra, "Ground contact heat losses: Simplified calculation method for residential buildings," *Energy*, vol. 48, no. 1, pp. 66–73, Dec. 2012, doi: 10.1016/j.energy.2012.04.013.

[5] I. Pokorska-Silva, M. Kadela, B. Orlik-Kożdoń, and L. Fedorowicz, "Calculation of Building Heat Losses through Slab-on-Ground Structures Based on Soil Temperature Measured In Situ," *Energies*, vol. 15, no. 1, p. 114, Dec. 2021, doi: 10.3390/en15010114.

[6] M. Deru, "A Model for Ground-Coupled Heat and Moisture Transfer from Buildings," National Renewable Energy Laboratory, Technical Report, 2003.

[7] "How To Improve Different Types Of Soil For Planting," *Wilson Bros Gardens*. https://www.wilsonbrosgardens.com/different-soil-types.html

[8] W. J. Rawls, D. L. Brakensiek, and K. E. Saxtonn, "Estimation of Soil Water Properties," *Transactions of the ASAE*, vol. 25, no. 5, pp. 1316–1320, 1982, doi: 10.13031/2013.33720.

[9] M. Kehrer and S. Pallin, "Hygrothermal Material Properties for Soils in Building Science," *Journal of National Institute of Building Science*, 2013.

[10] H. Brandl, "Energy foundations and other thermo-active ground structures," *Géotechnique*, vol. 56, no. 2, pp. 81–122, Mar. 2006, doi: 10.1680/geot.2006.56.2.81.

[11] N. H. Abu-Hamdeh, "Measurement of the Thermal Conductivity of Sandy Loam andClay Loam Soils using Single and Dual Probes," *Journal of Agricultural Engineering Research*, vol. 80, no. 2, pp. 209–216, Oct. 2001, doi: 10.1006/jaer.2001.0730.

[12] N. H. Abu-Hamdeh, "Thermal Properties of Soils as affected by Density and Water Content," *Biosystems Engineering*, vol. 86, no. 1, pp. 97–102, Sep. 2003, doi: 10.1016/S1537-5110(03)00112-0.

[13] E. I. Ekwue, R. J. Stone, and D. Bhagwat, "Thermal Conductivity of Some Compacted Trinidadian Soils as affected by Peat Content," *Biosystems Engineering*, vol. 94, no. 3, pp. 461–469, Jul. 2006, doi: 10.1016/j.biosystemseng.2006.03.002.

[14] M. P. Deru and A. T. Kirkpatrick, "Ground-Coupled Heat and Moisture Transfer from Buildings Part 1–Analysis and Modeling*," *Journal of Solar Energy Engineering*, vol. 124, no. 1, pp. 10–16, Feb. 2002, doi: 10.1115/1.1435652.

[15] N. N. Das and B. P. Mohanty, "Root Zone Soil Moisture Assessment Using Remote Sensing and Vadose Zone Modeling," *Vadose Zone Journal*, vol. 5, no. 1, pp. 296–307, Jan. 2006, doi: 10.2136/vzj2005.0033.

[16] G. C. Heathman, P. J. Starks, L. R. Ahuja, and T. J. Jackson, "Assimilation of surface soil moisture to estimate profile soil water content," *Journal of Hydrology*, vol. 279, no. 1–4, pp. 1–17, Aug. 2003, doi: 10.1016/S0022-1694(03)00088-X.

[17] R. F. Carsel and R. S. Parrish, "Developing joint probability distributions of soil water retention characteristics," *Water Resour. Res.*, vol. 24, no. 5, pp. 755–769, May 1988, doi: 10.1029/WR024i005p00755.

[18] M. G. Schaap and M. Th. van Genuchten, “A Modified Mualem-van Genuchten Formulation for Improved Description of the Hydraulic Conductivity Near Saturation,” *Vadose Zone Journal*, vol. 5, no. 1, pp. 27–34, Jan. 2006, doi: 10.2136/vzj2005.0005.
[19] “Soil Type Determination Guidelines,” Missouri departement of natural resources, 2006. [Online]. Available: https://dnr.mo.gov/env/hwp/mrbca.htm
[20] V. Gujisaite, “Transport réactif en milieux poreux non saturés,” PhD Thesis, Lorraine University, France, 2008.
[21] H. Janssen, J. Carmeliet, and H. Hens, “The influence of soil moisture transfer on building heat loss via the ground,” *Building and Environment*, vol. 39, no. 7, pp. 825–836, Jul. 2004, doi: 10.1016/j.buildenv.2004.01.004.
[22] G. S. Campbell and ristow Ristow K. L., “Underground power cable installations: soil thermal resistivity.” Decagon Devices, 2007.
[23] A. Piot, “Hygrothermique du bâtiment: expérimentation sur une maison à ossature bois en conditions climatiques naturelles et modélisation numérique,” p. 181, 2009.
[24] A. Evrard, “Transient hygrothermal behaviour of Lime-Hemp Materials,” 2008.
[25] F. Collet, “CARACTERISATION HYDRIQUE ET THERMIQUE DE MATERIAUX DE GENIE CIVIL A FAIBLES IMPACTS ENVIRONNEMENTAUX,” Institut National des Sciences Appliquées de Rennes, 2004.
[26] A. Fick, “Uber diffusion,” *Annalen der Physik und Chemie*, vol. 94, pp. 59–86, 1855.
[27] N. Wakao and J. M. Smith, “Difhsion in catalyst pellets,” p. 10, 1962.
[28] G. Costantine, “Etude et optimisation des performances énergétiques d’une enveloppe en béton de chanvre pour le bâtiment,” Université de Reims Champagne-Ardenne, Reims, 2018.
[29] S. P. Sutera and R. Skalak, “The History of Poiseuille’s Law,” *Annu. Rev. Fluid Mech*, p. 20, 1993.
[30] J.-F. Daïan, “Equilibre et transferts en milieux poreux I- Etats d’équilibre,” p. 189, 2010.
[31] WUFI, “WUFI Plus,” Jan. 13, 2020. https://wufi.de/en/software/wufi-plus/ (accessed Jan. 13, 2020).
[32] H. Dracy, *Les fontaines publiques de la ville de Dijon*. Paris, 1856.
[33] H. M. Künzel, *Simultaneous heat and moisture transport in building components: one- and two-dimensional calculation using simple parameters*. Stuttgart: IRB Verlag, 1995.
[34] W. Bahnfleth, “Three-Dimensional Modelling of Heat Transfer From Slab Floors,” US Army Corps of Engineers, 1989.
[35] M. Deru, R. Judkoff, and J. Neymark, “Whole-Building Energy Simulation with a Three-Dimensional Ground-Coupled Heat Transfer Model: Preprint,” p. 18, 2002.
[36] M. H. Adjali, M. Davies, S. W. Rees, and J. Littler, “Temperatures in and under a slab-on-ground ¯oor: two- and three-dimensional numerical simulations and comparison with experimental data,” *Building and Environment*, p. 8, 2000.
[37] W. Bahnfleth, “Three-Dimensional Modelling of Heat Transfer From Slab Floors,” *Ph.D. dissertation, also published as USACERL TM E-89/11, University of Illinois.*, pp. 1–200, 1989.
[38] ISO 10211, “ISO 10211:2017: Thermal bridges in building construction — Heat flows and surface temperatures — Detailed calculations,” 2017. [Online]. Available: https://viewer.afnor.org/Pdf/FileOpen/?token=7YaUn7Obvto1
[39] K. Dmytro, B. Maryna, S. Mykola, and S. Michael, “THE MAIN INSULATION PARAMETERS FOR THE DESIGN OF NZEB FROM BIOSOURCED MATERIALS,” p. 7, 2017.
[40] B. Nagy, “Comparative analysis of multi-dimensional heat flow modeling,” 2014, doi: 10.13140/2.1.2666.4003.
[41] M. Deru, “A Model for Ground-Coupled Heat and Moisture Transfer from Buildings,” p. 153, 2003.

[42] D. Bienvenido-Huertas, J. Moyano, D. Marín, and R. Fresco-Contreras, "Review of in situ methods for assessing the thermal transmittance of walls," *Renewable and Sustainable Energy Reviews*, vol. 102, pp. 356–371, Mar. 2019, doi: 10.1016/j.rser.2018.12.016.
[43] G. Mao and G. Johannesson, "Dynamic calculation of thermal bridges," *Energy and Buildings*, vol. 26, no. 3, pp. 233–240, Jan. 1997, doi: 10.1016/S0378-7788(97)00005-4.
[44] A. Hermelink *et al.*, "Towards nearly zero energy buildings," University of Wupperta, Italy, BESDE10788, 2013.
[45] Ministère de la transition écologique, "Réglementation thermique RT2012," 2020. https://www.ecologie.gouv.fr/reglementation-thermique-rt2012 (accessed Mar. 17, 2021).
[46] L. F. Goldberg and G. E. Mosiman, "High-Performance Slab-on-Grade Foundation Insulation Retrofits," The National Renewable Energy Laboratory, Denver, USA, 2015.
[47] A. Brás, F. Gonçalves, and P. Faustino, "Cork-based mortars for thermal bridges correction in a dwelling: Thermal performance and cost evaluation," *Energy and Buildings*, vol. 72, pp. 296–308, Apr. 2014, doi: 10.1016/j.enbuild.2013.12.022.
[48] G. Evola, G. Margani, and L. Marletta, "Energy and cost evaluation of thermal bridge correction in Mediterranean climate," *Energy and Buildings*, vol. 43, no. 9, pp. 2385–2393, Sep. 2011, doi: 10.1016/j.enbuild.2011.05.028.
[49] EST, "Enhanced Construction Details: Introduction and Use (Ed.)," Energy SavingTrust, London, UK, 2008.
[50] A. Tadeu, I. Simões, N. Simões, and J. Prata, "Simulation of dynamic linear thermal bridges using a boundary element method model in the frequency domain," *Energy and Buildings*, vol. 43, no. 12, pp. 3685–3695, Dec. 2011, doi: 10.1016/j.enbuild.2011.10.001.
[51] I. Abreu and J. Akander, "Energetic Rehabilitation in Buildings - Cost-Effective Solu-tions to Minimise Thermal Bridging.," Department of Construction and Planning,Polytechnic Institute of Braganc¸ a, Portugal, 2006.
[52] P. Levin and G. Mao, "The importance of thermal bridges for new Swedish multi-family buildings," *Proc. 3rd Syrup. Building Physics in the Nordic Countries*, Denmark, pp. 99–107, 1993.
[53] S. Hassid, "Thermal bridges in homogeneous walls: A simplified approach," *Building and Environment*, vol. 24, no. 3, pp. 259–264, Jan. 1989, doi: 10.1016/0360-1323(89)90040-1.
[54] S. Hassid, "Thermal bridges across multilayer walls: An integral approach," *Building and Environment*, vol. 25, no. 2, pp. 143–150, Jan. 1990, doi: 10.1016/0360-1323(90)90026-N.
[55] L. Zalewski, S. Lassue, D. Rousse, and K. Boukhalfa, "Experimental and numerical characterization of thermal bridges in prefabricated building walls," *Energy Conversion and Management*, vol. 51, no. 12, pp. 2869–2877, Dec. 2010, doi: 10.1016/j.enconman.2010.06.026.
[56] G. Mao, "Laboratory measurements and modelling of the dynamic thermal performance of a thermal bridge," *Nordic J. Build. Phys.*, 1998.
[57] K. Martin, A. Erkoreka, I. Flores, M. Odriozola, and J. M. Sala, "Problems in the calculation of thermal bridges in dynamic conditions," *Energy and Buildings*, vol. 43, no. 2–3, pp. 529–535, Feb. 2011, doi: 10.1016/j.enbuild.2010.10.018.
[58] "THERM Software." https://windows.lbl.gov/tools/therm/software-download (accessed May 12, 2020).
[59] Insulationshop.co, "Definition and Types of Thermal Bridges." https://www.insulationshop.co/definition_and_types_of_thermal_bridges.html
[60] Schoeck, "The causes of thermal bridging." https://www.schoeck.co.uk/en-gb/causes-of-thermal-bridging
[61] F. Ascione, N. Bianco, R. F. De Masi, F. de' Rossi, and G. P. Vanoli, "Simplified state space representation for evaluating thermal bridges in building: Modelling, application and validation

of a methodology," *Applied Thermal Engineering*, vol. 61, no. 2, pp. 344–354, Nov. 2013, doi: 10.1016/j.applthermaleng.2013.07.052.
[62] A. GhaffarianHoseini, N. D. Dahlan, U. Berardi, A. GhaffarianHoseini, N. Makaremi, and M. GhaffarianHoseini, "Sustainable energy performances of green buildings: A review of current theories, implementations and challenges," *Renewable and Sustainable Energy Reviews*, vol. 25, pp. 1–17, Sep. 2013, doi: 10.1016/j.rser.2013.01.010.
[63] M. Krarti, "Heat loss and moisture condensation for wall corners," *Energy Conversion and Management*, vol. 35, no. 8, pp. 651–659, Aug. 1994, doi: 10.1016/0196-8904(94)90048-5.
[64] BC Hydro, *Building envelope thermal bridging guide*. 2016.
[65] T. G. Theodosiou and A. M. Papadopoulos, "The impact of thermal bridges on the energy demand of buildings with double brick wall constructions," *Energy and Buildings*, vol. 40, no. 11, pp. 2083–2089, Jan. 2008, doi: 10.1016/j.enbuild.2008.06.006.
[66] M. Krus, R. Kilian, K. Sedlbauer, and H. M. Künzel, "Mould growth prediction by computational simulation," *ASHRAE Conference IAQ 2001*, 2001.
[67] S. Ilomets and T. Kalamees, "Evaluation of the criticality of thermal bridges," *J Build Rehabil*, vol. 1, no. 1, p. 11, Dec. 2016, doi: 10.1007/s41024-016-0005-6.
[68] S. Fantucci, F. Isaia, V. Serra, and M. Dutto, "Insulating coat to prevent mold growth in thermal bridges," *Energy Procedia*, vol. 134, pp. 414–422, Oct. 2017, doi: 10.1016/j.egypro.2017.09.591.
[69] M. H. Corvacho, "Pontes térmicas : análise do fenómeno e proposta de soluções," 1996.
[70] D. Glew, M. Brooke-Peat, and C. Gorse, "Modelling insulated coving's potential to reducing thermal bridging and moisture risk in solid wall dwellings retrofitted with external wall insulation," *Journal of Building Engineering*, vol. 11, pp. 216–223, May 2017, doi: 10.1016/j.jobe.2017.04.013.
[71] T. Theodosiou, K. Tsikaloudaki, K. Kontoleon, and C. Giarma, "Assessing the accuracy of predictive thermal bridge heat flow methodologies," *Renewable and Sustainable Energy Reviews*, vol. 136, p. 110437, Feb. 2021, doi: 10.1016/j.rser.2020.110437.
[72] ISO 13370, "ISO 13370:2017: Performance thermique des bâtiments — Transfert de chaleur par le sol — Méthodes de calcul," 2017. [Online]. Available: https://www.iso.org/fr/standard/65716.html
[73] ISO 13789, "ISO 13789:2017 Thermal performance of buildings — Transmission and ventilation heat transfer coefficients — Calculation method," 2017. [Online]. Available: https://www.iso.org/standard/65713.html
[74] ISO 6946, "ISO 6946:2017: Building components and building elements — Thermal resistance and thermal transmittance — Calculation methods," 2017. [Online]. Available: https://www.iso.org/standard/65708.html
[75] ISO 14683, "EN ISO 14683 "Thermal bridges in building construction - Linear thermal transmittance - Simplified methods and default values" is another European standard"," 2017. [Online]. Available: https://www.iso.org/obp/ui/#iso:std:iso:14683:ed-3:v1:en
[76] NECB, "'National Energy Code of Canada for Buildings,'" 2017. [Online]. Available: https://nrc.canada.ca/en/certifications-evaluations-standards/codes-canada/codes-canada-publications/national-energy-code-canada-buildings-2017
[77] ASHRAE 90.1, "ANSI/ASHRAE/IES Standard 90.1 'Energy Standard for Buildings Except Low-Rise Residential Buildings,'" 2001. [Online]. Available: https://www.cnmorn.com/wp-content/uploads/2018/12/ANSI-ASHRAE-IESNA-STANDARD-90.1-2001.pdf
[78] H. Erhorn-Kluttig, H. Erhorn, M. Citterio, M. Cocco, van Orshoven, and A. Tilmans, "Thermal Bridges in the EPBD context," p. 6, 2009.
[79] J. Kośny, H. Liu, C. Curcija, A. D. Fontanini, and E. Kossecka, "A New Approach for Analysis of Complex Building Envelopes in Whole Building Energy Simulations," p. 37, 2016.
[80] RT 2012, "Règles Th-bat – Ponts thermiques," Dcembre 2017.

[81] T. Andreeva, "REVIEW OF LINEAR THERMAL BRIDGES IN HIGH-RISE BUILDING," p. 133, 2013.
[82] B. Carmichael, "Thermal Bridging Sensitivity Analysis," p. 15, 2018.
[83] J. Ramalho de Freitas and E. Grala da Cunha, "Thermal bridges modeling in South Brazil climate: Three different approaches," *Energy and Buildings*, vol. 169, pp. 271–282, Jun. 2018, doi: 10.1016/j.enbuild.2018.03.044.
[84] F. Aguilar, J. P. Solano, and P. G. Vicente, "Transient modeling of high-inertial thermal bridges in buildings using the equivalent thermal wall method," *Applied Thermal Engineering*, vol. 67, no. 1–2, pp. 370–377, Jun. 2014, doi: 10.1016/j.applthermaleng.2014.03.058.
[85] E. Kossecka and J. Kosny, "Equivalent wall as a dynamic model of a complex thermal structure," *Journal of Thermal Insulation and Building Envelopes*, vol. 20, pp. 249–268, 1997.
[86] E. Kossecka and J. Kosny, "Influence of insulation configuration on heating and cooling loads in a continuously used building," *Energy and Buildings*, vol. 34, pp. 321–331, 2002.
[87] H. Viot, A. Sempey, M. Pauly, and L. Mora, "Comparison of different methods for calculating thermal bridges: Application to wood-frame buildings," *Building and Environment*, vol. 93, pp. 339–348, Nov. 2015, doi: 10.1016/j.buildenv.2015.07.017.
[88] J. Quinten and V. Feldheim, "Dynamic modelling of multidimensional thermal bridges in building envelopes: Review of existing methods, application and new mixed method," *Energy and Buildings*, pp. 284–293, 2016.
[89] F. Baba, "Dynamic Effect of Thermal Bridges on the Energy Performance of Residential Buildings," Master Thesis, Concordia University, Montréal, Québec, Canada, 2015.
[90] H. Ge and F. Baba, "Effect of dynamic modeling of thermal bridges on the energy performance of residential buildings with high thermal mass for cold climates," *Sustainable Cities and Society*, vol. 34, pp. 250–263, Oct. 2017, doi: 10.1016/j.scs.2017.06.016.
[91] H. Ge and F. Baba, "Dynamic effect of thermal bridges on the energy performance of a low-rise residential building," *Energy and Buildings*, vol. 105, pp. 106–118, Oct. 2015, doi: 10.1016/j.enbuild.2015.07.023.
[92] K. Martin, C. Escudero, A. Erkoreka, I. Flores, and J. M. Sala, "Equivalent wall method for dynamic characterisation of thermal bridges," *Energy and Buildings*, vol. 55, pp. 704–714, Dec. 2012, doi: 10.1016/j.enbuild.2012.08.024.
[93] T. Busser, "Etude des transferts hygrothermiques dans les matériaux à base de bois et leurs contributions à l'ambiance intérieure des bâtiments," 2016.
[94] M. Ben Mansour and B. Benhamou, "Caractérisation thermique d'un plâtre de gypse tunisien utilisé en tant que matériau de construction," 2013.
[95] G. H. dos Santos and N. Mendes, "Simultaneous heat and moisture transfer in soils combined with building simulation," *Energy and Buildings*, vol. 38, no. 4, pp. 303–314, Apr. 2006, doi: 10.1016/j.enbuild.2005.06.011.
[96] H. Janssen, "The influence of soil moisture transfer on building heat loss via the ground," PhD Thesis, Catholic university of Leuven, Belgium, 2004. Accessed: Mar. 17, 2021. [Online]. Available: https://linkinghub.elsevier.com/retrieve/pii/S0360132304000228
[97] C. Doughty and A. Nir Tsang, Chin-Fu, "Seasonal thermal energy storage in unsaturated soils: Model development and field validation," Master Thesis, Lawrence Berkeley Laboratory, Berkeley, California, 1991. doi: 10.2172/10176364.
[98] M. Sinka, V. Obuka, D. Bajare, and A. Jakovics, "Durability and hygrothermal performance of bio-based materials in Northern European climate," *Academic Journal of Civil Engineering*, pp. 371-377 Pages, Jun. 2019, doi: 10.26168/ICBBM2019.53.
[99] A. Wróbel and T. Kisilewicz, "Thermographic detection of thermal bridges - aims, possibilities and conditions," presented at the 2008 Quantitative InfraRed Thermography, 2008. doi: 10.21611/qirt.2008.05_07_08.

[100] J. Ge, Y. Xue, and Y. Fan, “Methods for evaluating and improving thermal performance of wall-to-floor thermal bridges,” *Energy and Buildings*, vol. 231, p. 110565, Jan. 2021, doi: 10.1016/j.enbuild.2020.110565.
[101] H. NYBERG, “Thermal bridges at foundations,” CHALMERS UNIVERSITY OF TECHNOLOGY, Sweden, 2011.
[102] B. Tiziana and A. Cottone, “Thermal bridges in industrialized building: the case of reinforced concrete wall floor junctions,” *The housing for the dignity of mankind Conference*, Naples, 2018.
[103] Brzyski, Grudzińska, and Majerek, “Analysis of the Occurrence of Thermal Bridges in Several Variants of Connections of the Wall and the Ground Floor in Construction Technology with the Use of a Hemp–lime Composite,” *Materials*, vol. 12, no. 15, p. 2392, Jul. 2019, doi: 10.3390/ma12152392.
[104] D. Borelli, P. Cavalletti, A. Marchitto, and C. Schenone, “A comprehensive study devoted to determine linear thermal bridges transmittance in existing buildings,” *Energy and Buildings*, vol. 224, p. 110136, Oct. 2020, doi: 10.1016/j.enbuild.2020.110136.
[105] M. Grudzińska and P. Brzyski, “The Occurrence of Thermal Bridges in Hemp-Lime Construction Junctions,” *Period. Polytech. Civil Eng.*, Feb. 2019, doi: 10.3311/PPci.13377.
[106] A. Capozzoli, A. Gorrino, and V. Corrado, “A building thermal bridges sensitivity analysis,” *Applied Energy*, vol. 107, pp. 229–243, Jul. 2013, doi: 10.1016/j.apenergy.2013.02.045.
[107] B. Brumă, L. Moga, and I. Moga, “Aspects Regarding Dynamic Calculation of Plan Building Elements Having Thermal Bridges,” *Energy Procedia*, p. 8, 2016.
[108] C. J. Hopfe and M. R. Hall, “Fabric insulation, thermal bridging and acoustics in modern earth buildings,” in *Modern Earth Buildings*, Elsevier, 2012, pp. 41–71. doi: 10.1533/9780857096166.1.41.
[109] A. Staszczuk, “Comparison of the calculation results of heat exchange between a single-family building and the ground obtained with the quasi-stationary and 3-d transient models. part 1: continuous heating mode,” p. 13.
[110] A. Staszczuk, “Comparison of the Calculations Results of Heat Exchange Between a Single-Family Building and the Ground Obtained with the Quasi-Stationary and 3-D Transient Models. Part 2: Intermittent and Reduced Heating Mode,” *Civil And Environmental Engineering Reports*, vol. 24, no. 1, pp. 133–144, Mar. 2017, doi: 10.1515/ceer-2017-0009.
[111] WUFI, “WUFI Plus.” https://wufi.de/en/software/wufi-plus/ (accessed Jan. 13, 2020).
[112] “DELPHIN Software.” http://bauklimatik-dresden.de/delphin/index.php?aLa=en (accessed May 12, 2020).
[113] “HEAT2 Software.” https://buildingphysics.com/heat2-3/ (accessed May 12, 2020).
[114] “HEAT3 Software.” https://buildingphysics.com/heat3-3/ (accessed May 12, 2020).
[115] “AnTherm Software.” http://www.antherm.at/antherm/EN/ (accessed May 12, 2020).
[116] “HAMLab Software,” *Build Up*. https://www.buildup.eu/en/learn/tools/heat-air-and-moisture-simulation-laboratory (accessed May 12, 2020).
[117] CESDB, “TERMUS BRIDGE.” https://www.cesdb.com/termus-bridge.html (accessed Feb. 25, 2021).
[118] Physibel, “2D & 3D Thermal simulation.” https://www.physibel.be/en/products/thermal-simulation (accessed Feb. 25, 2021).
[119] N. J. F. Kruis, “Development and Application of a Numerical Framework for Improving Building Foundation Heat Transfer Calculations,” 2015.
[120] N. Mendes, “DOMUS 2.0: A whole-building hygrothermal simulation program,” p. 8, 2003.
[121] A. Tilmans and D. Van Orshoven, “Software and atlases for evaluating thermal bridges,” Belgian Building Research Institute (BBRI), Belgium, 2010.

[122] G. G. Akkurt *et al.*, “Dynamic thermal and hygrometric simulation of historical buildings: Critical factors and possible solutions,” *Renewable and Sustainable Energy Reviews*, vol. 118, p. 109509, Feb. 2020, doi: 10.1016/j.rser.2019.109509.
[123] G. N. Walton, “Estimating 3-D heat loss from rectangular basements and slabs using 2-D calculations,” *Asgrae Transactions*, vol. 93, pp. 791–797, 1987.
[124] Blomberg. T, Lund Institute of Technology, and Department of Building Physics, “Heat conduction in two and three dimensions: Computer modelling of building physics applications,” Lund, 1996.
[125] AnTherm, “Analysis of Thermal behaviour of Building Constructions with Heat and Vapour Bridges.” Accessed: Mar. 11, 2021. [Online]. Available: http://help.antherm.kornicki.com/AnTherm_EN.pdf
[126] W. Heindl, K. Krec, E. Panzhauser, and A. Sigmund, *Wärmebrücken*. Springer-Verlag, 1987.
[127] A. W. M. van Schijndel, “Integrated heat air and moisture modeling and simulation,” PhD Thesis, Technische Universiteit Eindhoven, Eindhoven, 2007.
[128] B. R. Anderson, “The effect of edge insulation on the steady-state heat loss through a slab-on-ground floor,” *Building and Environment*, vol. 28, no. 3, pp. 361–367, Jul. 1993, doi: 10.1016/0360-1323(93)90040-A.
[129] K. A. Landman and A. E. Delsante, “Steady-state heat losses from a building floor slab with horizontal edge insulation,” *Building and Environment*, vol. 22, no. 1, pp. 57–60, Jan. 1987, doi: 10.1016/0360-1323(87)90041-2.
[130] M. Krarti, “Steady-state heat transfer from slab-on-grade floors with vertical insulation,” *International Journal of Heat and Mass Transfer*, pp. 2147–2155, Jan. 1993.
[131] D. Chen, “Heat Loss via Concrete Slab Floors in Australian Houses,” *Procedia Engineering*, pp. 108–115, 2017.
[132] A. Stolarska and J. Strzałkowski, “Modelling of Edge Insulation Depending on Boundary Conditions for the Ground Level,” *IOP Conf. Ser.: Mater. Sci. Eng.*, vol. 245, p. 042003, Oct. 2017, doi: 10.1088/1757-899X/245/4/042003.
[133] G. H. dos Santos and N. Mendes, “Hygrothermal bridge effects on the performance of buildings,” *International Communications in Heat and Mass Transfer*, vol. 53, pp. 133–138, Apr. 2014, doi: 10.1016/j.icheatmasstransfer.2014.02.018.
[134] J. Neymark *et al.*, “International Energy Agency Building Energy Simulation Test and Diagnostic Method (IEA BESTEST): In-Depth Diagnostic Cases for Ground Coupled Heat Transfer Related to Slab-on-Grade Construction,” NREL/TP-550-43388, 937333, Sep. 2008. doi: 10.2172/937333.
[135] C. Olivier, “Le coefficient de transmission thermique moyen d’une dalle sur sol,” 2011. https://energieplus-lesite.be/theories/l-enveloppe/les-echanges-de-chaleur/la-transmission-thermique/le-coefficient-de-transmission-thermique/le-coefficient-de-transmission-thermique-moyen-d-une-dalle-sur-sol/
[136] M. Grudzińska and P. Brzyski, “The Occurrence of Thermal Bridges in Hemp-Lime Construction Junctions,” *Period. Polytech. Civil Eng.*, Feb. 2019, doi: 10.3311/PPci.13377.
[137] A. Stefanoiu, “Towards performance evaluation of energy efficient buildings,” p. 221, 2017.
[138] ASHRAE, “62.1 User’s Manual: ANSI/ASHRAE Standard 62.1-2007 Ventilation for Acceptable Indoor Air Quality.” 2007.
[139] G. Florides and S. Kalogirou, “Annual Ground Temperature Measurements at Various Depths,” *CLIMA 2005 conference*, p. 6, 2005.
[140] G. P. Williams and L. W. Gold, “Ground temperatures,” *Canadian Building Digest*, p. 6 p., Jul. 1976, doi: 10.4224/40000712.
[141] European Standard EN 15026:2007, “Hygrothermal performance of building components and building elements — Assessment of moisture transfer by numerical simulation,” 2007.

[142] M. Vincent, “Profils hydriques dans les sols argileux. Premiers résultats sur deux sites expérimentaux,” p. 18, 2007.
[143] WUFI, “WUFI Support,” Sep. 04, 2019. https://wufi.de/en/service/support/
[144] T. Colinart, P. Glouannec, and P. Chauvelon, “Influence of the setting process and the formulation on the drying of hemp concrete,” *Construction and Building Materials*, vol. 30, pp. 372–380, 2012, doi: 10.1016/j.conbuildmat.2011.12.030.
[145] L. Arnaud and E. Gourlay, “Experimental study of parameters influencing mechanical properties of hemp concretes,” *Construction and Building Materials*, vol. 28, no. 1, pp. 50–56, 2012, doi: 10.1016/j.conbuildmat.2011.07.052.
[146] S. Benfratello, C. Capitano, G. Peri, G. Rizzo, G. Scaccianoce, and G. Sorrentino, “Thermal and structural properties of a hemp-lime biocomposite,” *Construction and Building Materials*, vol. 48, pp. 745–754, 2013, doi: 10.1016/j.conbuildmat.2013.07.096.
[147] F. Collet and S. Pretot, “Thermal conductivity of hemp concretes: Variation with formulation, density and water content,” in *Construction and Building Materials*, 2014, vol. 65, pp. 612–619. doi: 10.1016/j.conbuildmat.2014.05.039.
[148] F. Collet and S. Pretot, “Experimental investigation of moisture buffering capacity of sprayed hemp concrete,” *Construction and Building Materials*, vol. 36, pp. 58–65, 2012, doi: 10.1016/j.conbuildmat.2012.04.139.
[149] A. Shea, M. Lawrence, and P. Walker, “Hygrothermal performance of an experimental hemp-lime building,” *Construction and Building Materials*, vol. 36, pp. 270–275, 2012, doi: 10.1016/j.conbuildmat.2012.04.123.
[150] “chape chaux chanvre en isolation répartie - Weber Tradical,” *BCB Tradical*. https://www.bcb-tradical.com/le-beton-de-chanvre/beton-de-chanvre-chape-isolante/ (accessed Jun. 23, 2022).
[151] R. Garber, *Optimization stories: The impact of building information modelling on contemporary design practice*. 2009. [Online]. Available: https://doi.org/10.1002/ad.842
[152] E. Antipova, D. Boer, G. Guillén-Gosálbez, L. F. Cabeza, and L. Jiménez, “Multi-objective optimization coupled with life cycle assessment for retrofitting buildings,” *Energy and Buildings*, vol. 82, pp. 92–99, Oct. 2014, doi: 10.1016/j.enbuild.2014.07.001.
[153] J. Carreras, D. Boer, G. Guillén-Gosálbez, L. F. Cabeza, M. Medrano, and L. Jiménez, “Multi-objective optimization of thermal modelled cubicles considering the total cost and life cycle environmental impact,” *Energy and Buildings*, vol. 88, pp. 335–346, Feb. 2015, doi: 10.1016/j.enbuild.2014.12.007.
[154] R. Wu, G. Mavromatidis, K. Orehounig, and J. Carmeliet, “Multiobjective optimisation of energy systems and building envelope retrofit in a residential community,” *Applied Energy*, vol. 190, pp. 634–649, Mar. 2017, doi: 10.1016/j.apenergy.2016.12.161.
[155] P. Penna, A. Prada, F. Cappelletti, and A. Gasparella, “Multi-objectives optimization of Energy Efficiency Measures in existing buildings,” *Energy and Buildings*, vol. 95, pp. 57–69, May 2015, doi: 10.1016/j.enbuild.2014.11.003.
[156] R. Evins, “A review of computational optimisation methods applied to sustainable building design,” *Renewable and Sustainable Energy Reviews*, vol. 22, pp. 230–245, Jun. 2013, doi: 10.1016/j.rser.2013.02.004.
[157] Berkeley Lab, “GenOpt: Generic Optimization Program,” 2000. https://simulationresearch.lbl.gov/GO/
[158]M. Wetter, “Design Optimization with GenOpt,” vol. 21, p. 10, 2000.
[159] I. Moser, “Hooke-Jeeves revisited,” in *2009 IEEE Congress on Evolutionary Computation*, Trondheim, Norway, May 2009, pp. 2670–2676. doi: 10.1109/CEC.2009.4983277.
[160] J. A. Nelder and R. Mead, “A Simplex Method for Function Minimization,” *The Computer Journal*, vol. 7, no. 4, pp. 308–313, Jan. 1965, doi: 10.1093/comjnl/7.4.308.

[161] J. Kennedy and R. Eberhart, “Particle swarm optimization,” in *Proceedings of ICNN’95 - International Conference on Neural Networks*, Perth, WA, Australia, 1995, vol. 4, pp. 1942–1948. doi: 10.1109/ICNN.1995.488968.